INFORMATION TO USERS

The most advanced technology has been used to photograph and reproduce this manuscript from the microfilm master. UMI films the original text directly from the copy submitted. Thus, some dissertation copies are in typewriter face, while others may be from a computer printer.

In the unlikely event that the author did not send UMI a complete manuscript and there are missing pages, these will be noted. Also, if unauthorized copyrighted material had to be removed, a note will indicate the deletion.

Oversize materials (e.g., maps, drawings, charts) are reproduced by sectioning the original, beginning at the upper left-hand corner and continuing from left to right in equal sections with small overlaps. Each oversize page is available as one exposure on a standard 35 mm slide or as a 17″ × 23″ black and white photographic print for an additional charge.

Photographs included in the original manuscript have been reproduced xerographically in this copy. 35 mm slides or 6″ × 9″ black and white photographic prints are available for any photographs or illustrations appearing in this copy for an additional charge. Contact UMI directly to order.

Accessing the World's Information since 1938

300 North Zeeb Road, Ann Arbor, MI 48106-1346 USA

Order Number 8801690

Studies of substrates bound to horse liver alcohol dehydrogenase: Raman spectroscopy of NAD+, NADH and DABA *in situ*

Chen, De Huai, Ph.D.

City University of New York, 1987

U·M·I
300 N. Zeeb Rd.
Ann Arbor, MI 48106

PLEASE NOTE:

In all cases this material has been filmed in the best possible way from the available copy. Problems encountered with this document have been identified here with a check mark __✓__.

1. Glossy photographs or pages _____
2. Colored illustrations, paper or print _____
3. Photographs with dark background _____
4. Illustrations are poor copy _____
5. Pages with black marks, not original copy __✓__
6. Print shows through as there is text on both sides of page _____
7. Indistinct, broken or small print on several pages __✓__
8. Print exceeds margin requirements _____
9. Tightly bound copy with print lost in spine _____
10. Computer printout pages with indistinct print _____
11. Page(s) _____ lacking when material received, and not available from school or author.
12. Page(s) _____ seem to be missing in numbering only as text follows.
13. Two pages numbered _____. Text follows.
14. Curling and wrinkled pages _____
15. Dissertation contains pages with print at a slant, filmed as received _____
16. Other _____

_____

_____

STUDIES OF SUBSTRATES BOUND TO

HORSE LIVER ALCOHOL DEHYDROGENASE:

RAMAN SPECTROSCOPY OF NAD^+, NADH AND DABA IN SITU

BY

DE HUAI CHEN

A dissertation submitted to the Graduate Faculty in Physics in Partial fulfillment of the requirements for the degree of Doctor of Philosophy, The City University of New York.

1987

This manuscript has been read and accepted for the Graduate Faculty in Physics in satisfaction of the dissertation requirement for the degree of Doctor of Philosophy.

July 14 1987
date

Chairman of Examing Committee

July 14, 1987
date

Executive Officer

Supervisory Committee

The City University of New York

ABSTRACT

STUDIES OF SUBSTRATES BOUND TO

HORSE LIVER ALCOHOL DEHYDROGENASES:

RAMAN SPECTROSCOPY OF NAD^+, NADH AND DABA IN SITU

by

De Huai Chen

Adviser: Professor Robert H. Callender

In this thesis research we have studied the Raman spectra of reduced and oxidized nicotinamide adenine dinucleotide (NADH and NAD^+), adenosine 5'-diphosphate ribose (ADPR) and 1, 4, 5, 6 tetrahydronicotinamide adenine dinucleotide (H_2NADH) when bound to the coenzyme site of liver alcohol dehydrogenase (LADH). The bound NADH spectrum is calculated by comparisons the classical Raman spectrum of the binary complex, LADH/NADH, to that of LADH and by subtracting them. We have investigated how the bound NADH spectrum is affected when the ternary complexes with inhibitors are formed with dimethyl sulfoxide (DMSO), or iso-butyramide (IBA), i. e. LADH/NADH/DMSO or LADH/NADH/IBA. Similarly, the difference spectra of LADH/NAD^+/pyrazole, or LADH/ADPR, or LADH/H_2NADH with LADH are calculated. The magnitude of these difference spectral amplitudes are on the order of a few percent of the protein Raman spectrum. We present and discuss the experimental configuration and control procedures we use to reliably calculate such small difference signals. These sensitive difference techniques could be applied to a large number of problems where the classical Raman spectrum of a "small"

molecule, like adenine bound to the active site of a protein, is of interest. The spectrum of bound ADPR allows an assignment of the bands of the bound NADH and NAD^+ spectra to normal coordinates located primarily on either the nicotinamide and adenine moieties. This assigment has been confirmed from the studies of H_2NADH in solution and in situ. By comparing the spectra of the bound coenzyme with model compound data and through the use of deuterated compounds, we confirm and characterize how the adenine moiety is involved in coenzyme binding and discuss the validity of the suggestion that the adenine ring is protonated upon binding. The nicotinamide moiety of NADH shows significant changes upon binding, as evidenced by its spectrum. We find that the aromatic nature of the NAD^+ nicotinamide ring is disrupted in the ternary complex, LADH/NAD^+/pyrazole. We discuss various models which are consistent with the data and with the enzymatic mechanism of LADH. We note that the rather dramatic changes in the coenzyme molecular structure, that occur when NADH or NAD^+ binds, are not necessarily repeated at other dehydrogenase binding sites. For example, our preliminary results concerning coenzymes binding to yeast alcohol dehydrogenase show much fewer differences between solution and bound coenzymes.

To understand whether the substrate is directly bound to the active Zn (II) metal cation in the enzymatic hydrogenation by LADH, we have studied the pre-resonance Raman spectra of the aromatic aldehyde p-(dimethylamino) benzaldehyde (DABA) and its various isotopically labelled compounds in buffer solution, when bound to LADH/NADH and when complexed to Zn^{+2} in methylene chloride. The results suggest that the DABA-Zn complexes, that form in solvent like methylene chloride, are good models for DABA in situ. We find that DABA's bond character when bound to LADH/NADH retains a significant amount of essential double bond order.

ACKNOWLEDGEMENTS

I express my gratitude to Professor Robert H. Callender for his patient guidance and continued support during the course of this research.

I am greatly indebted to Dr.Donald L. Sloan for his guidance and many discussions of the chemistry in my thesis research.

I am grateful to the members of my thesis committee: Professor Myriam P. Sarachik, Professor Valeria Balogh-Nair, and Professor William V. Sweeney for their guidance and help.

I thank Professor Johan Lugtenberg for his generosity in providing isotopically labelled DABA samples.

I thank Dr. Kwok To Yue for his collaboration and assistance.

I thank Professor X. D. Xie, Professor Z. Y. Wang for their encouragement and help.

I also thank my husband Dr. S. L. Qiu for proofreading this thesis.

DEDICATION

I dedicate this thesis to my parents, my husband Shen Li Qiu, my daughters Dong Qiu and Shuang Qiu, my relatives and friends.

CONTENTS

LIST OF TABLES

LIST OF FIGURES

CHAPTER I

INTRODUCTION

The NAD-linked dehydrogenases form an important class of enzymes. They are involved in oxidation-reduction reactions and functions in all areas of metabolism. Many such dehydrogenases are known, and they catalyze the general reaction:

$$\text{reduced substrate} + NAD^+ \xleftrightarrow{\text{enzyme}} \text{oxidized substrate} + NADH + H^+$$

where a hydride ion is transferred from the reduced substrate to NAD^+ to form the oxidized substrate and NADH in the forward reaction. There are several intermediates in the overall reaction which involve binary and ternary complex of the enzyme, NAD^+ (or NADH), and substrate.

Horse liver alcohol dehydrogenase (EC 1.1.1.1), LADH, is a well known and well characterized dehydrogenase. It catalyzes the conversion of an alcohol (RCH_2OH) to an aldehyde (RCHO) along with the reduction of NAD^+ (Sund & Theorell, 1963). The kinetic mechanism of the ethanol-acetaldehyde transition is apparently compulsory ordered (eq. 1.1), with coenzyme dissociation rate limiting (Theorell and Chance, 1951; Wratten and Cleland, 1963).

$$E + NAD^+ \longleftrightarrow E(NAD^+) \longleftrightarrow E(NAD^+)(C_2H_5OH) \longleftrightarrow$$
$$E(NADH)(CH_3CHO) \longleftrightarrow E(NADH) \longleftrightarrow NADH + E \qquad (1.1)$$

Nicotinamide adenine dinucleotides (NAD^+ and NADH) are coenzymes for hundreds of oxidation-reduction reactions (Dalziel, 1975). Their roles in enzymatic reactions have been under investigation for the last few decades by various techniques (Kaplan, 1960; Colowick et al., 1966; Hollis, 1967; Fisher et al., 1969; Schlessinger et al., 1975; Subramanian & Ross, 1977, 1978; Rizzo

et al., 1986). A number of high resolution X-ray crystallographic studies on various NAD-linked dehydrogenases and their binary and ternary complexes have been reported (Bränden et al., 1975; Plapp et al., 1978; Eklund et al., 1981, 1984; Holbrook et al., 1975; Harris & Waters, 1976; Banaszak & Bradshaw, 1975; Rossman et al., 1975; Ohlsson et al., 1974;). However, detailed understanding of the coenzyme molecular properties in situ and interactions between the coenzyme in the active site and surrounding amino acid residues can only be surmized or examined indirectly.

Raman spectroscopy is known for its ability to provide detailed information concerning the molecular properties of biologically interesting molecules. Resonance Raman spectroscopy has been particularly useful in elucidating the properties of prosthetic group in the active site of proteins as in, for example, visual pigments, hemoproteins, and others (see e.g. Carey and Storer, 1984). A requirement of this technique, however, is that the prosthetic group must absorb visible or near ultra-violet light so as to be in resonance with the Raman exciting laser light. The resonance enhanced Raman cross-section of the prosthetic group is then much larger than the protein Raman spectrum and is, thus, easily obtained even though the prosthetic group is much smaller than the protein. Thus, resonance Raman studies are limited to proteins containing a chromophoric group. In principle, the Raman spectra of non-absorbing small molecules at the active sites of proteins can be obtained by classical Raman spectroscopy by employing sensitive difference techniques. The protein/small molecule binary complex can be measured, and the protein spectrum subtracted. The resulting difference spectrum yields the Raman spectrum of the in situ small molecule and, possibly, protein changes brought about by the binding of the small molecule. There are clearly a large number of interesting biological problems which could be very usefully studied by such measurements. Enzyme-substrate interactions are obvious examples. The idea of using classical Raman difference spectroscopy to obtain changes in a molecular spectrum resulting from small perturbation has been previously proposed (Bodenheimer et al., 1972; Kiefer, 1973). However, apart from our recent study (Yue et al., 1984b), the technique has not been applied to the studies

of proteins.

In our earlier study (Yue et al., 1984b), we employed sensitive difference techniques to obtain the Raman spectrum of bound NADH. We subtracted the Raman contribution of LADH from the binary LADH/NADH Raman spectrum. The difference between the binary complex and protein can be quite small, on the order of a few percent in that study. Apart from shot noise, the effects of systematic factors, such as spectrometer drift, on such small differences must be assessed. The previous reports where Raman difference spectroscopy has been applied to biological molecular systems, like those of Rousseau and his colleaques (Shelnutt et al., 1979; Rousseau, 1981), used split rotating cells and showed how to obtain very accurate frequency differences between normal modes of two nearly identical samples. Unfortunately, this instrumentation is not particularly suitable for studies of the type described here. Rotating cells with photomultiplier detectors and photon counting techniques can avoid a number of systematic errors by quickly switching from one sample to another. The signals are gated, fed to a computer, and subtracted appropriately. It is a powerful technique when the Raman signal is fairly strong. However, the classical Raman spectra of proteins in solution are typically weak. It is necessary to use optically faster optical multichannel analyzer (OMA) detectors rather than photomultipliers in order to obtain spectra within a reasonable period of time and with sufficiently small shot noise (i.e. less than one percent of signal). OMA's, however, do not lend themselves easily to measuring light signals arising from switching quickly from one sample to another. This is because there is significant noise superimposed on the signal each time OMA detectors are read. OMA's are most properly used when the Raman signal is integrated and read as infrequently as possible. We show below (in chapter II) how the effects of systematic errors can be estimated, under conditions where the two samples are infrequently changed. We show that problems associated with systematic errors can be sufficiently small, under one percent, to discern the spectrum of a protein bound nucleotide from the protein/nucleotide binary spectrum.

Using these difference techniques, we have extended our previous results on bound NADH by obtaining its Raman spectrum over a wider spectral range (350-1750 CM^{-1}), by examining

the changes on the spectrum of bound NADH over a broad pH range, and by studies of deuterated LADH/NADH complexes. We have also obtained the spectrum of ADPR bound to the active site of LADH. The purpose of this measurment is two-fold. A protein conformational change accompanies the binding of NADH to LADH (Eklund et al., 1984; Bränden et al., 1975). This conformational change does not occur when ADPR binds but the interactions between the adenosine moiety and the protein are similar to that of NADH (Eklund et al., 1984; Yonetani, 1963; Theorell and Yonetani, 1964). By comparing the spectrum of bound NADH with that of bound ADPR, we are able to conclude that none of the major bands of the bound NADH spectrum result from this conformational change. Moreover, ADPR lacks NADH's nicotinamide moiety, and this is very useful in assigning bands in the bound NADH Raman spectrum to particular NADH moieties. To confirm these assignments we have measured the Raman spectrum of H_2NADH in solution and in situ, since H_2NADH is a hydrogenated analogue of NADH where the double bond between C5 and C6 of the pyridine ring is saturated and it induces the same conformational change as NADH in liver alcohol dehydrogenase. We have also studied the Raman spectrum of bound NADH and NAD^+ in ternary complexes with LADH inhibitors, IBA and DMSO for NADH and pyrazole for NAD^+.

Our results reveal that the adenine moieties of both NADH and NAD^+ (in addition to ADPR and H_2NADH) are perturbed significantly upon binding. It is not clear, however, whether the adenine ring is protonated as suggested earlier by uv-vis difference spectroscopy (Fisher et al., 1967). The nicotinamide ring moiety of NADH is also modified upon binding. We discuss various molecular models which are consistent with the data and with the catalytic attributes of LADH. We also show, in agreement with previous reports (Theorell and Yonetani, 1963; Shore and Gilleland, 1970; Andersson et al., 1981; Eklund et al., 1982), that pyrazole interacts strongly with the nicotinamide moiety of NAD^+, forming a NAD-pyrazole adduct, when it binds to the binary complex of LADH/NAD^+.

The rather dramatic changes in molecular structure that occur when NADH binds to liver

alcohol dehydrogenase are not necessarily repeated in other NAD-linked dehydrogenases. We have investigated the Raman spectra of coenzymes binding to yeast alcohol dehydrogenase. Our preliminary results indicate much fewer difference between solution and bound coenzymes. This implies that much smaller molecular perturbations are imposed by this dehydrogenase on the bound coenzymes.

LADH contains Zn(II) at its active site. A very important question in enzymatic hydrogenation by LADH is whether the substrate is directly bound to the active Zn(II) metal cation. X-ray crystallography (Plapp et al., 1978), kinetic studies (Taniquchi et al., 1967) and absorption studies on colored substrates (Dunn, 1974) support direct bonding; whereas pH studies (Shore et al., 1974), NMR studies (Sloan et al., 1975; Drysdale & Hollis, 1980), and experiments concerning substituent effects in alcohol oxidation (Hardman et al., 1974; Blackwell and Hardman, 1975) suggest that the substrate binds in a second sphere coordination to the active metal. Generally speaking, we may expect to observe Raman bands arising from vibrational modes associated with the metal-liganded complex. Maret et al., (1983) have reported the resonance Raman spectrum of Cu(II) substituted LADH, showing that it is possible to detect Raman bands due to metal-ligand bonds. Dworschack & Plapp (1977) have studied p-dimethylamino benzaldehyde, DABA, as a substrate of LADH and showed that this aldehyde is readily converted to the corresponding alcohol in the presence of reduced coenzyme NADH and catalytic amount of enzyme. Peticolas and Coworkers (Jagodzinski et al., 1981, 1982) have shown that a stable ternary complex of LADH/NADH/DABA can be formed at higher pH and tentatively assigned the Zn-O band in the Raman spectrum of this ternary complex, thus suggesting direct binding of the substrate aldehyde oxygen to the active metal. However, confirmation is need since ^{18}O substitution on the aldehyde oxygen of DABA did not result in the expected change in this band. A careful study of the Raman spectra of DABA and ternary complexes of LADH with isotopically labelled substrates should be able to provide insight into this question.

For this purpose we have studied the pre-resonance Raman spectra of the aromatic

aldehyde DABA in pyrophosphate buffer (we called free DABA) and in complexation with zinc ion in methylene chloride (we called the DABA-Zn complex). We have also studied various isotopically labeled compounds of DABA complexed to Zn^{+2} in solution (we called bound DABA). From these experiments we have observed that the Raman spectra of bound DABA closely resemble that of the native DABA-Zn complex. Our results suggest that the aldehyde substrate DABA directly coordinates to active site metal ion of LADH. The major role of LADH to the binding of DABA is to provide a divalent zinc to form a first sphere Lewis acid complex. The data thus suggest that any other interaction between DABA at LADH's active site and its protein surroundings and the coenzyme, NADH, are quite minor. An estimate of the carbonyl bond character is made based on the respose of bands to isotopic labelling and trends observed in spectra taken of DABA in solvents of various polarities. We find that DABA's bond character when bound to LADH/NADH retains a significant amount of essential double bond order, but clearly less than that found in solutions of DABA.

CHAPTER II

DIFFERENCE RAMAN SPECTROSCOPY

A. Raman Scattering

A characteristic feature of Raman scattering is the frequency shift of the scattered light relative to the frequency of the incident light by amounts corresponding to the molecular normal mode frequencies. Raman spectra provide detailed information on the vibrational motions of atoms in molecules. Because these vibration are sensitive to chemical changes, the vibrational spectrum can be used as a monitor of molecular chemistry. For a complete description of the vibrational motion of a molecule, both Raman and infared spectra are needed. However, Raman spectra are richer and yield information not only concerning excited state structure (through the Raman intensities) but also ground state structrue (through the band frequencies). It is often impossible to obtain the infrared spectrum of a biological material in water, because water is a very strong absorber of IR. Under these conditions, the Raman data are the sole source of information.

Fig. 2.1 shows a quantum mechanical picture of Raman scattering. Raman scattering is depicted as a two-photon process. The first step in this process is the combination of a photon and a molecule to rise the molecule to a higher energy state of extremely short lifetime. This transition is depicted by the upward-pointing arrows in Fig. 2.1. The second step, indicated by the downward-pointing arrows in Fig. 2.1, involves the release of a photon after a very short time interval ($<10^{-13}$ sec). The lengths of the upward-pointing arrows are proportional to the frequencies of the incoming light while the lengths of downward-pointing arrows are proportional to the frequencies of the scattered light. In the Rayleigh scattering process, the upward and downward directed transitions have the same length, i.e. there is no change in frequency of the photon. If the downward-pointing arrow stops on a vibrational energy level that is higher than the starting level , then the frequency of scattered light is $\upsilon_s=\upsilon_0-\upsilon_{vib,}$ and a Stokes process is said to have occurred. Conversely, an anti-Stokes process results from the transition terminating at a vibrational energy

level lower than the starting level, i.e. $\upsilon_s=\upsilon_0+\upsilon_{vib}$. The range of $|\upsilon_s-\upsilon_0|$ is about 10 - 4000 cm^{-1}. In the normal Raman scattering process the upward-pointing arrow stops on a virtual energy state of the molecule; in the resonance Raman process the upper Raman state is a real quantized energy state of the molecule, i. e. the frequency of the incident light coincides with an electronic absorption center of the molecule. In the case of pre-resonance Raman scattering the frequency of the incident light is not at but close to the absorption center of the molecule. It will be shown later that band intensities in resonance (or pre-resonance) Raman spectra can be orders of magnitude greater than those in normal Raman spectra.

For randomly oriented molecules the total intensity of the scattered light resulting from a molecular transition between states m and n is:

$$I = K \upsilon_s^4 I_0 \sum_{\sigma\rho} |(\alpha_{\sigma\rho})_{mn}|^2 \qquad (2.1)$$

where

$$(\alpha_{\sigma\rho})_{mn} = \frac{1}{h} \sum_r \frac{\langle n|\mu_\rho|r\rangle\langle r|\mu_\sigma|m\rangle}{\upsilon_{rm}-\upsilon_0+i\Gamma_r} + \frac{\langle n|\mu_\sigma|r\rangle\langle r|\mu_\rho|m\rangle}{\upsilon_{rn}+\upsilon_0+i\Gamma_r} \qquad (2.2)$$

In these expression the molecule is considered to be in the molecular state m. It is perturbed by an electromagnetic wave of frequency υ_0 and intensity I_0, causing the transition to a state n and emission of scattering light of frequency $\upsilon_s=\upsilon_0\pm\upsilon_{mn}=\upsilon_0\pm\upsilon_{vib}$. The sum over index r covers all of the quantum mechanical eigenstates of the molecule, h is Planck's constant, and Γ_r is a damping constant which takes into account the finite lifetime of each eigenstate. The $\langle n|\mu_\rho|r\rangle$, etc., are the amplitudes of the electric dipole moment operator, μ, along direction ρ. Immediately, we see from (2.2) that as υ_0 approaches the energy of an allowed molecular transition υ_{rm}, $(\upsilon_{rm}-\upsilon_0+i\Gamma_r)$ becomes small, consequently, one term in the sum becomes very large. This is the resonance

condition. Apart from making spectra intrinsically easier to detect, the resonance (or pre-resonance) Raman effect introduces the possibility of selectively probing the vibrational spectrum of the a small but key part of an extremely complex biological system. This is achieved by choosing a system that contains a chromophore of interest which absorbs in or near the visible spectral region. By exciting the Raman spectrum with light that can be selectively absorbed by the chromophore the resonance Raman spectrum of that chromophore may thereby be obtained uncluttered by the normal Raman spectrum from the rest of the system, which, being orders of magnitude less intense, is lost in the spectral background.

It is important to emphasize that the positions of peaks in Raman and resonance Raman spectra are solely a property of the electronic ground state, while Raman peak intensities may be correlated with ground state properties, intensities under resonance conditions can only be understood by considering the excited electronic state of the molecule. By the same token, a study of resonance Raman intensities can provide unique information regarding excited states, and, in the biological context, this holds great promise for increasing the understanding of processes, such as photosynthesis and vision, which use excited states to perform chemical transformation.

As mentioned above, the resonance Raman process requires that the part of interest of the biological system must absorb in the visible or near ultra-violet region so as to be in resonance with the Raman exciting laser light (which are readily available in these region). Thus, resonance Raman studies are limited to those systems which contain chromophoric groups. The resonance Raman technique is used to study substrate DABA when binds to LADH in this thesis. A new technique is needed for studying the Raman spectra of non-absorbing small molecules, for example coenzymes and their analogs NADH, NAD^+, ADPR and H_2NADH, when bind to LADH. Before the discussion of the new technique---sensitive difference Raman spectroscopy, it is necessary to introduce the OMA system.

B. OMA System

OMA is an abbreviation of Optical Multichannel Analyzer. Our OMA system consists of a Triplemate spectrometer (Spex Industries, Metuchen, NJ) and a solid-state detector system of model 1420 water cooled photodiode array and model 1218 controller (EG&G, Princeton Applied Research, Princeton, NJ). All spectra lines measured with OMA system were calibrated against known Raman lines of toluene. The OMA system has an accuracy of $\pm$ 1.5 cm^{-1} in these measurements.

Triplemate Spectrormeter

Spex's 1877 Triplemate is a spectrograph specially tailored to provide the low-stray light and flat, undistrorted focal plane ideal for sensitive work with optical multichannel analyzer (OMA) detector.

The triplemate has two main sections as shown in Fig. 2.2. The first is an 0.22 m double monochromator with gratings locked in a subtractive-dispersion mode. Light passes into the entrance slit (S1) to be collimated by mirror M1 onto the first grating (G1) where it is dispersed onto mirror M2. After passing through the adjustable slit S2, which determines the bandpass of this section, the light strikes the spatial-filter mirror (M3) and passes through a fixed slit which eliminates much of the stray light. Again the light is collimated (M4), dispersed (G2) in an opposing direction to cancel the effects of the initial dispersion, then focused (M5) onto the exit slit of this section (S3) which controls the resolution of the next section. The calculated and measured results of the resolution will be given in a later section of this chapter. The entire first section acts as a variable-wavelength, selectable band-pass filter that feeds a non-dispersed segment of radiation from a sample into the entrance slit (S3) of the second section, or spectrograph stage. In the spectrograph stage, the light is again collimated (M6) and dispersed on a grating G3. To vary this dispersion and the spectral coverage at the focal plane, the spectrograph has provisions for mounting three gratings, of different groove densities, on a manually actuated turret. Whenever a new grating is selected, an internal microprocessor automatically drives the spectrograph stage to a

position that keeps the selected wavelength of the dispersed radiation centered on the detector. The camera mirror (M7), projects a flat image onto the focal plane where it is seen by OMA detector

Detector and Controller

The model 1420 is an intensified silicon photodiode array detector. This detector uses a large aperture photodiode array fiber optically coupled to a proximity focused microchannel plate intensifier to provide approximately 700 intensifier detector elements. The proximity focused intensifier allows fast gating with high on/off ratios. The model 1420 is specifically designed for use with the model 1218 Solid State Detector Controller. This controller was interfaced to a LSI---11 microcomputer (Digital Equipment Corp, Marlboro, MA), which was also used for data analysis.

All Raman spectra shown in the figures of this thesis were obtained using grating with grooves 1200/mm and either 488.0 or 514.5 nm lines of an argon ion laser (model 165, Spectra Physics, Mountain View, CA). Under this conditions, about 800 cm^{-1} segment of a spectrum can be detected simutaneously. Some spectra were also obtained with excitation at 413 and 468 nm with a krypton ion laser (model 2000 - CR, Coherent Radiation Inc., Palo Alco, CA). A typical measured 800 cm^{-1} segment of a spectrum of LADH/NADH required 1 to 2 hours to obtain using the OMA system and 150 mw of laser power incident on the sample. All the Raman data presented in this thesis are the result of many runs, each run obtained by integrating the incident Raman signal on the OMA detector for about 10 minutes. Details are discussed in a later section.

Resolution of OMA System

In order to compare the powers of different instruments to resolve spectral structrure, it is convenient to introduce a criterion of resolution:

$$R=\lambda/\Delta\lambda \qquad (2.3)$$

R is called the "resolving power" of the instrument (M. Born and E. Wolf, "Principles of Optics" p-333), where $\lambda \pm 0.5\ \Delta\lambda$ are the two neighboring wavelengths which are just resolved by

that instrument, $\Delta\lambda$ is the seperation of these two wavelengths.

By applying the Rayleigh Criterion to the case of grating, we can obtain the expression for the resolving power of a grating as:

$$R = \lambda/\Delta\lambda = KN \qquad (2.4)$$

Thus, the resolving power is equal to the product of the diffraction order number K and the total number of the grooves N.

It should be pointed out that the value of the resolving power calculated from expression (2.4) is the theoretical limit, because in the derivation of (2.4) an assumption of "indefinitely narrow slits" was taken. For practical purposes, considering a slit with finite width w, then we can derive the resolving power of a grating as (S. A. Chuster, "An introduction to the theory of optics"; G. Mu "Optics", in chinese):

$$R_g = K N \frac{\lambda}{W} \frac{f}{d} \frac{1}{\cos\theta} \qquad (2.5)$$

or

$$\frac{R_g}{R} = \frac{\lambda}{W} \frac{f}{d} \frac{1}{\cos\theta} \qquad (2.6)$$

where R is the theoretical limit of the resolving power of a grating given by (2.4), f and d are the focal length and diameter of the collimator lens respectivelly, θ is diffraction angle. The meanigs of K, N and λ are the same as above.

In the case of Spex's 1877 Triplemate, the size of G3 is 64 mm x 64mm with grooves 1200/mm.

$$\text{so } R = KN = 1\text{x}64\text{x}1200 = 76800 \qquad (2.7)$$

we take f/d = 10, λ = 5000Å, w (S3) = 100μ , for OMA system and cos $\theta \cong 1$, then

$$Rg = 3840, \text{ and } \Delta\lambda = 1.25Å, \text{ or } \Delta\upsilon = 5\ cm^{-1} \qquad (2.8)$$

This expression gives the calculated value of the resolution of OMA system ($\Delta\upsilon$= 5 cm^{-1}) which is in agreement of the experimental value of ~ 6cm^{-1}.

This experimental value was obtained by measuring the laser linewidth. The procedure of this measurement is as follows:

(1). A laser beam of wavelength λ = 514.5 nm is focused into toluene, and the Rayleigh scattering light from toluene was used as the light source. A 3 OD neutra lfilter was put in the front of slit S1 to reduce the intensity of the incident light.

(2). The slits were set as: S1 = 400 μ; S2 = 5000 μ; S3 = 100 μ. The grating with 1200/mm was selected.

(3). For measuring the laser line spectrum, the "center shifted" was set to zero, the "current setting" of triplemate was on 5145.

(4). The Raman spectrum of toluene was used to calibrate the 514.5 nm laser spectrum. In order to keep "current setting" unchanged, a laser beam of wavelength 488.0 nm was selected as the incident light for taking the Raman spectrum of toluene and the "center shift " was set to 1057 cm^{-1} (488.0 nm<------>20492 cm^{-1}; 514.5 nm<------>19435 cm^{-1}; 20492 cm^{-1}-19435 cm^{-1}=1057 cm^{-1}).

(5). The full width at half maximum of the 514.5 nm laser spectrum measured by using the procedure described above is of ~ 6 cm^{-1}.

C. Sensitive Difference Raman Spectroscopy

Over the past three years we have developed a methodology to obtain very sensitive Raman difference spectra. As mentioned above, resonance Raman studies are limited to proteins containing chromophoric groups. In principle, the Raman spectra of non-absorbing small molecules at the active sites of proteins can be obtained by classical Raman spectroscopy by employing sensitive difference techniques.

We discuss here the techniques and controls we use in obtaining the classical Raman difference spectrum between a protein and a protein/ligand binary complex. It might seem unlikely that the Raman signal from a molecular moiety like adenine, molecular weight 135, could be discerned from a 40000 molecular weight (per active site) protein like LADH. The respective classical Raman signals might be predicted to scale according to weight, suggesting that Raman signal of adenine would be about 0.3% that of LADH. However, the classical Raman bands observed from proteins are broad compared to nucleotide bands. For example, the amide I protein band near 1668 cm^{-1} is some 100 cm^{-1} wide compared to the 10 cm^{-1} (or less) width of a typical adenine band (see data below). This suggests that the peak intensity ratio of nucleotide to protein bands would be some ten times larger (3%) than predicted by simply scaling the relative molecular weights. As will be shown below, we find that adenine's classical Raman bands are on this order. Raman bands which we can assign to NADH's nicotinamide moiety are somewhat larger. The reduced nicotinamide moiety at the active site of LADH is characterized by a well-known absorption at 325 nm, which may result in some pre--resonance enhancement of nicotinamide's Raman bands. Modern detection equipment, such as that employed here, is capable of obtaining the Raman spectrum of a protein with a noise to signal ratio (due to shot noise) of greater than one percent within a couple of hours. Thus it is clearly feasible to obtain the classical Raman signal from a protein bound nucleotide (or other relatively small molecule) by employing sensitive difference techniques and by subtracting the protein spectrum from the binary complex spectrum.

The main experimental problem in measuring small differences in a spectrum is due to systematic factors. For example, varying ambient temperature or room vibration can lead to spectrometer drift. The power level of the laser light used to stimulate the Raman signal varies,

leading to signal variation. Optical multichannel detection equipment of the type used in the present investigation is more immune to those factors than detectors based on photomultipliers since an entire spectral segment is measured at once. There is a tendency, therefore, for the entire spectral segment to be affected equally by systematic factors so that the production of spurious bands in the difference spectrum is minimized. Moreover, the influence of these factors on the difference spectra from two samples may be decreased by obtaining spectra in an interleaved ABBAA.....BA fashion. Spectrometer drift will tend to affect the sum of the A measurements in the same way as the sum of the B measurements, and subtract out of the difference provided the drift time is larger than the time used in individual A and B measurements.

Our procedure for assessing the influence of systematic factors, which might adversely affect the A-B difference spectrum, involves adding every other A-spectrum in our ABBAA.....BA sequence and subtracting this from the remaining A spectra. This is repeated for the B spectra. In such a subtraction, the resulting A-A or B-B diference should result only in simple shot noise.

The results for this procedure for a typical data set are given in figure 2.3. This experiment made use of 8 runs of the enzyme alone and 8 runs of the binary LADH/NADH complex. Defining the i^{th} enzyme run as E_i and similarly the binary complex runs as B_i, the sequence can be defined as $B_1E_1E_2B_2B_3E_3E_4B_4B_5E_5E_6B_6B_7E_7E_8B_8$. Each run consisted of 10 minutes of integration time with 180 mW of the 488.0 nm line of an argon ion laser incident on the sample. Let $B^{odd} = B_1+B_3+B_5+B_7$ and $B^{even} = B_2+B_4+B_6+B_8$. Figure 2.3a shows the total binary spectrum, $B^{odd}+B^{even}$. The effective noise level and the effecs of any systematic problems are shown in fig. 2.3b, which contains the difference spectrum, $B^{odd}-B^{even}$. Note that the scale for figure 2.3b is 20 times that of figure 2.3a. On the same scale as in figure 2.3b, the binary spectrum minus the enzyme spectrum, $B^{odd}-E^{even}$, is plotted in figure 2.3c. These results show clearly that signal size is much larger than the spectral noise, whether due to shot noise or systematic errors. In this particular case, the noise level is represented in figure 2.3b and is at least five times smaller than the difference signal of figure 2.3c. Apart from shot noise, some small structure is evident near 1000

cm^{-1} in figure 2.3b. This is due to a (minor) incomplete subtraction of the sharp 1003 cm^{-1} phenylalanine band of LADH (figure 2.3a; Yue et al., 1984a). The difference spectra also contain Raman bands near 1000 cm^{-1} which arise from the phosphate buffers in our samples. Because of varying concentrations from sample to sample, these bands do not completely subtract out. Band that are due to buffer lines and/or incompletely subtraction of LADH's strong phenylalanine peak are marked with an "s" in the data shown below. Similar noise levels (data not shown) are obtained by examining various other possible control subtractions, i.e. E^{odd} -- E^{even}, B_1-B_7, etc. It is clear that no fewer than four measurements, ABBA, should be performed. Fewer than four would not permit any satisfactory assessment of adverse systematic factors which might affect the subtractions.

We are unable to control exactly the signal levels, sample concentrations, and sample alignments to better than a few percent. Thus, we must introduce a factor, x, in forming the difference spectrum, i.e. B - xE. The value of this factor is generally close to one (within 10%) but is otherwise not known a priori. In our case, this factor is determined when bands, clearly assignable to the protein, subtract out in calculating various B - xE spectra. Bands arising from the bound substrate are quite distinct and discernible from the protein bands in most cases. In general, protein bands are relatively broad, and their location and intensity patterns are known. It is, of course, quite possible that some protein conformation changes take place when a ligand binds. Sharp bands may be observed in the difference spectrum which result from this conformational change. The assignment of difference spectral bands arising from bound NADH, rather than from LADH conformational changes when NADH binds, must be made on an experimental basis. This is described in a later section.

In figure 2.4, we show a series of difference spectra, B - xE, where x is varied over a 10% range in order to assess the results of an over or under subtraction. It is evident from the figure which bands, in the difference spectra, can be assigned as arising from the presence of the bound NADH coenzyme and which bands are due to an over or under subtraction. These bands are

marked in panel d of figure 2.4. In our study, the δ-CH_2 protein band near 1450 cm^{-1} is particularly useful since the spectrum of NADH contains no bands near 1450 cm^{-1}. Moreover, it is known that δ–CH_2 protein bands are relatively insensitive to protein conformational changes. The bound coenzymes and their analogs Raman spectra are determined based on these two consideration.

CHAPTER III

CHARACTERIZATION AND PREPARATION OF SAMPLES

A. Enzyme LADH

Molecular Structure of LADH

Horse liver alcohol dehydrodenase, LADH, is a well known and well characterized dehydrodenase. It is an NAD-linked enzyme that catalyzes the oxidation of various primary and secondary alcohols to the corresponding aldehydes. The active enzyme has a molecular weight of 80000 and is a dimer of two identical subunits. The sequence of the 374 amino acids of the subunit has been determined by Jörnvall, (1970). X-ray crystallographic studies provide a great deal of information on the tertiary structure of LADH (Eklund, 1986). Each subunit is clearly divided into two domains, joined by a narrow neck region and separated by the deep active site cleft. One of these domains, called the coenzyme binding domain, binds the coenzyme. The second one is called the catalytic domain, binds the substrate. The two domains are unequal in size: the catalytic domain is larger and comprises 231 residues, whereas the coenzyme binding domain is built up from 143 residues. A schematic representation of the LADH dimer is shown in Fig. 3.1. The central part of the molecule illustrates two coenzyme binding domains bound together across a 2-fold axis perpendicular to the plane of the paper. The two catalytic domains are seperated from this central part by the coenzyme and substrate binding clefts. The binding sites for the coenzyme and substrate have been indicated for one of the subunits. The metal binding sites are located at the fringes of the catalytic domains. The rotation axis is marked, and the arrow specifies the direction of the rotation. The two subunits are joined together into the dimeric molecule through interactions within the coenzyme binding domains.

The coenzyme molecule binds in the cleft between the two domains and interacts with residues from both domains. The cleft is approximately 30 Å long and 7 Å in diameter. At the nicotinamide site the cleft continues into the substrate binding channel. The adenine moiety of coenzyme NADH (or NAD^+) molecules are located at the surface of the subunits, while the

nicotinamide ring pushed deep inside the protein. Almost theentire coenzyme is buried in the protein. The adenine ring is generally sandwiched by protein residues. The edge of the adenine ring is at the protein surface with N6A pointing towards the solution.

Native LADH contains four divalent Zn (II) ions per molecule (Akenson, 1964). Two of them are essential for catalytic activity and the other two have a structural role. X-ray studies suggest that the active Zn(II) cations are tetra- coordinated with two cysteine residues, one histidine residues and a water molecule, while the structural Zn (II) ions are coordinated with four cysteine sulfur atoms (Bränden et al., 1975; Bränden and Eklund, 1978). The structural Zn (II), located far from the active site, does not participate directly in the catalysis of the alcohol to aldehyde interconversion. Although it is bound near the surface of the molecule, this zinc cation is completely surrounded by the protein and is not accessible to chelating agents when the protein is in its native conformation. The catalytic Zn (II) cation is located centrally between the coenzyme and substrate binding sites. The distance between the two active-site zinc atoms of the dimer is 47 Å; the subunits are bound together through their coenzyme-binding substructures. The Lewis acid properties of the Zn (II) may be involved in the catalysis, and a variety of mechanisms have been proposed (Kvassman, 1980; Evans & Shore, 1980) with various roles assigned to the catalytic Zn (II).

The Zn (II) ions can be replaced with Co (II) and the enzyme retains most of its activity (Drum and Vallee, 1970); loss of activity accompanies Cu (II) replacement (Maret et al., 1980). In these replacements, chemical techniques have been developed to selectively replace either the catalytic or structural zinc ions (Sytkowski and Vallee, 1976; Maret et al., 1979). The absorption band of LADH with Zn(II) at the active site lines at 280 nm, while the Co(II) substituted enzyme has major absorption bands near 350 nm and 650 nm (Drum and Vallee, 1970; Maret et al., 1979) and Cu (II) substituted system contains an absorption band at 620 nm (Maret et al., 1980).

Preparation and Activity Measurement of LADH

LADH was purchased as a crystalline suspension in 10% ethanol from Boehringer Mannheim Co. and stored at 4 °C.

Before use, the LADH suspension was centrifuged at 4 C° at 6000 Xg for 20 minutes to collect the crystals. The pellet was redissolved in 0.05 M buffer (either phosphate or pyrophosphate) and then centrifuged again at 4 C° at 6000g for 10 minutes to remove denatured protein. The supernatant was then dialyzed overnight at least twice against 0.1 M buffer and then concentrated using either a collodion bag vacuum filtration apparatus (A. H. Thomas, Philadephia, PA) or a Centricon centrifuge concentrator (Amicon, Lexington, MA). The activity was measured by a method similar to that by Dalziel (1957) (details are given later). No enzyme preparation was used with an activity less than that reported by Dalziel. Deuterated samples were prepared by repeatedly concentrating enzyme solutions diluted by D_2O/deuterated buffer. Concentration of enzyme was determined spectroscopically, using $\varepsilon_{280} = 3.57 \times 10^4\ M^{-1}\ cm^{-1}$ for LADH. LADH contains two independent active sites; thus, the binary complexes were prepared by mixing a 1 :< 2 molar ratio of LADH to NADH, NAD^+, ADPR or H_2NADH. Depending on the pH and dissociation constant (see Table 3.1), the ratio was adjusted so that at least 90% of the coenzyme , ADPR, or H_2NADH molecules were bound (DeTraglia et al., 1977; Yonetani, 1963; Theorell and Yonetani, 1964; Li and Vallee, 1964; Taniguchi et al., 1967; Dunn, 1975). A typical concentration of LADH employed in the Raman studies was one millimolar. Ternary complexes with inhibitors were prepared by using excesses of the inhibitors as needed (Theorell & Mckinley-Mckee, 1961; Theorell & Yonetani, 1963; Shore and Gilleland, 1970). Samples were loaded into 3 mm X 3 mm fluorescence cuvettes. The cuvettes were transferred to a cuvette holder, maintained at 4 °C in a bath/circulator, for measurement. The LADH enzymatic activity was monitored before and after Raman measurement. No denaturation of the enzymes or their binary or ternary complexes was observed during the Raman measurement.

Enzyme activity of LADH was determined by measureing the rate of formation of NADH for a known amount of ethanol and NAD^+. A Perkin Elmer spectrophotometer was employed to record the absorption change in optical density at 340 nm. The procedure for measuring the activity of

LADH is as follows:

(1). stock solution of NAD^+ is prepared by adding 10 mg NAD^+ into 0.5 ml 0.1M pH 8.8 pyrophosphate buffer.

(2). 250 µl stock solution of NAD^+ was added into each of two labelled cuvettes with 10 mm pathlength.

(3). stock solution of ethanol, CH_3CH_2OH, was prepared by adding 0.1 ml of 100% CH_3CH_2OH into 0.9 ml distilled water. 30 µl stock solution of this 10% CH_3CH_2OH was added into reference and sample cuvettes respectively.

(4). 2.6 ml of 0.1M pH 8.8 pyrophosphate buffer was added into reference and sample cuvettes respectively.

(5). 0.1 ml 0.1M pH 8.8 pyrophosphate buffer was added into reference cuvette, while 0.1 ml LADH into sample cuvette. The stock concentration of LADH is about 1µM.

(6). The absorption spectrophotometer should be set at 340 nm and this assay should be performed at 20 °C.

(7). The change in optical density (OD) at 340 nm was recorded every 15 seconds for 5 minutes.

(8). Thus the slope of the initial linear part of the reaction can be obtained and expressed as activity units U: change in optical density at 340 nm per minute. These values are presented as specific activity units U per milligram of enzyme. The typical activity of our enzyme (LADH) is 7 - 9 U.

For comparison, we also used Dalziel's procedure to measure the activity of LADH. Both procedures and results are listed in table 3.2. Dalziel (1957) reported that their enzyme preparations

gave an increase in ε_{340} of .058 in 3 minutes per mg enzyme per ml. The activity of our sample is 0.061 in these units. It is clear that the activity of our sample is at the same level of Dalziel's sample.

B. Coenzymes and Analogues NADH, NAD^+, ADPR and H_2NADH

Fig. 3.2 shows the molecular schematics of NADH, NAD^+, ADPR and H_2NADH. The NAD molecule consists of six structural units: adenine, nicotinamide, two riboses and the two phosphates in the pyrophosphate group. These units can roughly be considered as rigid bodies except for the riboses, which can have different puckering. In addition the nicotinamide has a torsinal freedom between the ring and the carboxyamide group.

All observed NAD active conformations are anti with respect to the adenosine glycosidic bond. The adenine and nicotinamide rings are usually orinted at approximately right angles to each other and have their preferred energetic values for those conformations where their rings are roughly perpendicular to the plane of the ribose ring. The conformational paramaters for different NAD molecules free or bound to enzymes vary considerably. There are energetically preferred regions for torsion angles, but the local interactions determine the conformation of the coenzyme. These adapt to the geometry of the binding sites of the enzymes or to interactions between molecules in crystals of the free coenzyme (Eklund & Bränden, 1986).

ADPR lacks NADH's nicotinamide head. The ADPR moiety of the coenzymes is bound to the site of the enzyme-coenzyme binding common to NAD^+ and NADH (Theorell & Yonetani, 1964).

H_2NADH is a hydrogenated analogue of NADH where the double bond between C5 and C6 of the pyrdine ring is saturated. It is known that this analog does not provide a hydride ion in the dehydrogenase reaction scheme but will form stable binary and ternary complexes with the NAD-linked dehydrogenase (Dunn et al., 1975; Cedergren-Zeppezauer et al., 1982). The 1,4,5,6 tetrahydronicotinamide ring very likely assumes a nonplanar conformation with C5 out of the plane

defined by N1, C2, C3, C4 and C6 (Hope, 1969), while the nicotinamide ring of NADH is almost certainly planar (Koyama, 1963; Karle, 1961). Both NADH and H_2NADH bring about the same crystallographically identifiable conformational change in LADH (E. Zeppezauer et al., unpublished results).

Some usefull constants of NADH, NAD^+, ADPR and H_2NADH are listed in Table 3.1, where λ_{max} is the absorption maximum, ε is the extinction coefficient and K_d is the dissociation constant with LADH.

NADH, NAD^+, ADPR were purchased from either Sigma Chemical Co. (grade III; St. Louis, Mo) or Boehringer Mannheim Co. (Indianapolis, IN). and used without further purification. Concentrations of NADH, NAD^+, ADPR were determined spectroscopically, using ε_{340} = 0.622 X 10^4 $M^{-1}cm^{-1}$, ε_{259} = 1.44 X 104 $M^{-1}cm^{-1}$for NADH; ε_{259} = 1.53 X 10^4 $M^{-1}cm^{-1}$ for ADPR and ε_{259} = 1.8 X 10^4 $M^{-1}cm^{-1}$ for NAD^+.

The sample of H_2NADH used in these studies was prepared by a modification of the method of Biellmann and Jung (1971). In this modified method, 25 mg of 10% elemental palladium on charcoal is added to a solution of 100 mg of NADH dissolved in 5 ml of distilled water, and the resulting mixture is hydrogenated by bubbling hydrogen as previously described (Biellmann and Jung, 1971). The progress of the reaction is monitored by the UV spectral changes which accompany the formation of H_2NADH (see Fig. 3.4). Reduction is interrupted when a 288nm/ 265 nm OD ratio of 0.90 is attained. The purest H_2NADH had λ_{max} 265 nm, ε = 18500 M^{-1} cm^{-1} and λ_{max} 288 nm, ε = 15500 M^{-1} cm^{-1} (Biellmann and Jung, 1971) at 4 °C. The reaction mixture then is worked up by filtration using a collodion bag vacuum concentrator. (A. H. Thomas, Philadephia, PA). After removal of the catalyst by filtration, the solution was lyophilized and white a powder was obtained. This sample was stored in the refrigerator at 4 °C and was redissolved before use. It can

be stored for several months without change in the 288nm/ 265 nm OD ratio.

C. Substrate DABA

p-dimethylamino benzaldehyde (DABA) is an aldehyde substrate for LADH. The molecular structures of DABA (-CHO) and the isotopically labelled substrates are schematically shown in Fig. 3.3. DABA has a strong absorption band at 352 nm ($\varepsilon = 3.0 \times 10^4\ M^{-1}cm^{-1}$) in solution. Dworschack and Plapp (1977) have shown that DABA was converted to the corresponding alcohol in the presence of LADH and NADH around neutral pH. However, a stable ternary complex of LADH/NADH/DABA can be formed at pH 9.6 (Jagodzinski, et al., 1982) with the absorption shifted to 380 nm ($\varepsilon = 2.9 \times 10^4\ M^{-1}cm^{-1}$). It is expected that a pre-resonance Raman enhancement effect when using visible laser light will greatly enhance DABA's Raman cross section. Based on these two consideration, DABA was chosen as a substrate in studies of substrate binding behaviours.

DABA in methylene chloride has an absorption band at 337 nm, while Zn-DABA in CH_2Cl_2 at 372 nm. This feature is very similar to that of DABA in solution (λ= 350 nm) and in-situ (λ = 380 nm). Peticolas (1981) has suggested that Zn-DABA as a model of the bound substrate in the molecular environment of the enzyme active site.

DABA (-CHO) was purchased from Sigma Chemical Co. (St. Louis, MO). All isotopic labelled DABA used in this thesis were made by Prof. Lugtenburg and his colleagues. Zn-DABA model compounds were made as follows. $ZnCl_2$ was puchased from J.T. Baker Chemical Co. Phillipsburg, N. J.. CH_2Cl_2 was puchased from Fisher Scientific Company. A mixture of DABA and $ZnCl_2$ with a mole ratio 1 : <2 was placed in an oven at 80C° for two hours. $ZnCl_2$ is excess since it doesn't dissolve well in CH_2Cl_2. This was put then into CH_2Cl_2 solution with a desired concentration. All materials were used without further purification.

D. Inhibitors and Others

Iso-butyramide (IBA), dimethyl sulfoxide (DMSO) are inhibitors of NADH utilization, while pyrazole inhibits NAD^+ utilization (Theorell and McKinley-McKee, 1961; Theorell and Yonetani, 1963;Perlman 1968). IBA, DMSO, pyrazole were puchased from Sigma Chemical Co. Their concentration was determined by weighing procedures. All-trans retinol and retinal are good substrates of LADH. Retinal, an aldehyde, is efficiently catalyzed to the corresponding alcohol (retinol). The absorption maximum of all trans retinal is at 380 nm, while this maximum of all-trans retinol is at 330 nm. The conversion of retinal to retinol can thus be easily studied by absorption spectroscopy. All-trans retinol and retinal were puchased from Aldrich Chemical Co. Their concentration were determined spectroscopically (see appendix for details). All these material used without futher purification.

CHAPTER IV

STUDIES OF COENZYMES BOUND TO LADH

A. Bound NADH

Figure 4.1(a) shows the difference spectrum between the binary complex of LADH/NADH and LADH. The spectrum has been obtained using the procedure discussed above and represents the pooled results over many different runs. The measurements were performed at pH = 6.0, 7.0 and 9.6 and were repeated many times and at different excitation wavelengths (i.e. at 488 nm, 514.5 nm). The difference spectra were identical and all peaks, even the very small ones that are labelled in the figure, were consistently observed. No pH dependence was observed.

It is known that binding of NADH quenches the fluoresence of LADH (Luisi & Favilla, 1970; Theorell & Tatemoto, 1971). The Raman spectrum of LADH and that of the binary complex have slightly different fluorescence backgrounds. The backgrounds were removed, and any difference in concentration or collection optics between the two samples was corrected by comparing the peaks at 1450 cm^{-1} (see Fig 2.4 for detail). The 1450 cm^{-1} peak, which is due to the δ-CH_2 vibration(Lippert et al., 1976), is a covenient refrence because it is relatively insensitive to different secondary and tertiary structures of the protein. In addition, there is no peak in the Raman spectra of NADH in buffer solution around this region. There is a small residual broad peak around 1650 cm^{-1} due to different contribution of water in the original spectra.

The Raman spectrum of NADH in solution is shown in figure 4.1(b) for comparison (see e. g., Yue et al., 1986). The classical Raman bands in the solution spectra of NADH (0r NAD^+) have been found to arise from molecular motion from one or another of the adenine (A), nicotinamide (N), or, to a very limited extent, phosphate (P) moieties of the larger molecule (Yue et al., 1986). These have been so identified in figure 4.1(b). Similar assignments are made in the data of figure 4.1(a) based on the results below.

LADH undergoes a conformational change when NADH (or NAD^+) binds (Eklund et al.,

1984). Thus, the difference spectrum of figure 4.1(a) may arise from changes in the protein structure as well as from the presence of the bound substrate. It is known that Raman spectroscopy is sensitive to a few percent changes in protein structure (Yu et al., 1974; Kint & Tomimatsu, 1979). Changes in protein structure will appear as changes in the Raman spectrum in the amide I and/or amide III vibration at 1645-1680 and 1230-1300 cm^{-1} regions, respectively. That there are no negative peaks nor obvious "new" peaks in these regions suggests that the change in the structure of LADH upon NADH binding is small. We may, however, determine directly whether any of the peaks in the difference is due to protein conformational changes and, at the same time, help assign the difference spectrum peaks to either nicotinamide or adenine moieties by measurements on the binary LADH/ADPR complex.

ADPR lacks NADH's nicotinamide head and has been shown, in X-ray crystallographic studies (Eklund et al., 1984), to bind to LADH in the same way as NADH in that the adenosine moiety is in the same relative position to the amino acid residues of LADH. Moreover, the binding of ADPR does not induce a conformational change in LADH. (Eklund et al., 1984; Subramanian & Ross 1977,1978). Thus, the LADH/ADPR-LADH difference spectrum can show no difference bands due to a protein conformational change. By comparing the spectra of bound NADH with that of bound ADPR we are able to conclude that none of the major bands on the bound NADH spectrum results from the protein conformational change. (see the section of bound ADPR).

In obtaining the difference spectra for NADH (or ADPR and H_2NADH), we have observed consistently a negative peak at ca. 1003 cm^{-1}. There is a very strong peak in the spectrum of LADH at 1003 cm^{-1} due to phenylalanine. The negative peak may be an artifact of subtraction. However, it is also possible that the negative peak is real and shows that one or more of the 18 phenylalanine residues are involved in binding in such a way that the 1003 cm^{-1} mode is perturbed.

The difference spectra presented in this thesis contain contributions of the solvent to various degrees. The most significant contributions are a broad (110 cm^{-1} FWHM) peak at 1636 cm^{-1} due to water (1200 cm^{-1} for D_2O; 80 cm^{-1} FWHM) and two (pH dependent) buffer lines near

990 and 1076 cm^{-1}(for pH 7.0) and 990 and 1022 cm^{-1} (for pH 9.6).

Nicotinamide Binding

Upon binding, the nicotinamide moiety of NADH shows major molecular changes as deduced from the changes in Raman spectra. The most pronounced change in the NADH spectrum is the disappearance of the solution spectrum's nicotinamide 1546 cm^{-1} band (figure 4.1b) when NADH binds. Apart from these changes, the 1688 cm^{-1} and 526 cm^{-1} bands in the solution spectrum appear to shift downward slightly to 1681 cm^{-1} and 510 cm^{-1} respectively. There is a broad feature around 1084 cm^{-1} in the spectrum of NADH in solution and has been assigned to the NH_2 "rock" (Bowman & Spiro, 1980). As expected, the band shifts to around 900 cm^{-1} upon deuteration of NADH (Bowman & Spiro, 1980; Yue et al., 1986); the peak at 1109 cm^{-1}, which is not assigned to the NH_2 groups, remains unchanged. NADH contains two NH_2 groups, one associated with the nicotinamide ring and another with the adenine ring. The peak at 1084 cm^{-1} is absent in adenosine solution spectrum and present in NMNH solution spectrum. Based on these we have assigned the peak at 1084 cm^{-1} to nicotinamide carboxamide (Yue et al., 1986). The solution spectrum peak at 1084 cm^{-1} in figure 4.1(b) shifts to 1087 cm^{-1} with reduced intensity and appears to narrow upon forming the binary complex (figure 4.1(a)).

There are some suggested assignments of these bands but no studies, at this time, can unambiguously assign these bands to particular molecular motions. For example, it has been suggested (Bowman and Spiro, 1980) that the 1546 cm^{-1} band in the NADH solution spectrum arises from a ring C=C (out-of-phase) stretching motion. This assignment is based on an analogy with 1,4-cyclohexadiene spectral studies. Indeed C=C stretching motion lie in the ca. 1500-1600 cm^{-1} region. However, the 1546 cm^{-1} mode is upshifted to 1559 cm^{-1} upon deuteration of the amide's protons (Bowman and Spiro, 1980; Yue et al., 1984b), suggesting at least some influences of the carboxamide moiety. The intense solution NADH band at 1688 cm^{-1} has been assigned to carbonyl stretching of the carboxamide group by many different group (Patrick et al., 1974; Forrest

et al., 1976; Barrett, 1980; Nishimura and Tsuboi, 1980; Bowman and Spiro, 1980). Its unusually high intensity could result from a strong coupling between the C=O group and conjugated ring C=C bonds, both of which would undergo large bond length changes in the ground to excited electronic state transitions (Bowman and Spiro, 1980). Rodgers and Peticolas (1980) have questioned a strictly carbonyl assignment of the 1688 cm^{-1} band based on a number of observations, the most cogent being the insensitivity of this band to solvent and -NH_2 deuteration. They suggested that this band could result from a ring mode possibly with a contribution from -C=O stretching.

We can contribute to the assignment of the ca. 1688 cm^{-1} band by noting that a Raman study of a compound, H_2NADH (see the section of bound H_2NADH), where the nicotinamide C5-C6 double bond of NADH has been reduced, shows no 1688 cm^{-1} Raman band at all (it is also missing in NAD^+). The highest band in H_2NADH lies at 1632 cm^{-1} and is significantly broader and with diminished relative intensity than the 1688 cm^{-1} band of NADH. Moreover, the strong 1681 cm^{-1} band found in the binary complex, LADH/NADH (figure 4.1(a)), appears to be shifted to 1666 cm^{-1} in the ternary complex LADH/NAD^+/pyrazole data (figure 4. 7 (a)). As discussed below, it seems reasonable to ascribe this to the formation of a NAD^+-pyrazole adduct with covalent bond formation occurring between C4 of NAD^+ and N2 of pyrazole. All these results certainly suggest that ring C=C stretching is involved with the 1688 cm^{-1} mode. We find it plausible that this mode is a highly coupled vibration extending over the whole conjugated π-electron structure of NADH, i.e. extends over the nicotinamide ring -C=C- and, perhaps, also the carbonyl -C=O moiety. For a proper interpretation of our data, it is necessary to do experiments involving isotopically labelled NADH compounds and associated normal mode calculations.

While the exact nature of the molecular binding properties of the nicotinamide structure must await further study, it is clear that the nicotinamide moiety undergoes a substantial change. One or both of two general mechanisms may be operating to cause such changes. It has been suggested that strain is an important factor in the high efficiency of enzymes (Jencks, 1969). In this regard, Cook et al. (1981) have proposed possible bent chair conformations for the reduced

nicotinamide rings of NADH to explain secondary isotope effcts found in kinetic experiments of LADH. Certainly such conformations would have a marked effect on the normal modes of nicotinamide of the type observed here. A second general mechanism is the possible effects of electrostatic interactions between coenzyme and nearby enzyme amino acid residues. X-ray studies (Eklund et al., 1984) suggest hydrogen bonding between nicotinamide's carboxamide group with the peptide backbone of Val-292, Ala-317, and Phe-319. This hydrogen bonding is consistent with the change in the nicotinamide $-NH_2$ rocking mode at 1084 cm^{-1} (Yue et al., 1986) in the solution spectrum when NADH binds (figure 4.1(a)).

Adenine Binding

The adenine moiety is known to be important for the binding of NADH to LADH. NADH fragments without the nicotinamide ring can bind to LADH (Theorell & Yonetani, 1964), and X-ray crystallographic studies (Abdallah et al., 1975; Plapp et al., 1978; Eklund et al., 1981) showed that adenine binds in a cleft in the coenzyme binding domain of LADH. Difference ultravioled (Subramanian et al., 1981) and NMR (Hollis, 1967) studies have also indicated that the adenine moiety is perturbed by binding.

One obvious change when NADH binds to LADH is that the 1338 cm^{-1} band has appearently disappeared (figure 4.1(a)). It is well known that the 1338 cm^{-1} band is due to ring mode of the adenine moiety (Lord & Thomas, 1967; LaFleur et al., 1972; Rodgers & Peticolas, 1980). The disappearence of this band supports the fact that the adenine part of NADH is directly involved in binding.

The binding of NADH to LADH appears to be, at least, a two-step process. The binding of the AMP moiety of the coenzyme is apparently followed by a rather significant protein conformational change (see e.g. Eklund and Branden, 1986, for a review). This has been deduced by a variety of structural and binding studies which suggest that the adenosine binding site must be the recognition side for coenzyme binding. For example, coenzyme analogs, including ADPR, have

similar coenzymz-enzyme interactions (Kvassman et al., 1981; Samama et al., 1977, 1978; Cedergren-Zeppezauer et al., 1982; Eklund et al., 1984). The cleft between the AMP and NMN domains is open in the apoenzyme, permitting easy entrance of the nicotinamide ring. After coenzyme binding, the protein conformational change that occurs upon formation of the holoenzyme results in a closed form so that the coenzyme's nicotinamide ring is positioned deeper into the enzyme. UV-vis absorption studies (Fisher et al., 1967; Subramanian et al., 1981) showed significant changes in adenine's 260 nm absorption band upon coenzyme or ADPR binding. All these results suggested that the protein tightly binds the adenine moiety. It has been suggested that the adenine moiety is protonated upon binding (Fisher et al., 1967) as the changes in adenine's 260 nm absorption band upon binding are similar to those found when adenine in solution is titrated to low pH.

The environment of the adenine part of NADH bound to LADH has been determined by X-ray diffraction at 2.9 Å resolution. The site is largely hydrophobic, not particularly specific for adenine, and can accommodate many other hydrophobic groups (Einarsson et al., 1974; Biellman et al., 1979; Eklund et al., 1984). However, the polar group of Asp-223 and Arg-271 (which forms an ion pair with Asp-273) are very close to the adenine moiety. It is possible that a stable rearrangment of ion pairs or hydrogen bonding is formed at the adenine binding site consisting of these residues and/or hydrogen bonded water molecules with bound adenine.

Our Raman results show that a significant molecular effect takes place when the adenine moiety binds to LADH, as adenine's strong solution 1340 cm-1 band disappears. This mode has been assigned by Tsuboi and his colleagues (Tsuboi et al., 1973) to be mainly due to stretching motions of the adenine's C5-N7 and C8-N7 bonds. The other observed bands in adenine's solution spectrum, particularly the 1308 cm^{-1} and 1378 cm^{-1} bands, are assigned to be due to mainly C-H bending motions mixed with carbon-carbon and carbon-nitrogen stretching motions other than C5-N7 and C8-N7. Thus, it is feasible that the Raman data can be interpreted as resulting from a specific interaction on N7 of the adenine ring. Moreover, X-ray studies suggest that N7 is hydrogen

bonded to a water molecule when bound to LADH (Eklund et al., 1984). Such hydrogen bonding may be enough to disrupt this mode completely. However, it is not clear that these normal mode calculations have enough reliablity to warrant conclusions of such molecular detail. Studies employing isotopically labelled adenine are needed for more certain understanding of adenine's normal mode structure and its behavior when bound to LADH.

Deuteration Studies.

The triplet marker bands at 1308, 1338 and 1378 cm^{-1} in the solution spectrum of Figure 4.1b are readily assigned to the adenine component of NADH (see e. g. Yue et al., 1986). This triplet is quite modified when NADH binds. The central 1338 cm^{-1} band (figure 4.1(b)) either disappears, or its intensity is greatly reduced in the bound spectrum (figure 4.1(a)). In addition, new smaller bands appear in the bound NADH spectrum which are assigned to the adenine moiety, e. g. the 1324 cm^{-1} and 1172 cm^{-1} bands. We have observed earlier (Yue et al., 1986), in titration studies of NAD^+ or ADPR, that the adenine triplet marker bands are dramatically changed when the sample pH is below about 4. These results are consistent with a protonation of the adenine ring with a pK of 3.9 (Moore and Underwood, 1969). It has also been suggested that the adenine moiety is protonated when NADH or NAD^+ binds to LADH (Fisher et al., 1967).

In order to explore the possibility that the adenine's ring is protonated upon binding to LADH, we have measured the bound NADH and bound ADPR spectra in D_2O/deuterated buffer (the bound ADPR in D_2O buffer is not shown). The bound NADH in D_2O buffer is shown in Figure 4.2, which compares the protonated and deuterated spectra of bound NADH. A peak at 1340 cm^{-1} appears in both the bound deuterated NADH and bound deuterated ADPR spectra compared to the protonated spectra. In addition, the protonated NADH (figure 4.2(a)) band at 1415 cm^{-1} moves to 1425 cm^{-1} in the deuterated NADH spectrum (Fig. 2(b)), with an apparent increase in intensity. This peak is known to be associated with the nicotinamide moiety and was similarly upward shifted for NADH in solution upon deuteration (Yue et al., 1986).

Unfortunately, our studies on deuterated bound NADH are unable to confirm or exclude adenine protonation upon binding. The spectrum of deuterated bound NADH contains the strong adenine 1340 cm^{-1} band found in solution spectrum (compare figure 4.2(b) and 4.1(b)). This suggests to us that the adenine moiety is loosely bound to deuterated LADH compared to tightly bound in protonated samples. One would expect more dramatic changes in adenine's spectral features from exchange of a hydrogen by a deuteration in a protonated adenine ring. For example, the 1329 cm^{-1} band found in protonated adenine in solution at low pH (Yue et al., 1986) moves to 1342 cm^{-1} and the relative intensity of the 1411 cm^{-1} is halved in D_2O solutions at low pD (data not shown). It should be noted that NADH is clearly bound to LADH in D_2O since the strong NADH 1546 cm^{-1} nicotinamide band which is absent in the bound (protonated) NADH spectrum (figure 4.2(a)) is still absent (figure 4.2(b)). A looser binding affinity in D_2O is plausible. It is also possible that dissolving LADH/NADH in D_2O/deuterated buffer results in some protein conformational changes.

Effects of Inhibitors.

We examined the extent to which certain inhibitors affect the Raman spectrum of the bound coenzymes. IBA (isobutyamide) and DMSO (dimethyl sulfoxide) form tight ternary complexes with LADH/NADH (see table 3.1). Figure 4.5(a) and 4.5(b) show the spectrum of NADH in the ternary LADH/NADH/IBA and LADH/NADH/DMSO complexes respectively.

These spectra were generated in the same way as described above. The spectrum of LADH was subtracted from each ternary complex spectrum. The inhibitor concentration is in excess over the coenzyme in each case (LADH/NADH/IBA = 1:2:10; LADH/NADH/DMSO = 1:2:100). The Raman spectra of free IBA is relatively weak, and its solution spectrum did not contribute to the spectrum of Figure 4.5a (except at 1000 cm-1, where there is a IBA peak). The spectrum of DMSO in solution were present to an extent, and its solution spectrum has been subtracted out of Figure 4.5(b).

The addition of IBA and DMSO has similar effect on the bound NADH spectrum, i.e. the disappearence of the band at 1578 cm^{-1} and a shift of the band at 1087 cm^{-1} to 1080 cm^{-1}. The Peak at 1681 cm^{-1} is upshifted to 1685 cm^{-1} with addition of DMSO but not with IBA.

In the spectrum of NADH in solution (Figure 4.1(b)) there is a broad feature around 1084 cm^{-1}, which has been assigned to the rocking motion of $-NH_2$ of nicotinamide. This peak shifts to 1087 cm^{-1} with reduced intensity and appears narrower upon forming the binary complex of LADH/NADH (figure 4. 1(a)), while it shifts back to 1080 cm^{-1} with the addition of inhibitors to the LADH/NADH complex (Fig. 4.5 (a) and (b)). These results show clearly that the binding of nicotinamide moiety is influenced by inhibitors. This is in agreement of the results of the X-ray crystallography studies, which show that the inhibitors bind near the nicotinamide region and is very close to the active zinc atom of the enzyme (Eklund et al., 1981, 1982; Perlman 1968). In Fig. (4.1(b)) there is a shoulder at 1578 cm^{-1} in the spectrum of NADH in solution and is assigned to the adenine moiety (Yue et al., 1986). It is tempting to say that this mode remains upon binding. However, careful examination suggests otherwise. This mode disappears with the addition of inhibitors. DMSO has another effect. The mode at 1681 cm^{-1} in the bound spectrum is upshifed to 1685 cm^{-1}, showing that there can be subtle differences between the two inhibitors.

Theorell and Yonetani showed that IBA is an uncompetitive inhibitor of aldehyde function in the ternary LADH/NADH/IBA complex (Theorell and Yonetani, 1969). Uncompetitive inhibitors mainly alter the maximal velocity, but do not perterb the coenzyme binding Raman measurement requies a long accumulation time, i.e. equilibrium study. It is expected that IBA does not influence much on the Raman spectrum of bound NADH.

DMSO inhibition is competitive with the aldehyde substrate concentrations, and the K_i (inhibition constant) for DMSO determined kinetically is very close to the dissociation constant of the ternary complex determined fluorimetrically (Perlman, 1968). It is likely that DMSO binds at the carbonyl binding site of the LADH/NADH complex. This carbonyl binding site is thought to include the enzyme-bound zinc (perlman,1968); DMSO is known to form complexes with zinc salts (Cotton

& Fracis, 1960). In these complexes, zinc is thought to bind to the oxygen atom of DMSO (Cotton, 1960). In this regard, DMSO can be considered to be an analogue of acetone (Perlman, 1968), a very poor substrate for LADH (Eklund, 1982). The substrate may enter the active site causing alteration of the enzyme tertiary structure. This deformation of the enzyme may affect the nicotinamide binding. Thebinding interaction between the enzyme and substrate in such a case may be so spread over the substrate that the overall induced Raman changes upon binding would be small.

B. Bound ADPR

Our goal here is to assign the Raman bands of bound NADH to simpler molecular moiety by obtaining the bound Raman spectra of portions of these rather complicated molecules and comparing these properties to those of bound NADH. To do so, we have attempted to measure the difference spectra of various fragments of NADH when bound to LADH, e.g. LADH/NMN, LADH/AMP, LADH/ADP, LADH/ADPR. Since NMN, AMP and ADP binds only weakly with LADH (Li et al., 1964), the ratio of signal to noise in the difference spectra was very poor. Only the difference spectra of bound ADPR were successfully obtained. The ADPR interaction with protein is independent of substrates, and the ADPR moiety of the coenzyme is the site of the enzyme-coenzyme binding common to NAD^+ and NADH (Theorell & Yonetani, 1964). This conclusion was further supported by the following experiments. The 325 nm absorption maximum of LADH/NADH was shifted toward 340 nm upon an addition of excess ADPR. This shows bound NADH being displaced by ADPR. Similarly, the intensity of the 290 nm absorption maximum of LADH/NAD^+/pyrazole decreased appreciably upon the addition of excess ADPR. Nicotinamide, 1-methyl nicotinamide iodide, nicotinamide mononucleotide, adenine, adenosine, AMP, ADP and ATP were inactive as a potent inhibitor of LADH at pH 7.0. A combination of ADPR and each one of these substances did not affect the inhibitory effect of ADPR. Thus the ADPR moiety seems to be a minimal structure required for the unique firm binding of the coenzyme with LADH.

ADPR lacks NADH's nicotinamide head and has been shown to bind to LADH in the same way as NADH in that the adenosine moiety is in the same relative position to the amino acid residues of LADH (Eklund,1986). Moreover, the binding of ADPR does not induce a conformational change in LADH (Yonetani, 1963; Eklund et al., 1984). The same conclusion has been achieved for ADPR in solution by Subramanian & Ross (1977, 1978) who studied the calorimetry of NADH and NAD^+ binding for various dehydrogenases and found that there are large entropy changes only when NADH or NAD^+ binds to LADH, while binding of ADPR to LADH does not result in a large entropy change. Furthermore, LADH forms orthorhombic crystal normally, but the binary LADH/NADH compex (and almost all ternary complexes of LADH/NADH with various substrates or inhibitors) cannot form orthorhombic crystals. In contrast, many NADH fragments, without the nicotinamide part, including ADPR, form orthorhombic crystals with LADH (Bränden, 1965; Zeppezauer et al., 1967). It is possible that the nicotinamide moiety promots the activity of LADH by forcing a conformatinal change of the enzyme (Biellman & Jung, 1971). Thus, the LADH/ADPR-LADH difference spectrum can show no difference bands due to a protein conformational change.The difference spectrum between the binary complex of LADH/ADPR and LADH is shown in the Fig. 4.3 (a), which has been obtained using the same procedure as that for LADH/NADH. The measurements were performed at pH 7.0 and 9.6 and were repeated many times and at different excitation wavelengths (i.e. at 413, 468, 488 nm). The difference spectra were identical and all peaks, even the very small ones that are labelled in the figure, were consistently observed. No pH nor excitation wavelength dependence was observed. The Raman spectrum of ADPR in solution is shown in figure 4.3 (b) for comparison.

The most pronounced change in the bound ADPR Raman spectrum upon binding is the disappearence of the band at 1338 cm^{-1} and the appearence of two small peaks at 1324 and 1340 cm^{-1} respectively. The peaks at 1484 cm^{-1} and 1582 cm^{-1} in ADPR solution spectrum shift to 1471 and 1576 cm^{-1} respectively in bound ADPR spectrum. This is an evidence that the adenine moiety is involved in the binding.

We have also measured the bound ADPR spectrum in D_2O/deuterated buffer (data not shown). The major changed in the bound ADPR spectrum is the enhancement of the peak at 1340 cm^{-1}. This is also true for the bound NADH in D_2O/deuterated buffer.

Figure 4.4 shows the spectra of bound NADH and bound ADPR. The bands at 1575, 1510, 1375, 1340, 1324, 1303, 1245 and 1172 cm^{-1} in figure 4.4 (a) can be clearly assigned to the adenine moiety since they appear essentially at the same positions and relative intensities (except for the 1375 and possibly 1575 cm^{-1} bands) in the bound ADPR spectrum of figure 4.4 (b). The 1375 cm^{-1} band in the bound NADH spectrum is relatively more intense than the corresponding bands in the bound ADPR. These bands very likely contain also a contribution from a mode located on the nicotinamide moiety. This is true of the solution data, figure 4.1 (b). We have labelled bands in figure 4.1(a) as adenine bands as a result of these correspondences. The 1114 cm^{-1} band in figure 4.1(a) is found in the bound and solution spectra of ADPR (figure 4.3 (b)). This peak has been assigned to a pyrophosphate mode with ribose contribution (Yue et al., 1986). We have labelled this peak in figure 4.1(a) as a phosphate mode based on this close correspondence. We note that the relatively intense bands at 1681, 1616, 1600 and 1415 cm^{-1} found in NADH's difference spectrum (Figure 4.4 (a) and 4.1(a)) are absent in figure 4.4 (b). These correspond quite closely to bands found in solution spectrum of NADH which have been previously assigned to reduced nicotinamide (figure 4.1 (b)). It seems quite reasonable to assign those lines in figure 4.1(a) to NADH's nicotinamide head rather than to protein conformational changes on this basis.

There is a peak at 1471 cm^{-1} in the bound ADPR spectrum (figure 4.4(b)) which is absent in the bound NADH spectrum (figure 4.4 (a)). This may be due to different interaction of the ribose and phosphate, as concluded from the X-ray results by Eklund (1984). There is another example, that the conformation of ADPR when bound to LADH is very similar to the AMP part of the full coenzyme while the rest (i. e. ribose or phosphate) differs considerably and has a conformation different from that of coenzymes. (Eklund et al., 1984).

C. Bound NAD^+ with Pyrazole

Pyrazole and its derivatives have been extensively studied as inhibitors for LADH. Theorell et al. demonstrated that pyrazole inhibition is attributable to the formation of an abortive enzyme-NAD^+-pyrazole complex showing a characteristic difference absorption band at about 295 nm. In the ternary complex LADH/NAD^+/pyrazole, NAD^+ was found to bind more tightly than if no pyrazole was present. The dissociation constants of NAD^+ and pyrazole in the ternary complex are very small ($K_{EP,O}$= 0.1 μM and $K_{EO,P}$= 0.1 μM at pH 7.0). The stoichiometry between LADH, pyrazole and NAD^+ was founed to be 1:2:2 by spectrophotometric titrations with pyrazole and with NAD^+ (Theorell & Yonetani, 1963). They proposed, based on model systems, that pyrazole is bound to the zinc atom of the liver dehydrogenase and carbon 4 of the nicotinamide ring of NAD^+ with concomitant release of a hydrogen ion. Due to the stability and chromophoric properties of this ternary complex, pyrazole has turned out to be a most useful ligand from a methodological point of view. Transient-state kinetic methods based on the absorbance changes associated with pyrazole binding have been applied to monitor formation of the enzyme-NAD^+ complex during catalysis and to study the process of ternary complex formation with non-chromophoric substrate and coenzyme analogues.

Kinetic studies of the complex LADH/NAD^+ with pyrazole (Shore et al., 1970) showed that dissociation constants of pyrazole from the ternary complexes were the same for complexes with NAD^+ and NHD^+ (nicotinamide hypoxanthine dinucleotide). The results of this studies indicate that pyrazole interacts with the nicotinamide ring of NAD^+ in the ternary complex. McFarland et al. (1972) has reported that pyrazole does not inhibit any reaction or interaction involving NADH or aldehyde based on stopped-flow experiments. X-ray diffraction measurements for the complex of LADH/NAD^+/pyrazole (Eklund et al., 1982) showed that one of the nitrogen atoms of the pyrazole ring is very close to the active-site zinc atom with a Zn-N bond distance of 2.1 Å. The other nitrogen atom of pyrazole is 2 Å from the C4 atom of the nicotinamide ring of the coenzyme. The structure of LADH/NAD^+/pyrazole complex was investigated by ^{15}N nuclear magnetic resonance (NMR)

spectroscopy (Becker & Roberts, 1984). The N1 nicotinamide chemical shift of the coenzyme of the LADH/NAD^+/pyrazole complex demonstrates that the pyrazole in the ternary complex is consistent with covalent bond formation between pyrazole N1 and the nicotinamide ring of the coenzyme. The N2 chemical shift of the pyrazole in the ternary complex indicates that the nucleus of this nitrogen is about 40 ppm more shielded than those of the N2 nitrogens of typical pyrazole. Such shielding is expected as the result of direct complexation of N2 to the active-site zinc.

No Raman studies of the complex LADH/NAD^+/pyrazole were reported. We have measured both the UV-absorption spectra and Raman spectra of this complex. Our results suggest, in agreement with previous reports (McFarland, 1972; Eklund, 1982; Becker & Roberts, 1984), that pyrazole interacts strongly with the nicotinamide moiety of NAD^+, forming a NAD-pyrazole adduct, when it binds to the binary complex of LADH/NAD^+.

The absorption measurements of LADH/NAD^+/pyrazole were carried out with a Perkin-Elmer digital double wavelength spectrophotometer. The stoichiometry between LADH, NAD^+, pyrazole was chosen as 1:2:5. Fig. 8.6 shows the obsorption spectra of (a) LADH, (b) LADH/NAD^+, (c) the subtraction of (a) and (b). This subtraction gives the absorption spectrum of bound NAD^+. The peak at 325 nm indicates that some NAD^+ reduction occurred. A detail discussion will be given in next section.

The absorption spectra of bound NAD^+ with pyrazole are shown in Fig. 4.6. In contrast with the spectrum (c) in Fig. 8.6 there is no peak at 325 nm but a peak at 290 nm appears which is considered to be due to the fomation of a new ternary complex LADH/NAD^+/pyrazole.

We have also measured the absorption spectra of bound NADH with pyrazole (data not shown). There is no peak at 290 nm but a peak at 325 nm is present. A similar absence of a peak at 290 nm was obtained for the complex of LADH/ADPR/pyrazole which indicates that the adenine moiety does not affect the formation of this ternary complex.

Fig. 4.7 (b) shows the Raman spectrum of bound NAD^+ in the LADH/NAD^+/pyrazole complex. The molar ratio of this ternary complex was LADH/NAD^+/pyrazole = 1:2:5 which was the

same as that used in the absorption measurement.

The major change in the Raman spectrum of bound NAD^+ upon formation of the NAD^+-pyrazole ternary complex is that the peak at 1681 cm^{-1} in the binary LADH/NADH complex (Fig. 4.1 (a)) appears to be shifted to 1666 cm^{-1} in the ternary complex LADH/NAD^+/pyrazole (Fig. 4. 7 (b)). For comparison, the Raman spectrum of bound NADH in the LADH/NADH/pyrazole complex is shown in Fig. 4. 7 (a). The positions of the all main peaks in this spectrum remain unchanged compared to that in the spectrum of the binary LADH/NADH (see Fig. 4.1 (a)).

We have also measured the Raman spectrum of bound ADPR in the LADH/ADPR/pyrazole complex (data not shown). No change was observed compared to that in the binary complex LADH/ADPR.

Our results (both Raman data and absorption data) indicate that NAD^+ and pyrazole form a covalently bound adduct in the LADH/NAD^+/pyrazole ternary complex and suggest that pyrazole covalently binds to the nicotinamide ring of NAD^+ but not to the carboxamide and adenine moiety.

The Raman spectrum of NAD^+ in solution is charecterized by an intense narrow 1032 cm^{-1} band which arises from oxidized nicotinamide (see, e.g., Yue et al., 1986). Such a sharp intense band near 1000 cm^{-1} is characteristic of aromatic rings. For example, benzene's spectrum contains an intense band near 991 cm^{-1}, which has been assigned to a ring breathing mode. A similarly intense mode at 1029 cm^{-1} is observed (unpublised result) with n-methylated pyridine, the simplest analogue for oxidized nicotinamide. The absence of this mode in the data (Fig 4. 7 (b)) shows that the aromatic nature of NAD^+ nicotinamide ring is completely disrupted in the LADH/NAD^+/pyrazole complex. Moreover, the spectrum of this complex strongly resembles that of bound NADH, for example the 1666 cm^{-1} and 1415 cm^{-1} bands (Fig. 4. 7 (b)) are reminiscence of the 1681 and 1415 cm^{-1} bands of bound NADH (Fig. 4.1 (a)) which we have assigned to the nicotinamide moiety. It would seem reasonable to suggest that the bonding in the NAD^+-pyrazole ternary complex takes place at C4 position of the nicotinamide ring. Indeed, X-ray crystallographic studies at 2.9 Å resolution show that the distance between pyrazole N1 and nicotinamide C4 to be very close, 2 Å

(Eklund et al., 1982).

NAD^+ is more tightly bound to the LADH/pyrazole complex than to LADH, this suggests that the LADH/NAD^+/pyrazole complex is a model for the transition state of the enzyme catalyzed reaction (Theorell and Yonetani, 1963). Such a concept coupled with the above results are in agreement with the generally accepted pathway for catalysis by dehydrogenases. Hydride transfers occur from substrate to the C4 position of NAD^+ nicotinamide ring. During this transfer, the aromatic nature of oxidized nicotinamide would be disrupted, presumably, with substantial positive charge developing at C4. This could result in a structure for NAD^+ which would resemble NADH.

D. Bound H_2NADH

The role of the coenzyme is a double one: that of giving up or accepting a hydride ion during the oxido-reduction and that of modifying the conformation of the enzyme on binding. H_2NADH is a hydrogenated analogue of NADH where the double bond between C5 and C6 of the pyridine ring is saturated. It has been shown that this analog can not provide a hydride ion in the dehydrogenase reaction scheme but can form stable binary and ternary complexes with the pyridine linked dehydrogenase (Dunn et al., 1975; Cedergren-Zeppezauer et al., 1982). H_2NADH was very useful in demonstrating that the reduced coenzyme beside being a hydride donating group induced a conformational change to the active forms. The use of such inactive analogues may provide more information about the active site than can be deduced from the use of common inhibitors, since it permits the study of stabilized intermediates along the reaction pathway. For example, LADH, p-dimethylamino cinnamaldehyde (DACA), and H_2NADH form a stable ternary complex whose spectroscopic properties are similar to those transiently observed with NADH as coenzyme (Dunn, 1973, 1975; Bignetti and Zeppezauer, 1979). The complex with H_2NADH does not change with time as does that with NADH. The crystal structure of the ternary complex LADH/H_2NADH/DACA has been determined (Zeppezauer, 1982). The X-ray results show that a complex LADH/H_2NADH/aldehyde whose structure is likely to be similar to that of the active

complex LADH/NADH/aldehyde. Thus, inactive coenzyme analogue, H_2NADH, and the real substrate, DACA, form a simulated transient complex that provides a suitable model for studying substrate binding to LADH.

H_2NADH induces the same conformational change as NADH in liver alcohol dehydrogenase as shown by crystallographic (E. Zeppezauer, Bränden, Eklund, unpublished results) and spectroscopic (Dunn, Biellmann and Branlant, unpublished results) studies. These features of H_2NADH can be used to check the band assignment by comparing the Raman spectra of H_2NADH with that of NADH. Since the structural difference between NADH and H_2NADH is in the nicotinamide part, for the Raman spectra of NADH and H_2NADH, we expect to see that the bands due to adenine moiety will be unchanged and the bands due to both adenine and nicotinamide could be partially changed. We have for the first time measured the Raman spectra of H_2NADH both in solution and in situ. These spectra were generated in the same way as described in chapter II.

Fig 4. 8 shows the Raman spectra of H_2NADH and NADH in solution. The peak at 1308, 1338, 1484 and 1578 cm^{-1} which have been assigned to adenine (Yue et al., 1986), remain unchanged in the positions. The relative intensities of the 1336 to 1303 cm^{-1} of H_2NADH is the same as that of the 1338 to 1308 cm^{-1} of NADH. The peaks at 998, 1182, 1546, 1618 and 1688 cm^{-1} which have been assigned to pure mode of nicotinamide moiety, are dramatically modified. The peaks at 998 and 1546 cm^{-1} are shifted to 992 and 1530 cm^{-1} respectively. There are no peaks at 1182, 1618 and 1688 cm^{-1} at all in the spectrum of H_2NADH. The highest band in the Raman spectrum of H_2NADH lies at 1630 cm^{-1} and is significantly broader and with diminished relative intensity than the 1688 cm^{-1} band of NADH. Notice that the relative intensities of the 1530 and 1303 cm^{-1} bands of H_2NADH in solution remains relatively unchanged comparing to that of the 1546 and 1308 cm^{-1} bands of NADH in solution.

The bands at 1246,1378 and 1422 cm^{-1} of NADH in solution, which are assigned to modes arising from both adenine and nicotinamide, are changed in the spectrum of H_2NADH in

solution. The peaks at 1378 and 1422 cm^{-1} in the spectrum of NADH are replaced by the peaks at 1383 and 1415 cm^{-1} respectively in the solution spectrum of H_2NADH and the intensity of the peak at 1415 cm^{-1} is greatly reduced. The peak at 1246 cm^{-1} is absence in H_2NADH solution spectrum.

As expected that the bands at 1084, 1112 and 1578 cm^{-1} in the spectrum of NADH in solution remain unchanged in the spectrum of H_2NADH in solution, since the band at 1084 cm^{-1} has been assigned to the rocking motion of $-NH_2$ of the amide of the nicotinamide; the band at 1112 is mainly due to ribose with small influence of phosphate (Yue et al., 1986); the peak at 1578 cm^{-1} is due to adenine.

Fig. 4.9 (b) and (c) show the Raman spectra of H_2NADH in situ and in solution respectively. For comparison the Raman spectrum of NADH in situ is shown in (a). The spectrum of LADH was subtracted from the binary complex spectrum. The major changes in the Raman spectrum of H_2NADH upon binding are as follows:

(a). The intensity of the band at 1338 cm^{-1} of H_2NADH in solution is greatly reduced in the bound spectrum. In addition, new smaller band at 1326 cm^{-1} appears in the bound H_2NADH spectrum. A similar change can be seen in the Raman spectrum of NADH (Fig 4. 4 (a)) or ADPR (Fig 4. 4 (b)) upon binding.

(b). The most intense and broad peak at 1530 cm^{-1} of H_2NADH in solution is shifted to about 1575 cm^{-1} upon binding and its broad feature remains.

(c). The intensity of the band at 1630 cm^{-1} of H_2NADH in solution is enhanced in the bound spectrum with the position unchanged.

(d). The peak at 1383 cm^{-1} with a shoulder at 1415 cm^{-1} of H_2NADH in solution are replaced by three sharp peaks at 1374, 1400, 1418 cm^{-1} in the bound spectrum.

From Fig 4. 9 (a) and (b) we can see that both bound NADH and H_2NADH have bands at 1302, 1326, 1338 and 1375 cm^{-1} which are the characteristic features of the adenine moiety upon binding. Not only the band positions but also the relative intensities of these bands are very similar for the bound NADH, bound ADPR and bound H_2NADH. This indicates that the adenosine moiety

in both NADH and H_2NADH has the same conformation when bound to LADH.

The bands which are due to nicotinamide are quite different between the bound H_2NADH and bound NADH. The most intense peak at 1681 cm^{-1} in bound NADH spectrum is replaced by 1632 cm^{-1} with similar shape feature in bound H_2NADH spectrum.

The peaks at 1616, 1600 and 1681 cm^{-1} in the bound NADH spectrum are not observed in the bound H_2NADH spectrum. In contrast, the peaks at 1400 and 1418 cm^{-1} in the bound H_2NADH spectrum are not observed in the bound NADH spectrum. These differences show that the nicotinamide moiety are quite different when NADH and H_2NADH are bound to LADH.

In summary, the comparison of the Raman spectra of H_2NADH with that of NADH in both solution and in situ leads to the conclusion that all the bands assigned to the adenine moiety remain unchanged (i.e. the bound adenine bands remain the same and the free adenine bands are the same), while the bands due to nicotinamide are dramatically modefied in either position or intensities.

The dramatic changes of those bands that are assigned to nicotinamide moiety can be understood as follows: X-ray studies show that the analogue H_2NADH has a geometry that is different from NADH, in that the bonds C5--C6 and N1--C6 are longer than in NADH. Furthermore, the 1,4,5,6-tetrahydronicotinamide ring very likely assumes a nonplaner conformation with C5 positioned out of the plane defined by N1, C2, C3, C4 and C6 (Hope, 1969), while the nicotinamide ring of NADH is almost certanly planar (Koyama, 1963; Karle, 1961). This structural difference between the reduced nicotinamide moieties of H_2NADH and NADH causes the dramatic changes in the Raman spectrum of the H_2NADH and NADH.

CHAPTER V

STUDIES OF BOUND SUBSTRATE DABA

In this chapter, we present the Raman spectra of DABA bound to LADH/NADH without the contribution of the enzyme and coenzyme. In order to understand the spectroscopy of DABA, we have also measured the bound spectra of DABA with various atoms isotopically substituted. As a model, we have obtained the Raman spectra of zinc-complexes of DABA and its various isotopically labelled compounds. We have also studied the Raman spectra of DABA in various solvents with different dielectric constants in an attempt to identify the carbonyl band(s).

A. Free, Bound and Zn-complexed DABA

Fig. 5.1(a) shows the Raman spectrum of the ternary complex LADH/NADH/DABA with a molar ratio of 1 : 2 : 0.67. The spectrum agrees with previous report by Jagodzinski et al. (1982). For comparison, the binary complex of LADH/NADH is also shown (Fig. 5.1(b)). Virtually all this signal arises from protein bands of LADH. It is clear that the bound DABA gives very sizable contribution to the ternary complex spectrum. This is almost certainly due to some pre-resonance enhancement of DABA 's Raman cross section, since bound DABA's λ_{max}=380 nm is close to the excitation wavelength of 488 nm. Fig. 5.2(b) shows the Raman spectrum due only to the bound DABA with the contribution from LADH and NADH subtracted, using the method described in chapter II. The subtraction is easier because of the much larger intensity of bound DABA. It is possible that the difference spectrum contains changes in LADH and NADH upon DABA binding. This is, however, not the case. In the first, x-ray studies show no major conformation difference between binary and ternary complexes of LADH, including those of DACA (Zeppezauer et al., 1982), a closely related substrate to DABA. Moreover, as will be evident below, most of the bands in Fig.5.2(b) respond to isotopic labelling of the bound DABA and the spectra resemble very closely those of zinc complex model compounds. For comparison, the Raman spectrum of DABA in

buffered solution is shown in Fig. 5.2(a). The agreements between the two spectra are not bad in most regions, with small changes in band positions and relative intensity. However, one region of the spectra is quite different. Around 1400 cm^{-1}, there are two bands of considerable intensity for bound DABA, but only one for free DABA in buffered solution. Fig. 5.2(c) shows the spectrum of DABA in the complex with zinc chloride in nonaqueous methylene chloride; we'll call this the Zn-complex. It is clear that the bound DABA spectrum is much closer to that of the Zn-complex, particularly in the region around ca. 1400 cm^{-1}. The general pattern is identical, and most peaks differ only in frequencies of less than 10 cm^{-1}. There are some intensity differences in the high wavenumber region around 1600 cm^{-1}.

B. Isotopically Labelled DABA

To understand the normal mode pattern of DABA, we have examined four isotopically labelled samples which have been named as DABA (-CDO), (-^{13}CDO), (-^{13}CHO) and (^{2}D) (see Fig. 3.2). Fig. 5.3(b)--->(e) show the Raman spectra of these four samples in buffered solutions from 1000 cm^{-1} to 1700 cm^{-1}. Fig. 5.3(a) repeats the Raman spectrum of unlabelled DABA in this range for comparison. The corresponding Raman spectra of bound DABA, and Zn-complexes--- in the order of unlabelled DABA(-CHO), (-CDO), (-^{13}CDO), (-^{13}CHO), and (-^{2}D)--- are shown in figures 5.4 and 5.5 respectively. Because of the low solubility of DABA in methylene chloride, the raw data of Zn-complexes have various amounts of free DABA in methylene chloride. In Fig. 5.5, the contributions of free DABA and the solvent have been subtracted.

It is clear that there are significant differences between bound DABA and free DABA in buffered solutions (compare figures 5.3 and 5.4). On the other hand, the similarities between all corresponding samples of bound DABA and Zn-complex are striking (compare figures 5.4 and 5.5). The most significant similarity is around the region 1400 cm^{-1} (where bound and solution spectra show the most differences). Even the relative intensity of the two bands around 605-635 cm^{-1} is the same for bound DABA and Zn-complex (data not shown for isotopically labelled samples). Morever, the relative intensity of these two peaks revers compared Fig. 5.7 and 5.8.

C. DABA in Various solvents

Fig. 5.6 shows the Raman spectra of DABA in different solvents arranged with decreasing redshift of the absorption peak from Fig. 5.6(b) to Fig. 5.6(f). The Zn-complex in diethyl ether, with the largest redshift, is also shown in Fig. 5.6(a) for comparison. The amount of redshift also increases with increasing dielectric constant. Almost all the peaks above 1300 cm^{-1} are sensitive to the polarity of the solvents, supporting the idea that the normal modes of DABA are quite extended. One obvious change is the relative intensities of the two peaks at 1440 and 1392 cm^{-1}. For DABA in diethyl ether (Fig.5.6(f)) the intensity of the band at 1392 cm^{-1} is relatively weaker than that of the band at 1440 cm^{-1}, but the intensity of 1392 cm^{-1} band increases with increasing the dielectric constant of the solvent (Fig.5.6(e)--->(a)) and it becomes much intense than that of the 1440 cm^{-1} band for DABA/$ZnCl_2$/diethyl ether (Fig.5.6(a)). Of particular interest is the behavior of the group of bands from 1550 to 1700 cm^{-1}. All the peaks in this region shift to lower frequencies as the environment becomes more polar, with the largest downshift in the Zn-complex in diethyl ether.

D. Assignments of Peaks

DABA is basically a planar molecule with 16 "atoms"(the two methyl group can be treated as two heavy "atoms") and shows a rich Raman spectrum below 1800 cm^{-1}. It is a relatively simple molecule but the normal mode pattern seems to be quite complicated with many extended modes involving many parts or all of the molecule. For example, when the aldehyde's hydrogen atom is replaced by a deuteraium, almost all the peaks between 1000-1700 cm^{-1} are affected (compare Fig. 5.3(a) and 5.3(b)). Similar drastic effects can also be seen with the other isotopically substituted samples. Therefore, care must be taken in assigning a peak to a particular bond streching or bending. It is also important to note that the changes seen in isotopically substituted samples are not the same for bound DABA and DABA in solution, indicating that the normal mode patterns of

the two are quite different.

1500-1700 cm^{-1} region: It is very tempting to assign the highest frequency peak in solution to be due to the carbonyl streching. This peak is sensitive to different solvents (Jagodzinski et al., 1982) and is in the expected region for carbonyl streching. Our results (Fig. 5.6) show that the highest frequency peak is most affected by the different solvents and it clearly splits into at least two different peaks in different solvents. The two peaks seem to have different behavior as a function of redshift. Both these peaks are probably modes involving a lot of carbonyl stretching. In the Zn-complex, the highest frequency peak is considerably narrower. It is possible that one of the two peaks "disappears" in forming the Zn-complex. A more likely scenario is the following. As the environment becomes more polar, the mode(s) that is (are) predominantly due to carbonyl stretch is downshifted until it is (they are) mixed in with the other stretching modes of the ring. The characters of the resulting modes have changed so much that it is not appropriate to think of a particular mode shifting in frequency, although the general trend that the modes are at lower frequencies as the environment becomes more polar, is probably still valid.

It is clear that all the peaks in bound DABA are sensitive to isotopic substitutions (Fig. 5.4), indicating that they are very extended modes, involving both bond stretching and bending. It is interesting to note that isotopic substitutions do not have a drastic effect on the mode pattern of DABA in buffered solution (Fig. 5.3). The effect is minimal with those involving substitution of hydrogen by deuterium (sample CDO and ^{2}D; Fig. 5.3(b) and 5.3(e)), indicating that bending of hydrogen/deuterium has a small role in these modes.

Of particular interest are modes that involve carbonyl stretch. By comparing Fig. 5.4(a) and 5.4(d), it is easy to see that the carbonyl stretch is important in all the modes in this region since all the peak frequencies are changed by substituting the carbonyl carbon by ^{13}C. Here again one has to be careful of possible change in mode characters. Nevertheless, it is likely that the characters of these modes remain essentially the same with isotopic substitutions. The ^{13}C substitution has the most effect on the peak at 1578 cm^{-1}, downshifting it by 15 cm^{-1}. A downshift of 35 cm^{-1} is expected for a "pure" carbonyl stretch. The same peak, however, is also drastically affected by

deuterating the aldehyde's hydrogen (downshifted by 9 cm^{-1}; Fig. 5.4(b)) and to a lesser extend by deuterating two of the ring's hydrogens (downshifted by 3 cm^{-1}; Fig. 5.4(e)). It is interesting to note that there may be two modes at this frequency. There is a clear shoulder on the lower frequency side of the corresponding peak in the Zn-complex CDO sample (Fig. 5.5(b)). The unlabelled DABA(-CHO) in Zn-complex shows a broader peak (Fig. 5.5(a)). The peak is also not symmetric in the ^{13}CHO sample, with more intensity on the lower frequency side (Fig. 5.5(d)).

The other peaks in this region show fairly consistent changes upon isotopic substitutions. The 1624 cm^{-1} peak is downshifted slightly and with reduced intensity in almost all substituted samples; the intensity does not seem to change in the ^{2}D sample (Fig. 5.4). There is a clear shoulder on the low frequency side of the 1545 cm^{-1} peak (Fig.5.4(a)). The two modes are separated more in substituted samples, with the intensity of the low frequency mode much enhanced by ^{13}C substitution (samples ^{13}CDO and ^{13}CHO; Fig. 5.4(c) and 5.4(d)). It is not clear whether there are two modes in the ^{2}D sample.

We have found a small peak above 1700 cm^{-1} in CDO samples (bound and Zn-complex) only (data not shown). The origin of this peak is not known. We have also found excitation wavelength dependence of the relative intensities of the two highest frequency peaks (data not shown). As the excitation wavelength becomes shorter, the intensity of the highest frequency peak increases whereas that of the second highest frequency peak decreases.

1250-1500 cm^{-1} region: This region contains peaks that are mostly due to bending motions and are relatively insensitive to different solvents (Fig. 5.6). The peak at 1444 cm^{-1} remains unchanged in all samples --- bound, Zn-complex and in buffered solution--- with substitutions in the aldehyde (Fig. 5.3-5.5(a)-(d)). It disappears in all ^{2}D samples and a new peak appears at a lower frequency (1416 cm^{-1} in the bound spectrum). This mode is assigned to the bending motions of the ring's hydrogen. There are two modes of considerable intensity around 1390 cm^{-1} in the bound DABA (1393 and 1378 cm^{-1}) and Zn-complex (1398 and 1378 cm^{-1}) spectra whereas only one peak is present in the "free" spectrum (1403 cm^{-1}). It is very tempting to assign one of the two bound peaks to the weakened carbonyl stretch since single bond carbonyl

stretching is expected to have frequency in this range. This is not the case. ^{13}C substitution has only minimal effect on these two modes (Fig. 5.4(d) and 5.5(d)). On the other hand, CDO sample has no peak in this range (Fig. 5.4(b) and 5.5(b)). Instead, two new peaks appear, one at 1038 cm^{-1} and the other at 1284 cm^{-1}. A similar downshift of the 1403 cm^{-1} peak to 1044 cm^{-1} is seen with the free DABA in solution. A "pure" hydrogen bending mode at around 1400 cm^{-1} will be shifted to 1024 cm^{-1} upon deuteration. This mode (1394 cm^{-1} in bound and 1403 cm^{-1} in free DABA) is clearly predominantly due to the aldehyde's hydrogen bending. Its intensity is also much reduced in the ^{2}D sample (Fig.5.3(e)). It is tentatively assigned to coupled hydrogen's bendings in both the ring and the aldehyde group. The two smaller peaks at 1353 and 1321 cm^{-1} are not very sensitive to isotopic substitutions.

Below 1250 cm^{-1}: The two peaks at ca. 1180 and 1228 cm^{-1} in the bound DABA spectrum (Fig. 5.4(a)) are basically independent of any isotopical substitution and are probably due to the ring skeleton stretching. They are slightly different in the solution spectrum and in the zinc-complex spectrum (Fig. 5.3(a)and 5.5(a)). It is interesting to note that in the solution spectrum only, they are drastically changed in the ^{2}D sample, indicating that they must contain a significant amount of ring hydrogen bending. There are minor changes in the region below 1000 cm^{-1} with no new peak in the bound or zinc-complex spectrum as compared to the solution spectrum (Fig.5.7 and 5.8). The peak at 848 cm^{-1} in the bound spectrum (Fig. 5.2(b) and Fig.5.8(a)) is probably consisted of at least two modes since it is split into two peaks at 848 and 819 cm^{-1} in the ^{2}D sample (Fig5.8(e)). It is also significantly downshifted in all three aldehyde-substituted samples, CDO(to 815 cm^{-1}), ^{13}CDO(to 808 cm^{-1}), and ^{13}CHO(to 836 cm^{-1}) (Fig.5.7 and Fig.5.8). Similar changes on substituted samples are observed for zinc-complex spectra (data not shown). The two peaks at 605 and 635 cm^{-1} in the bound spectrum (Fig. 5.2(b) and 5.8(a)) are insensitive to aldehyde's carbon or hydrogen substitution but downshifted by about 10 cm^{-1} in the ^{2}D sample (Fig.5.8 (b), (c), (d), (e)). Similar behavior is observed for the solution and zinc-complex labelled spectra. As mentioned above, the intensity pattern of these two peaks of bound DABA agrees with that of the zinc-complex but is just the opposite to that of the solution spectra (compare Fig. 5.7 and Fig.5.8).

The broad peak at 367 cm^{-1} in the bound spectrum is relatively insensitive to our isotopic substitutions, a feature also shared by the solution and zinc-complex samples. It is interesting to note that the peak in the bound spectrum is slightly closer to that of the solution (at 359 cm^{-1}) than to that of the zinc-complex (at 382 cm^{-1}).

We noticed that the relative peak intensity is different using excitation wavelengths between 407 to 514.5 nm. This is not unexpected from resonancely or preresonancely enhanced Raman spectra as the normal modes of the various observed bands may couple differently to the electronic excited states of the molecule which can give rise to different Raman cross section. We have performed all measurements reported here using the same excitation wavelength, 488.0 nm.

Discussions

It has been known that aromatic aldehydes can be used as substrates for LADH (Dworschack & Plapp, 1977). In particular, DABA is readily converted to the corresponding alcohol in the presence of catalytic amount of LADH. Peticolas and his co-workers have shown that a stable ternary complex of LADH/NADH/DABA can be formed in excess enzyme and coenzyme (Jagodzinski & Peticolas, 1981; Jagodzinski et al., 1982). There is, however, the problem whether this ternary complex is a true intermediate of the reaction or just a trapped "dead-end" product. The fact that this ternary complex can be obtained by starting from either NADH and DABA or NAD^+ and the alcohol shows that the ternary complex is the most preferred state of the system (Jagodzinski et al., 1982). It does not, however, exclude the possibility that it is a "dead-end "product. That is, the complex is not kinetically relevant. We have found that the Raman spectra of the ternary complexes of LADH/H_2NADH/DABA and LADH/NADH/DABA are identical (data not show). H_2NADH is an inactive analog of the reduced coenzyme which preserves most binding properties but cannot afford the transfer of a hydride ion (Dunn et al., 1975). More recently, X-ray diffraction showed that H_2NADH binds in the same way as NADH (Cedergren-Zeppezauer et al., 1982). Therefore, it is likely that the ternary complex is a true intermediate.

The involvement of the catalytic zinc ion of LADH as a Lewis acid catalyst has been proposed by many investigators (Theorell & McKinley-McKee, 1961; Creighton & Sigman, 1971; Dunn & Hutchison, 1973; Dunn et al., 1975; Angelis et al., 1977; Jagodzinski et al., 1982). A coordination between the catalytic zinc and the substrate's carbonyl oxygen is suggested by many of these authors. For example, Dunn and his co-workers studied another aromatic substrate, DACA, and concluded that the red shift due to ternary complex formation of this substrate is indicative of zinc acting as a Lewis acid. Jagodzinski et al. (1982) correctly pointed out that there can be other reasons for redshift. They reported Raman studies, which are more sensitive to detailed bonding changes, on the ternary complex with DABA and concluded (correctly) that zinc-complex of DABA in nonaqueous solution of methylene chloride or diethyl ether is a good model for the role of LADH. DABA, however, shows fairly complicated and extended normal mode pattern (see Results above), making it difficult to compare the Raman spectra of DABA in zinc-complex and the ternary complex of LADH/NADH/DABA, which contains sizable contribution of enzyme and coenzyme (Jagodzinski et al., 1982). In fact, our data show that the mode characteristic changes in going from solution to bound state, so much that it is sometimes incorrect to say a certain peak has shifted in frequency. A more appropriate way to describe the change is that a certain mode has disappeared and another mode, which may have quite different characters, appears.

Our results show an amazing correspondence between bound DABA and DABA in zinc-complex. The correspondence is especially striking with the isotopically substituted samples, excluding the possibility of accidental similarity between bound DABA and DABA in zinc-complex. It is clear that one of the roles of LADH in catalysis is to provide a zinc ion as a Lewis acid. The success of the zinc-complex model eliminates the possibility of a second sphere interaction of catalytic zinc and this substrate. We cannot, however, find a peak in the bound spectrum that corresponds to a direct zinc- carbonyl oxygen bond. There is also no clear evidence of a single bonded carbonyl stretching mode in the bound spectrum since the modes are very extended. The peak at 1578 cm^{-1} has a good contribution from the carbonyl stretch, but a carbonyl single

bond is expected to be at ca. 1400 cm^{-1} (assuming that a pure carbonyl double bond is at ca. 1700 cm^{-1}). Studies with DABA in different solvents show that the absorption peak position and the trend of the peaks around 1550-1700 cm^{-1} correlate well with the polarity of the solvents. Thus, the general idea that the carbonyl double bond is weakened upon complex formation is probably valid from the amount of redshift of the bound DABA and the general downshift trend of all the high frequency bands.

It has been established that the catalytic zinc is tetrahedrally coordinated in the native enzyme, with three ligands in the protein and a water molecule as the fourth ligand (Bränden et al., 1975). Kanno & Hiraishi (1980) showed that in $ZnCl_2$ solution, the most stable ionic entity is the tetrahedral $ZnCl_2$- ion. It is thus very likely that the tetrahedral coordination of the catalytic zinc is preserved in substrate binding, with the water molecule replaced by the substrate. Indeed, X-ray crystallographic studies on the ternary complex with a very similar aromatic aldehyde, DACA, shows that the substrate pocket is too small for any water molecules and that the zinc ion is very close to the carbonyl oxygen (Cedergren-Zeppezauer et al., 1982). They found that the only substantial interaction between the protein and the substrate is through the zinc atom. Furthermore, the pyridine ring of the coenzyme is not particularly close to the aldehyde group of the substrate. Such a proximity is necessary for direct hydride transfer from the coenzyme to the substrate in normal catalytic reaction. Our results are consistent with this picture. The close correlation between the bound DABA and DABA in zinc-complex for all isotopically substituted samples suggests that the only significant interaction between DABA and the protein is through the catalytic zinc ion. It also eliminates the possibility of any strong interaction between the coenzyme and this substrate. Such interaction, if exists, will undoubtedly alter the normal mode pattern of the substrate. This is also consistent with the fact that the Raman spectrum of the ternary complexes with NADH is the same with H_2NADH.

CHAPTER VI

STUDIES OF COENZYMES BOUND TO YADH

Yeast alcohol dehydrogenase (YADH) is a NAD-dependent enzyme composed of four seemingly identical subunits which catalyses the interconversion of acetaldehyde and ethanol. There are four Zinc atoms per molecule (Vallee, 1955). Many kinetic mechanism studies are available (Nygaard & Therorell, 1955; JAN & Kaplan, 1957; Klinman, 1975; Dickinson, 1973, 1975, 1977, 1978; Cook and Cleland, 1981) and it now appears that the enzyme obeys a preferentially ordered mechanism whose equilibrium favors aldehyde reduction, with NADH binding first and NAD^+ dissociating as the last product. Ethanol oxidation also proceeds with a preferentially ordered mechanism, but in this case an appreciable reactant random binding may be occur (Dickinson, 1973). The interaction of coenzyme with the enzyme has been investigated by several authors (Dickinson, 1970, 1974; Yamada et al., 1973; Temler et al., 1974; Karloric et al., 1976;Chi-Yu Lee and Kaplan, 1974; Gronenborn et al., 1982). Dickinson (1974) has suggested that the tetrameric enzyme has only two binding sites for NADH. Yamada and Yamato (1973) and Pavkov-Pericin (1974) have presented data in support of this claim. However, in the studies of Hayes and Vellick, it has been shown that there are four equal and independent sites for binding NAD^+ and NADH. This is in ageement with Vallee's observation that there are four Zinc atoms per molecule of enzyme. Temler and Kagi (1974) reported on the basis of circular dichroism measurements that the molecule of YADH binds 4 molecules of NADH in a non-cooperative fashion.

The molecular weight (1.5×10^5 g) of the yeast enzyme is about twice that of the mammalian ADH and it is about 100 time more active. Both dissociation constants of NAD^+ and NADH when bound to YADH are higher ($K_{E,R}$ = 11 μM; $K_{E,O}$ = 270 μM; Dickinson 1978) than that when bound to LADH ($K_{E,R}$ =0.3 μM; $K_{E,O}$ = 133 μM; Taniguchi et al., 1967).

The reaction catalyzed by yeast ADH is identical with that catalyzed by horse liver ADH, but it was shown that there are considerable differences between YADH and LADH in their physical properties, substrate specificities and kinetic behavior. The binding of NADH by the two enzymes

appears to be different, a shift of the 340 nm absorption band to 325 nm of NADH can be observed when the enzyme-coenzyme complex is formed with the mammalian enzyme but not with the yeast dehydrogenase. For the liver enzyme, binding of NAD^+ results in perturbation of the pK_a of an enzyme group from 9.6 in the free enzyme to 7.6-8.0 in the enzyme-NAD^+ complex (Dalziel, 1963; Shore et al., 1974). For the yeast enzyme the dissociation constant of the enzyme-NAD^+ complex is practically constant over the pH range 6.0-8.5 (Dicknson et al., 1975), and there is no evidence for the participation of a similar functional group with this enzyme. Yamada (1973) has reported that the interactions between the coenzyme binding site and substrate binding site in presence of YADH are so weak that substrate binding does not affect coenzyme binding.

The considerable differences between YADH and LADH as mentioned above suggest very difference enzyme-coenzyme interaction which can be studied by the Raman spectra of bound coenzymes. We have studied the Raman spectra of coenzymes when bound to YADH using the same method as described in chapter II.

YADH was purchased as crystalline suspension in 10% ethanol from Boehringer Mannheim CO. The preparation procedure of YADH was the same as that of LADH except that the sample of YADH was centrifuged at a higher speed, 7000 Xg. The activity was measured by the method of Bert L. Vallee et al.,(1955). For the measurement of the rate of the formation of NADH, the following 3.0 ml reaction mixture was employed at 23 °C : NAD^+ 5 μmoles; ethanol 1000 μmoles; 1.0 ml of 0.1 M pyrophosphate buffer, pH 8.8; approximately 5 μg of YADH in 0.2 ml. A typical set of the data for making such reaction mixture is listed in table 6.1. The activity of our sample of YADH is about 560 U.

Fig 6.1 shows the Raman spectra of (a) NADH in solution, (b) the bound NADH with YADH, (c) the bound NADH with YADH and IBA. The ratio of the binary complex is YADH : NADH = 1 : 3 for binary complex and YADH : NADH : IBA = 1: 3 : 10 for ternary complex. In order to ensure that most of the molecules of NADH are in the bound state, we have used a ratio of 1 : 2 for the binary complex YADH/NADH, and obtained the same result as that obtained by using a ratio of 1 : 3 for the

binary complex.The major changes in the Raman spectra of NADH upon binding to YADH are as follows:

The intensity of the band at 1338 cm^{-1} in the solution spectrum is reduced when NADH binds. The relative intensity of the 1422 and 1378 cm^{-1} bands of NADH in solution is considerably reduced in the bound spectrum. The bands at 1112 cm^{-1} and 1084 cm^{-1} are unresolved in the solution spectrum but resolved in the bound spectrum and the intensity of the band at 1112 cm^{-1} is enhanced when NADH binds to YADH.

The similarity and difference in the binding behaviours of NADH with LADH and YADH can be seen from the Raman spectra of NADH bound respectively to these two enzymes. The intensity of the band at 1338 cm^{-1} of NADH in solution is reduced when NADH binds to LADH or YADH. This indicates that the adenine binding is very similar in these two cases. The band at 1546 cm^{-1} of NADH in solution completely disappears when NADH binds to LADH but remains when NADH binds to YADH. The band at 1688 cm^{-1} of NADH in solution is shifted to 1681 cm^{-1} for NADH bound to LADH while there is no shift for NADH bound to YADH. These are in agreement with that of the absorption measurement. The absorption maximum at 340 cm^{-1} of NADH in solution is shifted to 325 cm^{-1} upon binding to LADH but there is no shift when NADH bound to YADH. Both Raman and absorption data clearly show that the nicotinamide moiety of NADH undergoes major molecular changes upon binding to LADH but is almost unaffected when NADH bound to YADH.

We have also measured the Raman spectrum of the bound NAD^+ with YADH (data not shown) which is similar to the solution spectrum of NAD^+.

All the measurements mentioned above have been repeated several times and the results are reproducible, which indicates that there are much fewer differences between solution and bound NADH and NAD^+.

The affinity of NAD^+ to YADH is rather poor. In order to increase this affinity and investigate the spectroscopic properties of the oxidized coenzyme in ternary complex, we have carried out experiment of NAD^+/YADH in the presence of pyrazole (data not shown). The result shows that the inhibitor pyrazole has a different effect on NAD^+ in the two cases of NAD^+/YADH and NAD^+/LADH

(see Fig 4. 5 (c)). This result is in agreement with that from the x-ray studies, which concluded that there is an important difference between yeast and liver alcohol dehydrogenase (Reynier, 1969) on the effect of substitutions made at the 4 position of the pyrazole ring. Such substitutions drastically decrease the inhibitory power of the derivative with yeast alcohol dehydrogenase. This can be correlated with differences in the amino acid sequence in the active site (Jörnvall et al., 1978) which decreases the space available for substrate or inhibitor binding.

CHAPTER VII

SUMMARY

Difference Raman spectroscopy has been used to study the bound substrate DABA and the coenzymes as well as their analogues (NADH, NAD^+, ADPR and H_2NADH) bound to either LADH or YADH.

Our Raman results show clearly that significant molecular effects take place when the adenine or nicotinamide moieties bind to LADH. The most pronounced change in the NADH Raman spectrum is the disappearence of the solution spectrum's nicotinamide 1546 cm^{-1} band when NADH bounds to LADH. It has been suggested that this 1546 cm^{-1} band arises from a ring C=C stretching motion. However, this mode is upshifted to 1559 cm^{-1} upon deuteration of the amide's protons, suggesting at least some influences of the carboxamide moiety. We have for the first time measured the Raman spectra of H_2NADH, where the nicotinamide C5-C6 double bond of NADH has been reduced. H_2NADH shows no Raman band at 1688 cm^{-1} which is the intense solution Raman band of NADH. The strong 1681 cm^{-1} band found in the binary complex, LADH/NADH, appears to be shifted to 1666 cm^{-1} in the ternary complex LADH/NAD^+/pyrazole data. It seems reasonable to ascribe this to the formation of a NAD^+-pyrazole adduct with covalent bond formation occurring between C4 of NAD^+ and N2 of pyrazole. All these results certainly suggest that ring C=C stretching is involved with the 1688 cm^{-1} mode. We find it plausible that this mode is a highly coupled vibration extending over the whole conjugated π-electron structure of NADH, i.e. it extends over the nicotinamide ring -C=C- and, perhaps, also the carbonyl -C=O moiety. The adenine binding feature is the same for NADH, ADPR and H_2NADH, that is the disappearence of the adenine's strong solution 1338 cm^{-1} band upon binding. It is feasible that the Raman data can be interpreted as resulting from a specific interaction on N7 of the adenine ring. However, studies employing isotopically labelled adenine are needed for more certain understanding of adenine normal mode structure and its behavior when bound to LADH.

ADPR lacks NADH's nicotinamide head and the binding of ADPR does not induce a conformational change in LADH. By comparing the spectra of bound NADH with that of bound ADPR we can conclude that none of the major bands of the bound NADH spectrum results from the protein conformational change. The spectrum of bound ADPR allows an assignment of the bands of the bound NADH and NAD^+ spectra to normal coordinates located primarily on either the nicotinamide and adenine moieties. For example, the bands at 1575, 1510, 1375, 1340, 1324, 1303, 1245 and 1172 cm^{-1} in the Raman spectrum of bound NADH can be clearly assigned to the adenine moiety since they appear essentially at the same positions and relative intensities in the bound ADPR spectrum. This assignment has been confirmed from the Raman studies of H_2NADH.

We have examined the extent to which certain inhibitors affect the Raman spectrum of the bound coenzymes. The addition of IBA and DMSO has little effect on the bound NADH spectrum. Pyrazole binds tightly to the nicotinamide ring moiety of NAD^+ and not the carboxamide.

The considerable differences between YADH and LADH suggest very different enzyme-coenzyme interactions. We have studied both the Raman and absorption spectra of coenzymes when bound to YADH. The Raman results indicate that the adenine binding is similar for NADH/YADH and NADH/LADH. Both absorption and Raman spectra show clearly that the nicotinamide moiety of NADH undergoes major molecular changes upon binding to LADH but is almost unaffected when NADH bound to YADH.

A careful study of the Raman spectra of DABA and its various isotopically labelled compounds complexed to Zn^{+2} in methylene chloride has been made. The close correlation between the bound DABA and DABA in Zn-complex for all isotopically substituted samples suggests that the only significant interaction between DABA and the protein is through the catalytic zinc ions. The success of the Zn-complex model eliminates the possibility of a second sphere interaction of catalytic zinc and this substrate. The carbonyl double bond retains a high degree of double bond character when DABA binds to LADH/NADH, but clearly less than that found in solution of DABA.

CHAPTER VIII

APPENDIX

DETERMINATION OF THE REDUCTION OF NAD^+

Fig. 8.1 shows the Raman spectra of bound NAD^+ and bound NADH respectively. A most striking result is that these two spectra are virtually the same. There are two posibilities which cause this result: (1) the binary LADH/NAD^+ has been converted to binary LADH/NADH due to alcohol as an impurity in LADH preparations. (2) the conformation of NAD^+ when binds to LADH is the sama as that of NADH. It has long been known that crystalline preparation of LADH retain some alcohol despite all attempts at removal by dialysis or other means, and despite the relatively large values of the dissociation constant ($K_{E,\ alcohol}$), for the dissociation of ethanol from the active sites of LADH, which have been proposed (4.6 or 6.0 mM, Therorell et al., 1961). Taniquchi (1967) has reported that the amount of residual alcohol can be minimized by carefully controlled diaysis procedures to far less than one molecule of alcohol per coenzyme-binding site (0.165 molecules for $LADH_E$ and 0.305 molecules for $LADH_S$).

For the study of NAD^+, after the treatmant by using the procedure which is described in chapter III, our samples of LADH were extensively dialyzed against buffer solutions over 3 days (the buffer was changed twice a day) to remove the ethanol. A simple calculation shows that the ethanol concentration would be no more than 0.02 μM (assume all ethanol is unbound to LADH) compared to the ~ 1 mM LADH concentration in the final preparation.

In order to estimate how much NAD^+ has been reduced due to the residual alcohol during the Raman measurement, the following experiments were performed.

A. Measurement of the Retinol ---> Retinol Conversion

All trans retinol and retinal, the chromophore of visual pigments, from a very efficient alcohol-aldehyde pair of substrates for LADH. All trans retinol and retinal have absorption maxima at

330 and 380 nm, respectively, so that the amount retinol or retinal in a solution can be easily monitored by measuring its absorption spectrum. It is thus possible to determine spectroscopically the concentration of NAD^+ in the presence of LADH by titrating this solution against retinol and observing retinal formation. A pH = 7.0 solution of one mN LADH (remenber LADH contains two independent active sites), one mM NAD^+, and 100 mM iso-butyramide (IBA) was prepared. IBA forms a tight (K_d = 0.14 μM at pH = 7.0) ternary, LADH/NADH/IBA, complex (Therorell & McKinley-McKee, 1961) and is added to trap any NADH formed from NAD^+ by preventing the NADH ---> NAD^+ back reaction. Part of this solution was used to obtain a difference Raman spectrum against LADH. The result, apart from the appearence of known bands due to IBA, was the same as in Fig. 8.1(a). An absorption spectrum of a second part of solution was taken using a 0.5 mm cell; the result was the same as for solutions of LADH/NAD^+. A third portion of the sample was titrated against retinol.

Fig. 8.2 shows the conversion of retinol to retinal as a function of time. Curve (1) is the absorption spectrum of bound NAD^+ (18.6 μM) which was obtained by subtracting the contribution of LADH from that of the binary LADH/NAD^+. For doing so, the samples of LADH/NAD^+ and LADH were placed in sample side and reference side of the spectrometer respectively.

Curve (2) is the absorption spectrum of bound NAD^+ with inhibitor IBA. In this measurement, 8 μL 100 mM IBA was added into the sample of LADH/NAD^+ (392 μl) and the same amount of buffer was added into the LADH sample. The intensity of the band at 325 nm increases a littile bit (Fig.8.2).

Curve (3) was taken just after (< 1 min.) 40 ml 0.33 mM all trans retinol was added into the sample of LADH/NAD^+/IBA and the same amout buffer was added into the LADH sample. The intense peak at 330 nm is a characteristic of retinol while the shoulder at 380 nm is due to retinal.

Curves (4), (5) and (6) show the evolution of both the bands at 330 and 380 nm as a function of time. These three curves were taken respectively 5-, 15-, and 90 minutes after the curve (3) was taken. We can thus determine how much all trans retinol has been formed from the intensity

of the band at 380 nm by using the equation as follows:

$$C = O.D./\varepsilon X L \qquad (8.1)$$

where C is the concentration to be calculated.

ε is the extinction coefficient, for retinal $\varepsilon_{380} = 4.5 \times 10^4\ M^{-1}cm^{-1}$.

L is the opitical pathlength, L = 0.2 cm in this experiment.

O.D. is the optical density, from curve (6) in Fig.8.2 we have O.D. = 0.16 (at 380 nm).

Substituting the values of ε, L and O. D. into eq. (8.1) we obtain the concentration of retinal as 17.7 μM.

This result implies that an amount of 17.7 μM NADH has been converted from NAD^+. In other wards, our sample contains 90% of LADH/NAD^+ in the binary complex.

The sample of LADH/NAD^+ used in this conversion experiment is 32 times less concentrated than that used in the Raman measurement. It is limited by the solubility of all trans retinol in buffer/H_2O. Tween 80 as a detergent was added. The higher concentration of retinol to be made the more Tween 80 has to be added. Unfortunately high concentration of Tween 80 causes the dissociation of retinol, as a consequence, the characteristic peak of all trans retinol at 330 nm will be shifted to 315 nm and broader. The highest concentration of all trans retinol we have obtained without dissociation is less 1 mM. In the conversion experiment the stock concentration of retinol was 0.3 -- 0.4 mM.

The extinction coefficiencets of all trans retinol and retinal in water with Tween 80 were determined to be $\varepsilon = 4.5 \times 10^4\ M^{-1}cm^{-1}$ by weight. We have only found from literature that the extinction coefficients in ethanol (not in water) as: $4.57 \times 10^4\ M^{-1}cm^{-1}$ for all trans retinol and $4.61 \times 10^4\ M^{-1}cm^{-1}$ for all trans retinal (Frolik C. and Olson J. 1984).

We have also performed conversion experiment without IBA. The possibility of this

experiment is based on the fact that NADH binds to LADH more tightly than NAD^+ does, which favors the conversion along the direction NAD^+ ---> NADH. The result is shown in Fig.8.3.

Curve (0) is the absorption spectrum of bound NAD^+ (16 μM) without retinol.

The absorption spectrum (1) was taken just after the all trans retinol (final concentration 22 μM) was added into the sample of LADH/NAD^+.

The spectra (2), (3), (4), (5) and (6) were taken respectively 10, 30 minutes and 1, 42, 66 hours latter. Finally 20 μM all trans retinal was formed. These results show that the conversion from NAD^+ to NADH in this experiment was much slower than that in the presence of IBA. This slower conversion process is most likely due to that the reverse process still exists. Therefore, it is not accurate enough to estimate quantitively the reduction of NAD^+ by using the result of this experiment.

similar results were obtained by using both the fresh sample of LADH/NAD^+ and the sample used for Raman measurement. This indicates that the laser beam doesn't affect the conversion of NAD^+ to NADH.

B. HPLC Measurements

We have also performed HPLC (high pressure liquid chromatography) measurement to determine the reduction of NAD^+ in the binary complex LADH/NAD^+ due to residual alcohol.

A Waters HPLC instrument equipped with a Model 6000A solvent delivery system, Model U6K sample injector, Model 440 absorbance detector, and a Houston Omniscribe chart recorder was used in the assay procedure. A single 4 mm X 40 cm Waters μBondapak C_{18} column (equilibrated with 10 % methanol) was placed on-line with the solvent delivery system at a flow rate of 1 ml/min. Samples (100 μl) were injected into the column with a Hamilton 801 microliter syringe and eluted under 700-1000 psi pressure. Nucleotides and bases in the eluet were detected at 254 nm with 0.1 absorbance setting. All of the solvents used in the chromatographic procedures were eluted, by vacuum filtration, through a 0.45 mm HA Millipore filter.

Using 0.1M pH 7.0 phosphate with 20 % triethanol buffer we are able to separate NAD^+ and NADH. It is necerssary to remove the protein by filtration from the binary complex LADH/NAD^+ before adding the buffer to it, since the buffer contains alcohol. Quanidine hydrochloride was used to denature the enzyme.

Both the binary complexes LADH/NAD^+ and LADH/NADH have the concentration of 0.47 mM/0.7 mM. 8 samples were made for each binary complex according to the time at which the quanidine hydorchloride was added in after the complex was made. These samples are listed in table 8.1.

The absorption spectrum of each sample was taken just before the quanidine hydrochloride was added in and a 0.5 mm pathlength cuvette was used.

After denaturation and filtration, 450 (μl) phosphate buffer with 20 % triethanol at pH 7.0 was added to each sample (50 μL), which then was ready to be injected into HPLC.

For comparison of binary sample with solution sample, the same procedure of denaturation and filtration was used for the solution sample.

Fig. 8.4 shows the results of the HPLC measurement for (a) NAD^+ in solution; (b) NAD^+ in situ (sample $S_8(+)$); where the peak (Q) is the characteristic of quanidine hydrochloride, the peak (+) is the feature of NAD^+ and the peak (H) is the feature of NADH. In Fig. 8.4, it is clear that the peak at 4.9 cm in the HPLC spectrum of NAD^+ in situ (b) is absent in the HPLC spectrum of NAD^+ in solution (a). This indicates that there is a reduction of NAD^+ in the binary complex of LADH/NAD^+ which can be estimated from the intensities of the peaks (H) and (+).

The results of the HPLC measurement for NADH in solution and in situ (sample $S_8(H)$) are shown in Fig. 8.5. The peak at 3.5 cm appears in both spectra (a) and (b) of Fig. 8.5. It is due to the impurity of NAD^+ in NADH samples.

Fig. 8.6 and Fig. 8.7 show the absorption spectra of NAD^+ (sample $S_8(+)$) and NADH (sample $S_8(H)$) respectively.

By using the equation (8.1), we can also estimate the amount of reduction of NAD^+. The extinction coefficient of bound NADH can be obtained from the absorption spectrum measurement which is given in next section.

The average value of the reduction of NAD^+ over the 8 samples is 20 % from the HPLC measurement which is in agreement with that from the absorption measurement.

Our results from both HPLC and absorption measurements show that the reduction of NAD^+ is not a linear function of time. There is a fluctuation in the values of the reduction over the 8 samples, but almost the same value of the reduction was obtained from both HPLC and absorption measurements for each sample.

For obtaining more convincing conclusion on the structural change from free NAD^+ to bound NAD^+, a control experiment need to be done, i.e. all the measurements of Raman, absorption and HPLC measurement should be carried out using same sample.

C. The Extinction Coefficient for Bound NADH Measurement

The band at 340 nm of NADH in solution ($\varepsilon = 0.622 \times 10^4\ M^{-1}cm^{-1}$) is shifted to 325 nm when NADH binds to LADH. Thus, this band can be used as a monitor of the formation of LADH/NADH and shows as an indicator of the reduction of NAD^+ in the presence of LADH. For quantitatively estimating the reduction of NAD^+, it is necessary to know the extinction coefficient of band at 325 nm.

The measurements of extinction coefficient was performed as follows:

(1). 250 µl (1mM) of NADH was added into a cell with a 2 mm pathlength and its absorptionspectrum was measured, which is shown in Fig. 8.8 curve (1). The band at 340 nm is the characteristic of free NADH.

(2). 20 µl (.7 mM) of LADH was added into the cell, the absorption spectrum is shown in Fig. 8.8 curve (2). The band at 340 nm of the NADH is shifted to 335 nm due to some of the NADH bound to LADH.

(3). Another 20 µl (.7 mM) of LADH was added into the cell and the absorptin spectrum was recored, then this step was repeated for about 10 times. The absorption peak was blue shifted, finally moving to 325 nm with more LADH added.

(4). the percentage of bound NADH can be calculated from the equation as follows:

$$K_{E,R} = \frac{[LADH][NADH]}{[LADH/NADH]} \qquad (8.2)$$

where $K_{E,R}$ is the dissociation constant (.2 µM, Theorell et al.,1961)

The concentration of bound NADH is the product the total concentration of NADH and the percentage obtained from eq. (8.2).

(5). The extinction coefficient of bound NADH can be calculated from the equation (8.1).

The results of this calculation is listed in table 8.2. The average extinction coefficient is 5.5 X 10^3 $M^{-1}cm^{-1}$ which is in agreement with 5.8 X $10^3 M^{-1}cm^{-1}$ obtained by Theorell (1951).

A parallel experiment has been performed for NAD^+. The results are shown in Fig. 8.9. Curve (1) is the absorption spectrum of free NAD^+. There is no peak at neither 340 nor 325 nm. Curve (2) shows the absorption spectrum after adding 20 ml (0.7mM) LADH into 250 ml (1mM) NAD^+. A peak at 325 nm appears and its intensity increases with more LADH added. This indicates that some of the NAD^+ is converted to NADH.

Table 3.1

	molecular weight (g)	λ_{max} (nm)	ε ($mM^{-1}\ cm^{-1}$)	dissociation costant (mM) pH 7.0	dissociation costant (mM) pH 9.0
LADH	84000	280	3.5×10^4		
NADH	663.5	340 260	$.622 \times 10^4$ 1.44×10^4		
IBA	87.12				
DMSO					
LADH/NADH/ IBA		325 260		a. 0.14	
LADH/NADH		325 260		a. 0.0003	a. 0.0006
LADH/NADH/ DMSO		325 260			b. 0.004
NAD^+	661.5	260	1.8×10^4		
pyrazole	68.08				
LADH/NAD^+/ pyrazole		290		c. 0.001	
LADH/NAD^+		325 260		d. 0.133	d. 0.005
ADPR	259	260	1.5×10^4		
LADH/ADPR		260		e. 0.13	e. 0.08
H_2NADH	665.5	265 288	1.85×10^4 1.55×10^4		
LADH/H_2 NADH					f. 0.008
all trans retinol	286.46	330	4.57×10^4		
all trans retinal	284.45	380	4.61×10^4		

a. Theoerll & Mckinley Mckee (1961)
b. Perlman (1968)
c. Theorell &yonetani (1963)
d. Taniqushi & Teorell (1967)
e. Theorell & Yonetani (1964)
f. Dunn & Biellman (1975)

Table 3.2

		stock concentration (mM)	volume (ml)	final concentration (mM)	ratio
our method	NAD^+	30	0.25	2.5	0.5×10^5
	alcohol	1700	0.030	17	5.4×10^5
	buffer		2.6		
	LADH	1.2×10^{-3}	0.10	0.048×10^{-3}	1
Dalziel's method	NAD^+	1.25	1	0.42	10^4
	alcohol	17	0.15	8	2×10^5
	buffer		1.85		
	LADH	5.6×10^{-3}	0.022	0.041×10^{-3}	1

Table 6.1

	stock conc. (mM)	volume (ml)	ratio	final conc. (mM)
NAD^+	15	.333	1.5×10^5	1.5
CH_3CH_2OH	17000	.06	3×10^7	300
YADH	.35/2000	.19	1	.00001
buffer		2.417		

Table 8.1

sample for LADH/NAD^+	sample for LADH/NADH	the time at which the quanidine hydrochloride was added in after the binary complex was made
S_1 (+)	S_1 (H)	5 min
S_2 (+)	S_2 (H)	10 min
S_3 (+)	S_3 (H)	30 min
S_4 (+)	S_4 (H)	1 hr
S_5 (+)	S_5 (H)	5 hr
S_6 (+)	S_6 (H)	8 hr
S_7 (+)	S_7 (H)	16 hr
S_8 (+)	S_8 (H)	24 hr

Table 8.2

	NADH (ml)	NADH(cal) (mM)	bound NADH (cal) %	peak (nm)	peak (O.D.)	LADH (ml)	LADH (mM)	bound LADH %	*boud NADH extin. coeff.
1	.25	1	0	340	1.22	0	0	0	
2	.25	.93	11	335	1.09	.02	.052	100	
3	.25	.86	22	333	0.97	.04	.097	100	
4	.25	.81	33	331	0.88	.06	.135	100	
5	.25	.758	44	330	0.82	.08	.17	100	
6	.25	.714	56	328	0.72	.10	.20	99.9	
7	.25	.676	67	328	0.72	.12	.227	99.8	
8	.25	.64	78	328	0.68	.14	.25	99.6	
9	.25	.61	89	325	0.65	.16	.273	99.6	
10	.25	.58	98	325	0.62	.18	.293	97.0	$5.5X10^3$
11	.25	.556	99.5	325	0.61	.20	.311	87	$5.5X10^3$
12	.25	.532	99.7	325	0.59	.22	.328	79	$5.6X10^3$
13	.25	.51	99.8	325	0.57	.24	.343	73	$5.5X10^3$

*. unit is $M^{-1} cm^{-1}$

FIGURE CAPTIONS

Figure 2.1: Some of possible consequences of a photon-molecule interaction. The lengths of the upward-pointing arrows are proportional to the frequencies of the incoming light while the lengths of the downward-pointing arrows are proportional to the frequency of the scattered (or in the case of fluorescence, emitted) light. The vibrational quantum numbers in the upper and lower electronic states are υ' and υ'' respectively. The energy spacing between the lower state vibrational levels is equal to υ_{vib}.

Figure 2.2: Schematic drawing of the Spex's 1877 Triplemate. The triplemate has two main sections. The first section, from s_1 to s_3, acts as a variable-wavelength, selectable band-pass filter. The second section is a spectrograph stage. The resolution of this section is controlled by the exit slit s_3.

Figure 2.3: Sum and Difference spectra of B^{even} (binary complex), B^{odd} and E^{even} (enzyme) from a particular set of experiments as defined in the text. (a) $B^{odd} + B^{even}$; (b) $B^{odd} - B^{even}$; (c) $B^{odd} - E^{even}$. The intensity scale of (b) and (c) is 20 times that of (a). Samples were in 0.1 M phosphate buffer pH=6.0.

Figure 2.4: The difference spectra between the spectrum of the LADH/NADH complex (B) and that of LADH (E), B-xE, showing various different scaling factors, x, between x=0.94 and x=1.14. The optimal value of x is 1.04 (d) for this set of data. Peaks associated with bound NADH (see figure 4.1(a)) are marked in (d). Samples were in 0.1M pyrophosphate buffer pH=9.6. Difference between the spectra in figures 2.3(a) and 2.4 (a) near 1000 cm^{-1} are due to pH sensitive buffer bands.

Figure 3.1: Schematic drawing of the LADH dimer, designed by Bo Furugren. The central part of the molecule illustrates the two coenzyme binding domains bound together across a 2-fold axis perpendicular to the plane of the paper. The two catalytic domains are separated from this central part by the coenzyme and substrate binding clefts. The binding sites for the coenzyme and substrate have been indicated for one of the subunits. The metal binding sites are located at the fringes of the catalytic domains.

Figure 3.2: Molecular structure of NADH, NAD^+, ADPR and H_2NADH.

Figure 3.3: Molecular structure of DABA and its isotopically labelled DABA.

Figure 3.4: Preparation of H_2NADH by hydrogenating NADH. The absorption spectra represent the time course following the mixture of 25 mg of 10% palladium on charcoal with 100 mg o fNADH dissolved in 5 ml of distilled water . The coenzyme is hydrogenated by bubbling hydrogen for 1, 4, 5, 5.5 and 6 hours respectively.

Figure 4.1: Raman spectra of (a) bound NADH (LADH:NADH=1 mM:2 mM) at 4°C; (b) NADH in solution (54 mM) at room temperature. Both were in 0.1 M pyrophosphate buffer pH=9.6. Assignments of the solution peaks in (b) are from Yue et al. (1986); see text for the assignments of the bound NADH peaks: A=adenine; P=phosphate; N=nicotinamide.

Figure 4.2: Raman spectra of (a) bound NADH(LADH:NADH=1mM:2mM) in 0.1M pyrophosphate buffer pH=9.6; (b) bound NADH(LADH:NADH=1mM:2mM) in 0.1M phosphate buffer pD=7.0; both were at 4°C.

Figure 4.3: Raman spectra of (a) bound ADPR (LADH:ADPR=1.2 mM:1.8 mM); (b) ADPR in solution (80 mM). Both were in 0.1M pyrophosphate buffer pH=9.6 at 4°C.

Figure 4.4: Raman spectra of (a) bound NADH (LADH:NADH=1mM:2mM); (b) bound ADPR(LADH:ADPR=1.2mM:1.8mM). Both were in 0.1M pyrophosphate buffer pH=9.6 at 4°C.

Figure 4.5: Raman spectra of (a) bound NADH with IBA (LADH:NADH:IBA=1.4mM:2.8mM:14mM); (b) bound NADH with DMSO (LADH:NADH:DMSO=1.0mM:2.0mM:105mM); (c)bound NAD^+ with pyrazole (LADH:NAD^+:pyrazole=1.1mM:2.0mM:5.0mM); all were in 0.1M pyrophosphate buffer pH=9.6 at 4°C.

Figure 4.6: Absorption spectra of (a) LADH(0.11mM); (b) LADH/NAD^+/pyrazole (0.11mM:0.2mM:0.5mM); (c) subtraction of (a) from (b). The full scale is 1 O.D. for (a), 2 O.D. for (b) and 0.7 O.D. for (c). Samples were in 0.1M pyrophosphate buffer pH=9.6 at 15°C.

Figure 4.7: Raman spectra of (a) bound NADH with pyrazole (LADH:NADH:pyrazole=1.1mM:2mM:5mM); (b) bound NAD^+ with pyrazole (LADH:NAD^+:pyrazole=1.1mM:2mM:5mM). Samples were in 0.1M pyrophosphate buffer pH=9.6 at 4°C.

Figure 4.8: Raman spectra of (a) H_2NADH(42mM) in solution; (b) NADH(50mM) in solution. Samples were in 0.1M pyrophosphate buffer pH=9.6 at 4°C.

Figure 4.9: Raman spectra of (a) bound NADH(LADH:NADH=1mM:2mM); (b) bound H_2NADH(LADH:H_2NADH=1.2mM:2.2mM); (c) H_2NADH(42mM) in solution. Samples were in 0.1M pyrophosphate buffer pH=9.6 at 4°C.

Figure 5.1: Raman spectra of (a) the ternary complex LADH/NADH/DABA(CHO) with a molar ratio of 1 mM:2 mM:0.67 mM; (b) the binary complex of LADH/NADH with a molar ratio of 1mM:2 mM. Both were in 0.1 M pyrophosphate buffer pH=9.6 at 4°C.

Figure 5.2: Raman spectra of (a) DABA(CHO) (4.6 mM) in 0.1M pyrophosphate buffer pH=9.6; (b) bound DABA(CHO) (LADH:NADH:DABA(CHO)=1mM:2mM:0.67mM); (c) DABA(CHO) (10mM) Zn-complexed in methylene chloride. All were at 4 °C.

Figure 5.3: Raman spectra of (a) DABA(CHO) (4.6 mM); (b) DABA(CDO) (7.3 mM); (c) DABA(^{13}CDO) (2.2mM); (d) DABA(^{13}CHO) (4.3 mM); (e) DABA(2D) (2.5 mM). All were in 0.1 M pyrophosphate buffer pH=9.6 at 4 °C.

Figure 5.4: Raman spectra of bound (a) DABA(CHO); (b) DABA(CDO); (c) DABA(^{13}CDO); (d) DABA(^{13}CHO); (e) DABA(2D). The molar ratio is LADH:NADH:DABA=1mM:2mM:0.67mM. All were in 0.1M pyrophosphate buffer pH=9.6 at 4 °C.

Figure 5. 5: Raman spectra of Zn-complexed (a) DABA(CHO)(20mM); (b) DABA(CDO)(28mM) ; (C) DABA(^{13}CDO)(40mM); (d) DABA(^{13}CHO)(20mM); (e) DABA(2D)(19mM). All were in methylene chloride at 4°C.

Figure 5.6: Raman spectra of DABA (CHO) in different solvents: (a) Zn-complexed DABA (10mM) in diethyl ether; (b) DABA (4.6mM) in 0.1 M pyrophosphate buffer pH=9.6; (c) DABA (~100mM) in methyl ethanol; (d) DABA(~100mM) in methylene chloride; (e) DABA (~100mM) in toluene; (f) DABA (~100mM) in diethyl ether. All were at 4°C.

Figure 5.7: Raman spectra of (a) DABA(CHO) (4.6mM); (b) DABA(CDO) (7.3mM); (c) DABA(^{13}CDO) (2.2mM); (d) DABA(^{13}CHO) (4.3mM); (e) DABA(2D) (2.5mM). All were in 0.1 M pyrophosphate buffer pH=9.6 at 4°C.

Figure 5.8: Raman spectra of bound (a) DABA(CHO); (b) DABA(CDO); (c) DABA(^{13}CDO); (d) DABA(^{13}CHO); (e) DABA(2D). The molar ratio is LADH:NADH:DABA=1mM:2mM:0.67mM. All were in 0.1 M pyrophosphate buffer pH=9.6 at 4°C.

Figure 6.1: Raman spectra of (a) bound NADH with YADH and IBA (YADH:NADH:IBA= 0.5mM:1.5mM:5mM); (b) bound NADH with YADH (YADH:NADH=0.5mM:1.5mM); (c) NADH in solution. All were in 0.1 M pyrophosphate buffer pH=9.6 at 4°C.

Figure 8.1: Raman spectra of bound NAD^+ (LADH:NAD^+=0.9mM:1.6mM); (b) bound NADH (LADH:NADH=1mM:2mM). Both were in 0.1 M pyrophosphate buffer pH=9.6 at 4 °C.

Figure 8.2: The conversion of retinol to retinal as a function of timein the presence IBA.

(1) absorption spectrum of bound NAD^+ (18.6 μM),

(2) absorption spectrum of bound NAD^+ in the presence IBA,

(3) absorption spectrum was taken just after (<1min.) all trans retinol was added into ternary complex (LADH:NAD^+:IBA:retinol=0.01mM:0.015mM:1.8mM:0.03mM),

(4), (5) and (6) absorption spectra were taken respectively 5-, 15- and 90 minutes after (3). The left scale is for spectra (3), (4), (5), (6) while the right scale is for spectra (1) and (2).

Figure 8.3: The conversion of retinol to retinal as a function of time in the absence of IBA.
(0) absorption spectrum of bound NAD^+ (16 μM),
(1) absorption spectrum was taken just after the all trans retinol was added into LADH/NAD^+ (LADH:NAD^+:retinol=10 μM:16 μM:22 μM),
(2), (3), (4), (5) and (6) absorption spectra were taken respectively 10, 30 minutes and 1, 42, 66 hours after (1). The left scale is for spectra (1), (2), (3), (4), (5), (6) while the right scale is for spectrum (0).

Figure 8.4: HPLC elution profile of (a) NAD^+ in solution; (b) NAD^+ in situ (sample $S_8(+)$). Where the peak(Q) is a characteristic of quanidine hydrochloride, the peak (+) is the feature of NAD^+ and the peak(H) is the feature of NADH.

Figure 8.5: HPLC elution profile of (a) NADH in solution; (b) NADH in situ. The peak at 3.5 cm appears in both spectra which is due to the impurity of NAD^+ in the NADH sample.

Figure 8.6: Absorption spectra of (a) LADH(0.47 mM), (b) LADH/NAD^+ (0.47 mM:0.7 mM) and (c) LADH/NAD^+-LADH. The scale for (b) is double of that for (a) and (c). Samples were in 0.1M phosphate buffer pH=7.0 at 15 °C.

Figure 8.7: Absorption spectra of (a) LADH(0.47mM), (b) LADH/NADH(0.47mM:0.7mM), (c) LADH/NADH-LADH. Samples were in 0.1M phosphate buffer pH=7.0 at 15 °C. The scale for(b) is double of that for (a) and (c).

Figure 8.8: Evolution of the absorption spectrum of NADH as a function of concentration of LADH. (1) is the absorption spectrum of 250 μl (1mM) of NADH. The spectra from (2) to (13) were taken in sequence by adding 20 μl (0.7 mM) of LADH. Samples were in 0.1 M phosphate buffer pH=7.0 at 15 °C.

Figure 8.9: Evolution of the absorption spectrum of NAD^+ as a function of concentration of LADH. (1) is the absorption spectrum of 250 µl(1 mM) 0f NAD^+. The spectra from (2) to (7) were taken in sequence by adding 40 µl (0.7 mM) of LADH. Samples were in 0.1M phosphate buffer pH=7.0 at 15°C.

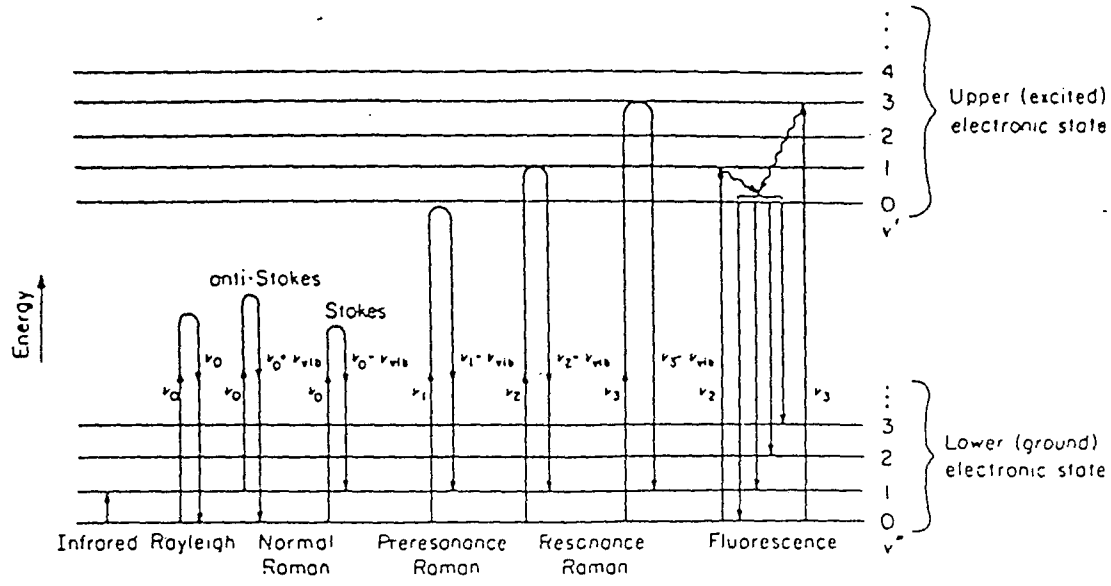
Energy
anti-Stokes
Stokes
Upper (excited) electronic state
Lower (ground) electronic state
Infrared
Rayleigh
Normal Raman
Preresonance Raman
Resonance Raman
Fluorescence

2.1

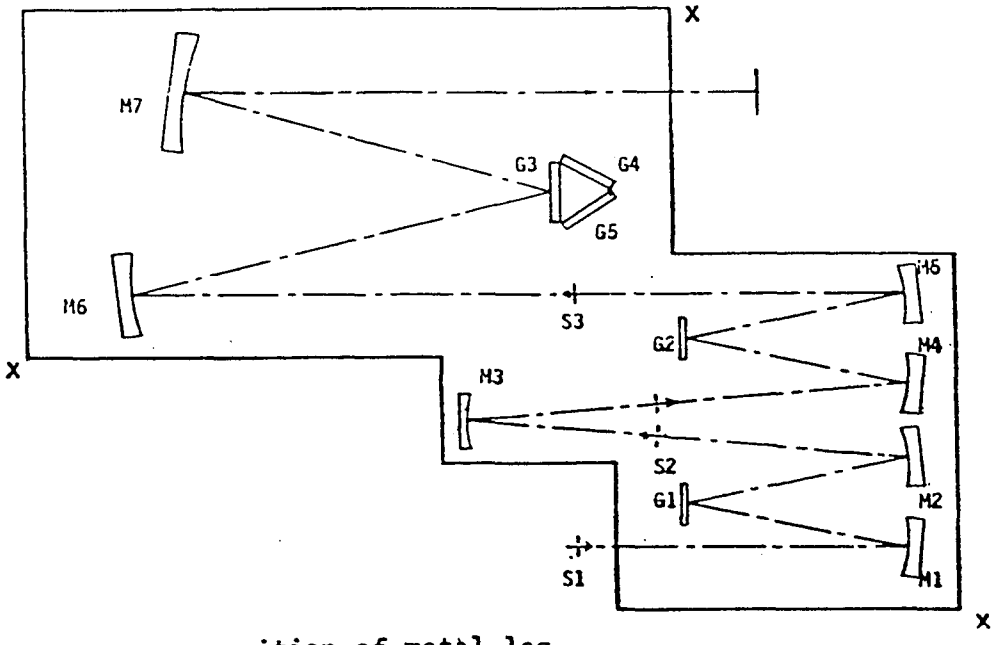

x = position of metal leg

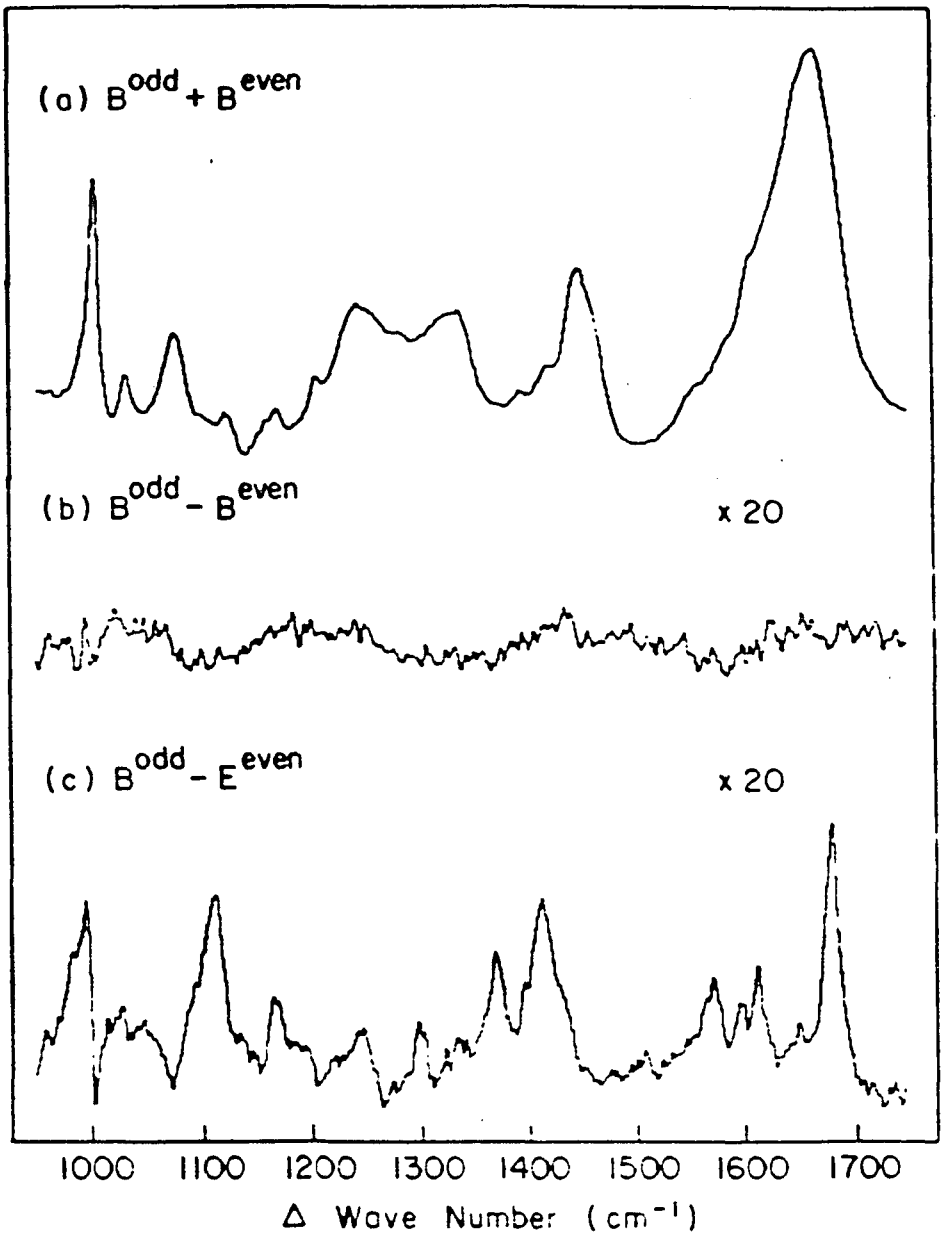
(a) $B^{odd} + B^{even}$
(b) $B^{odd} - B^{even}$
x 20
(c) $B^{odd} - E^{even}$
x 20
1000
1100
1200
1300
1400
1500
1600
1700
Δ Wave Number (cm^{-1})

2.3

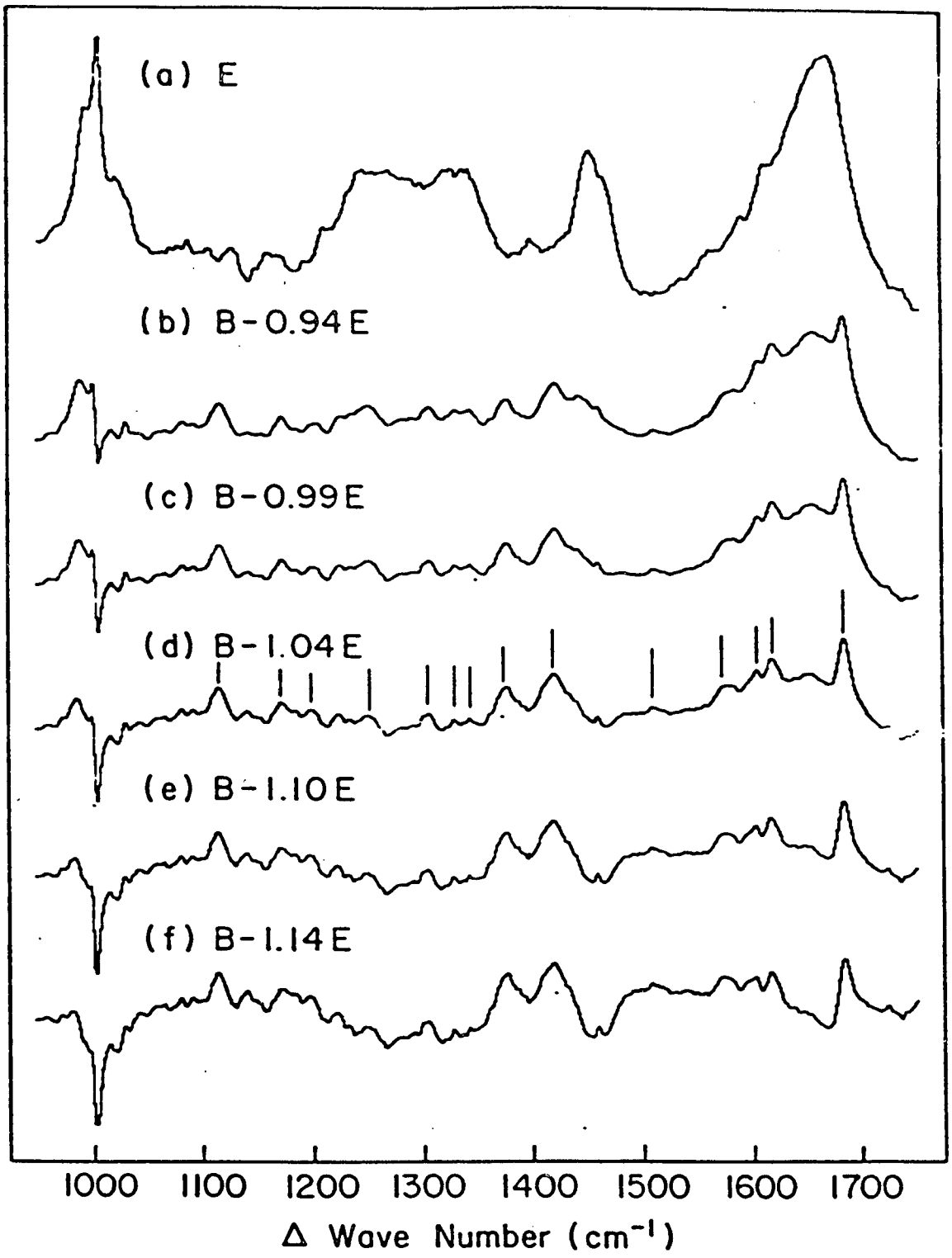
(a) E
(b) B-0.94E
(c) B-0.99E
(d) B-1.04E
(e) B-1.10E
(f) B-1.14E
1000
1100
1200
1300
1400
1500
1600
1700
Δ Wave Number (cm⁻¹)

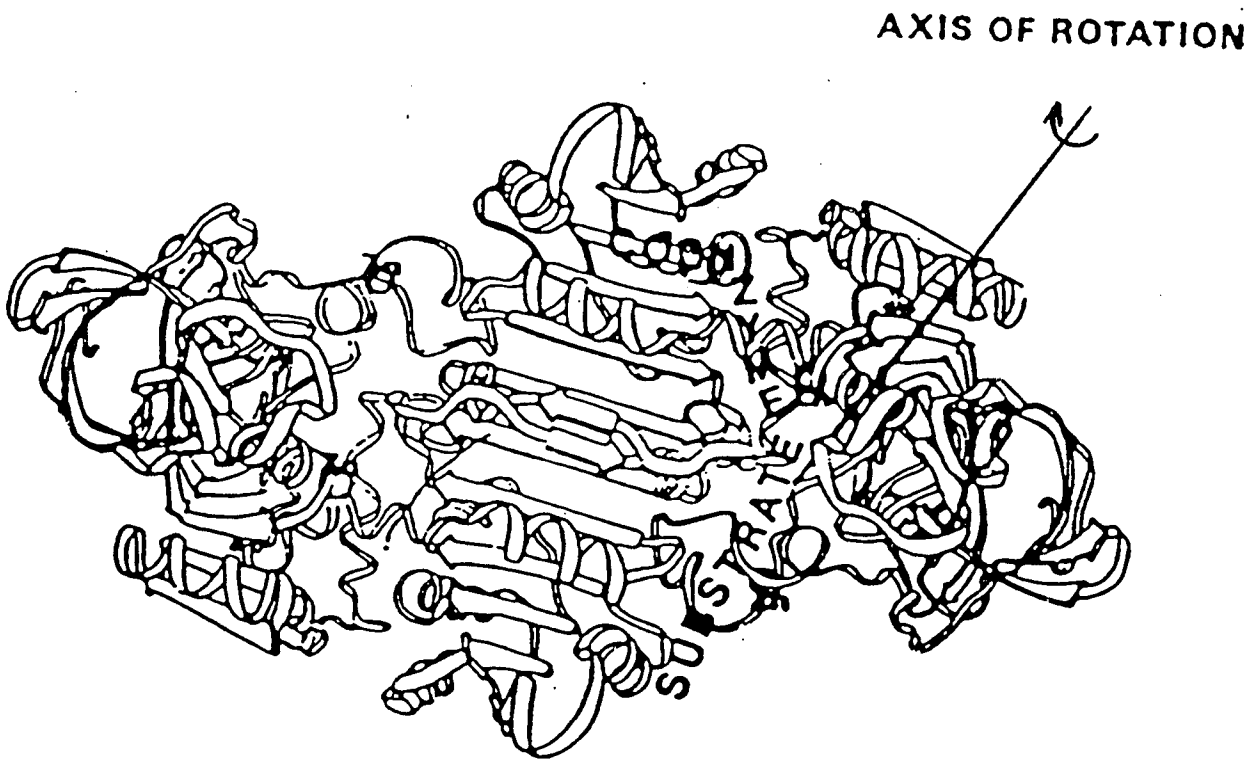

3.1

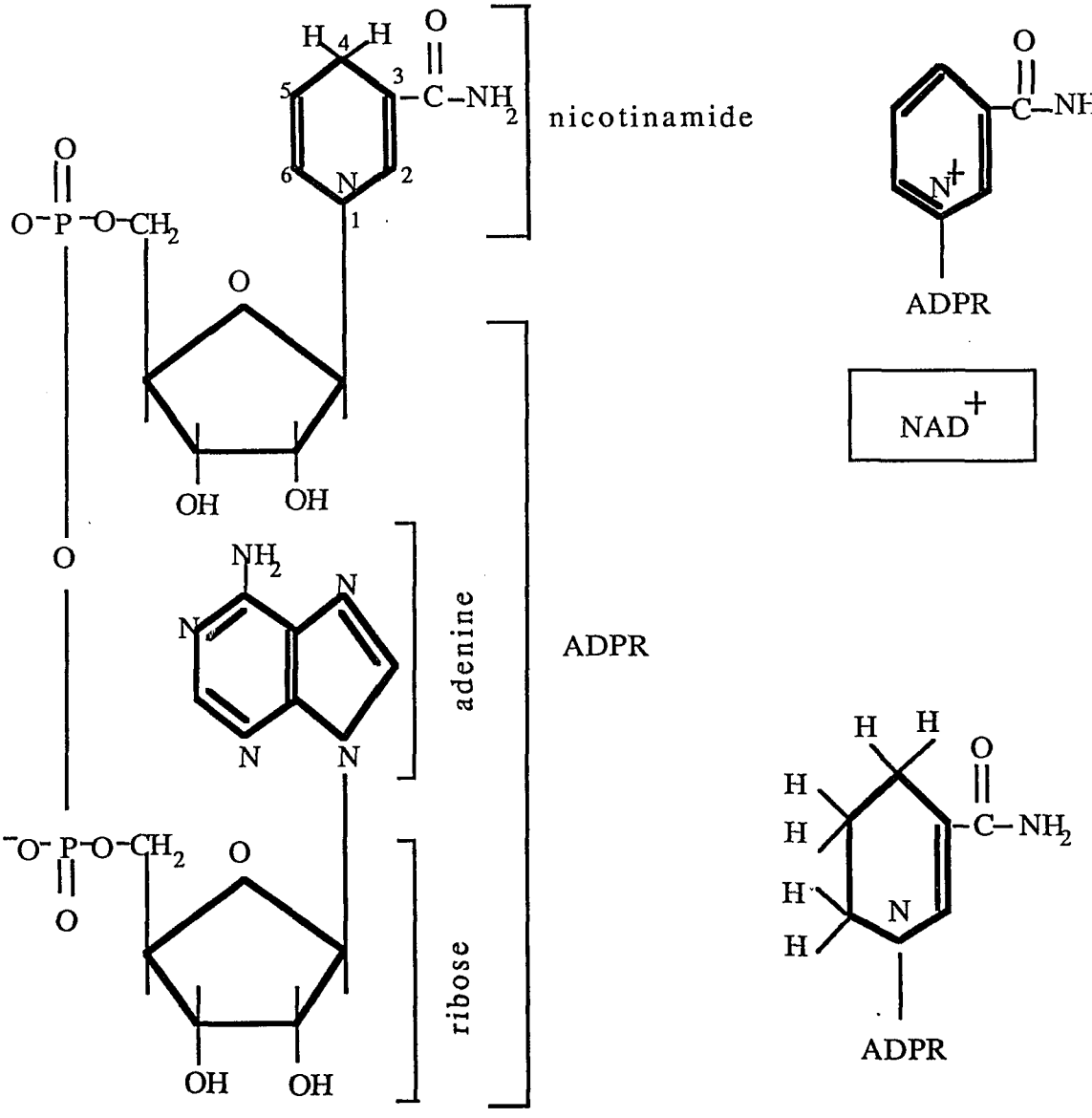
nicotinamide
adenine
ribose
ADPR
ADPR
ADPR
NAD+
NADH
H2NADH

3.2

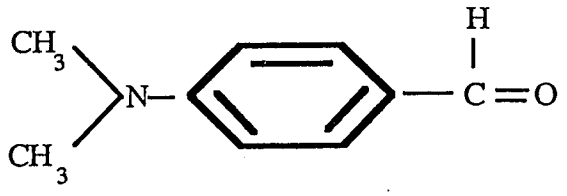

—DABA(CHO)

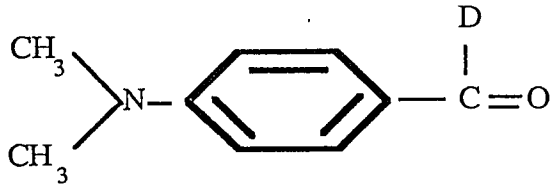

—DABA(CDO)

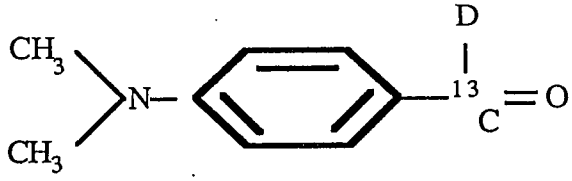

—DABA(^{13}C+D)

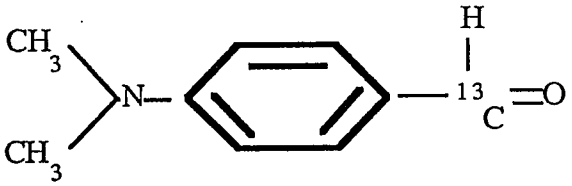

— DABA(^{13}C)

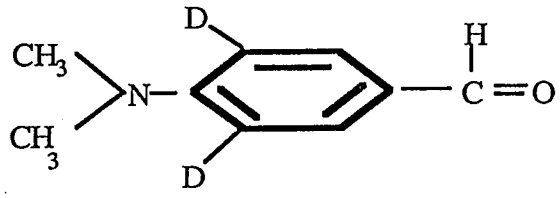

—DABA(^{2}D)

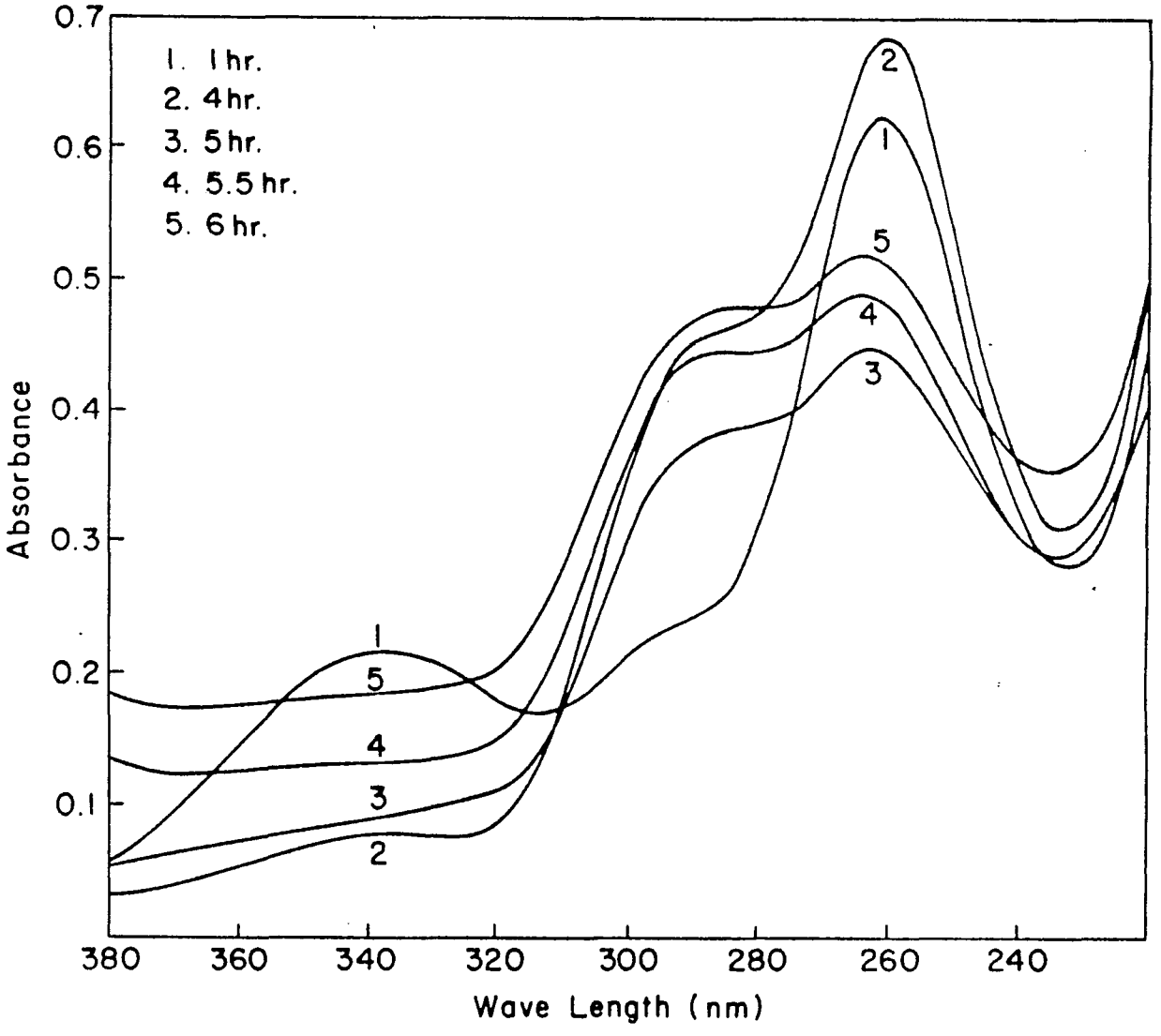
1. 1 hr.
2. 4 hr.
3. 5 hr.
4. 5.5 hr.
5. 6 hr.
Absorbance
0.7
0.6
0.5
0.4
0.3
0.2
0.1
380
360
340
320
300
280
260
240
Wave Length (nm)

3.4

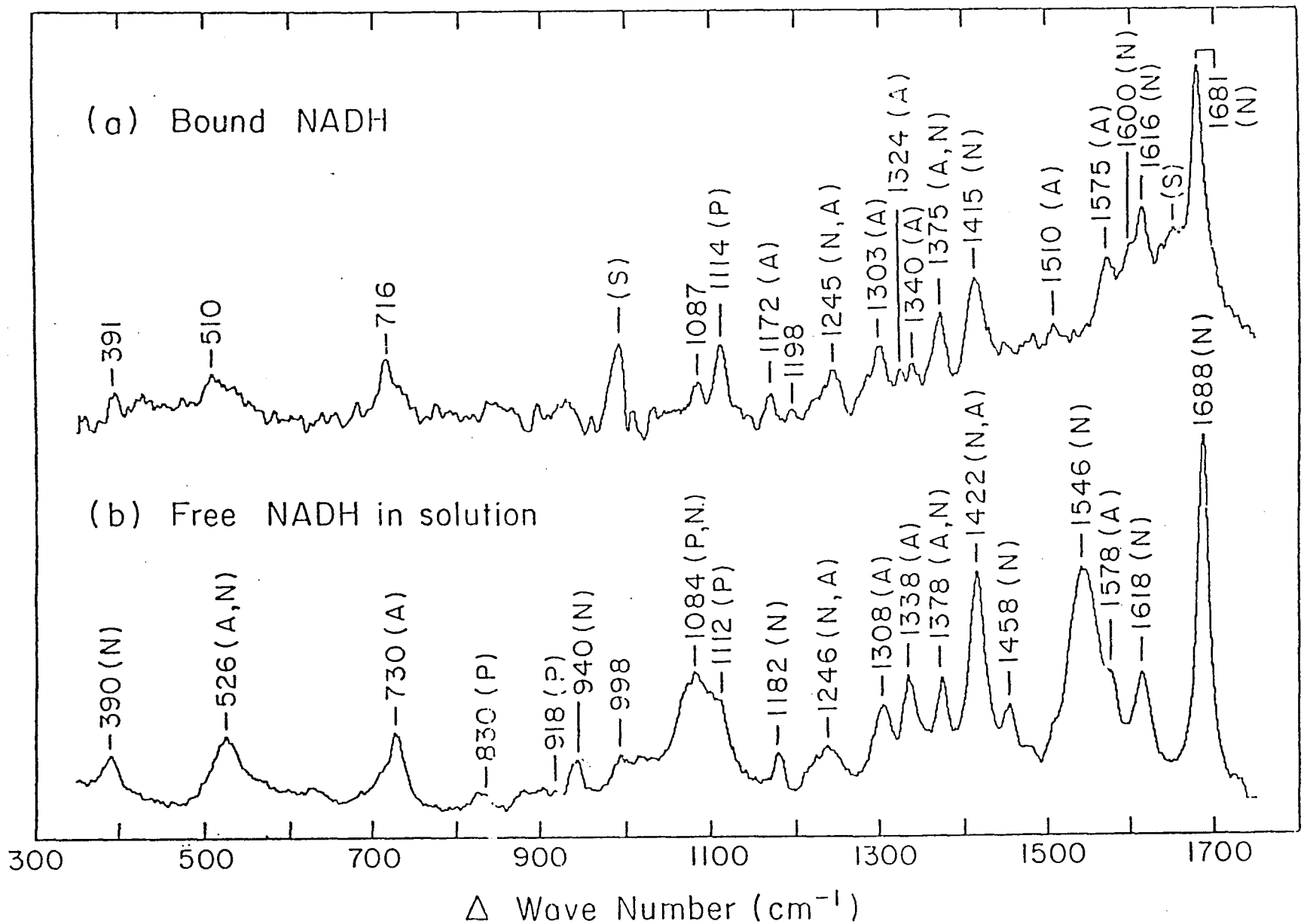
(a) Bound NADH
391
510
716
(S)
1087
1114 (P)
1172 (A)
1198
1245 (N,A)
1303 (A)
1324 (A)
1340 (A)
1375 (A,N)
1415 (N)
1510 (A)
1575 (A)
1600 (N)
1616 (N)
(S)
1681 (N)
(b) Free NADH in solution
390 (N)
526 (A,N)
730 (A)
830 (P)
918 (P)
940 (N)
998
1084 (P,N)
1112 (P)
1182 (N)
1246 (N, A)
1308 (A)
1338 (A)
1378 (A,N)
1422 (N,A)
1458 (N)
1546 (N)
1578 (A)
1618 (N)
1688 (N)
300
500
700
900
1100
1300
1500
1700
Δ Wave Number (cm⁻¹)

4.1

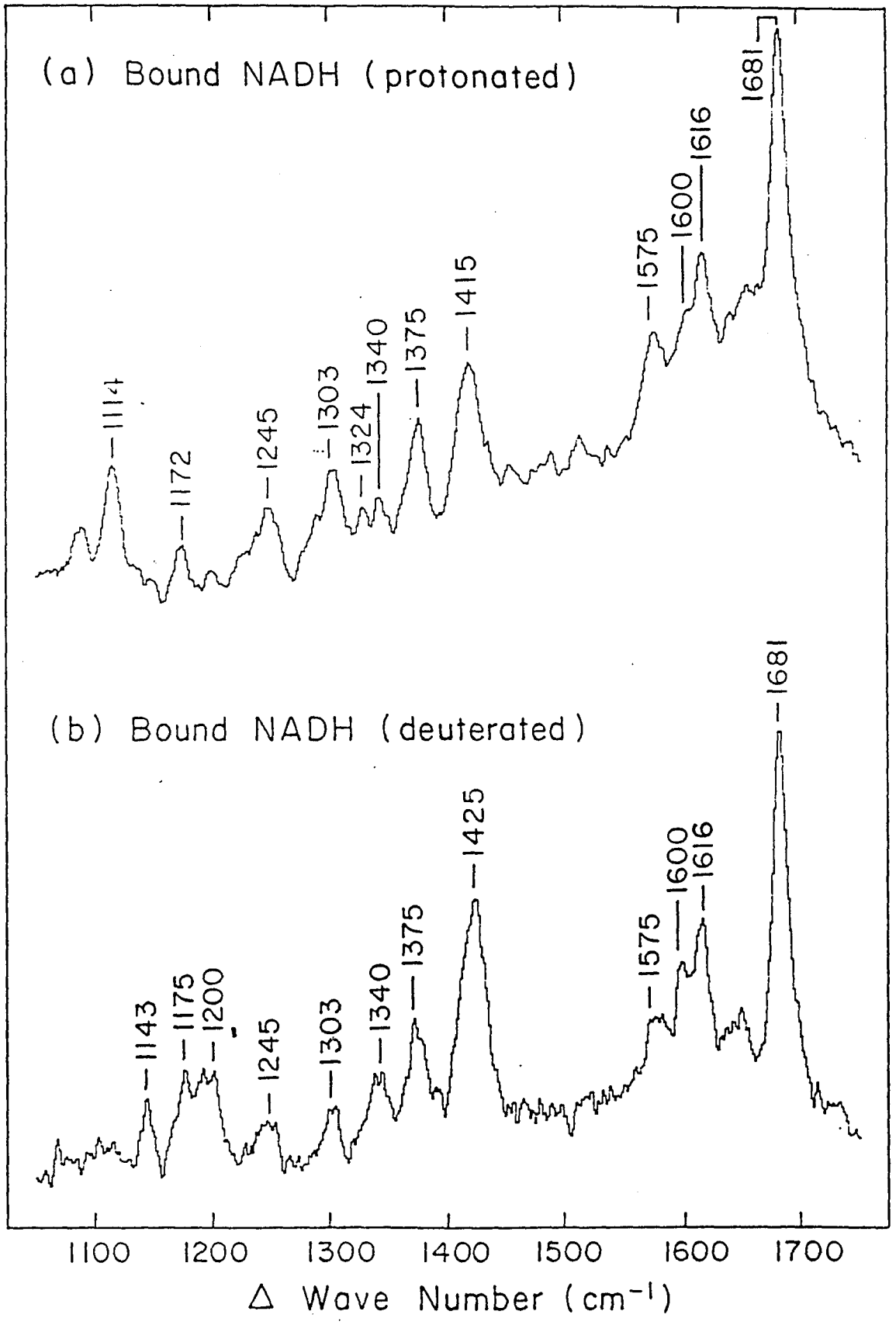
(a) Bound NADH (protonated)
1114
1172
1245
1303
1324
1340
1375
1415
1575
1600
1616
1681
(b) Bound NADH (deuterated)
1143
1175
1200
1245
1303
1340
1375
1425
1575
1600
1616
1681
1100
1200
1300
1400
1500
1600
1700
Δ Wave Number (cm⁻¹)

4.2

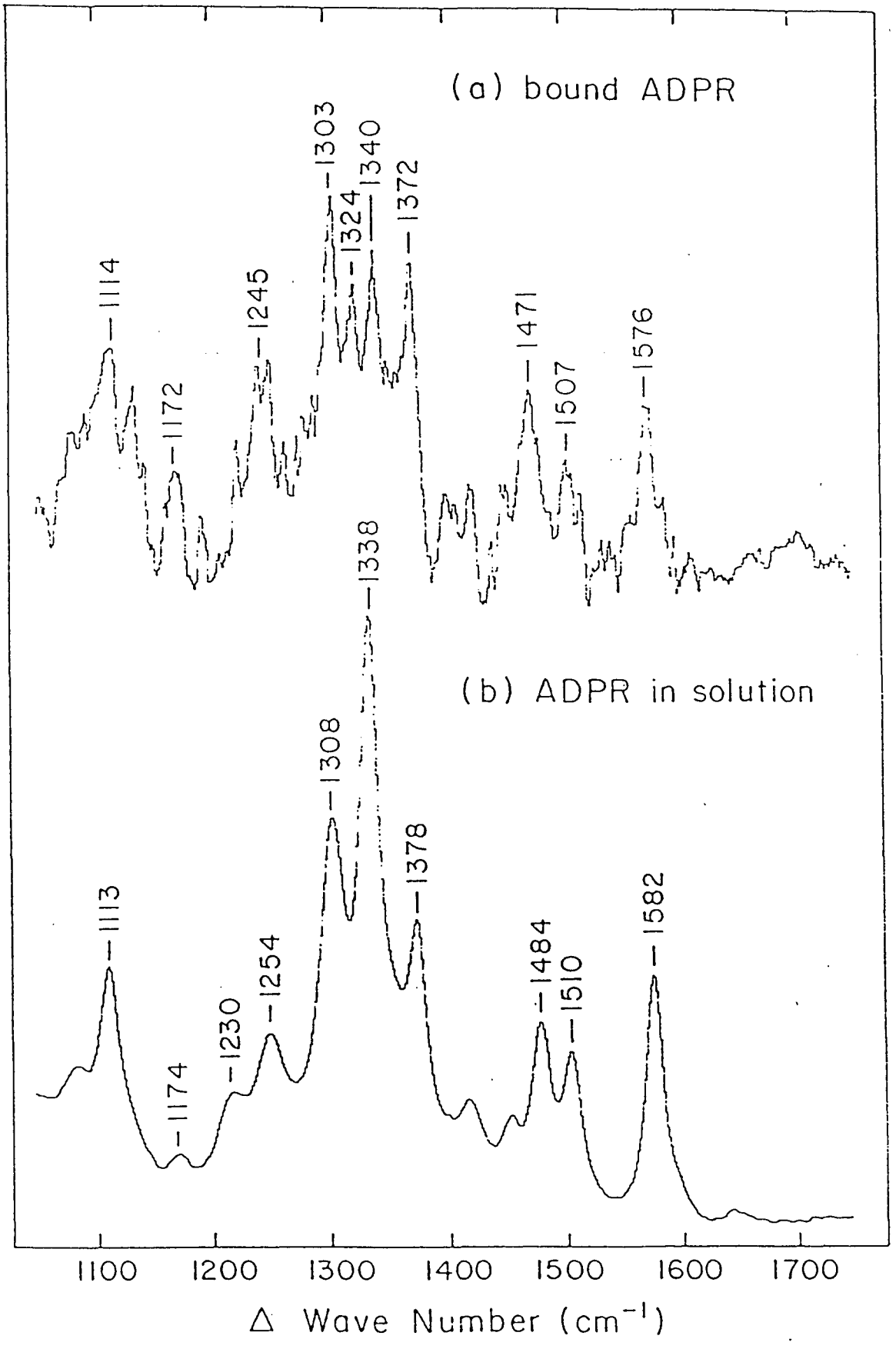
(a) bound ADPR
1114
1172
1245
1303
1324
1340
1372
1471
1507
1576
1338
(b) ADPR in solution
1113
1174
1230
1254
1308
1378
1484
1510
1582
1100
1200
1300
1400
1500
1600
1700
Δ Wave Number (cm⁻¹)

4.3

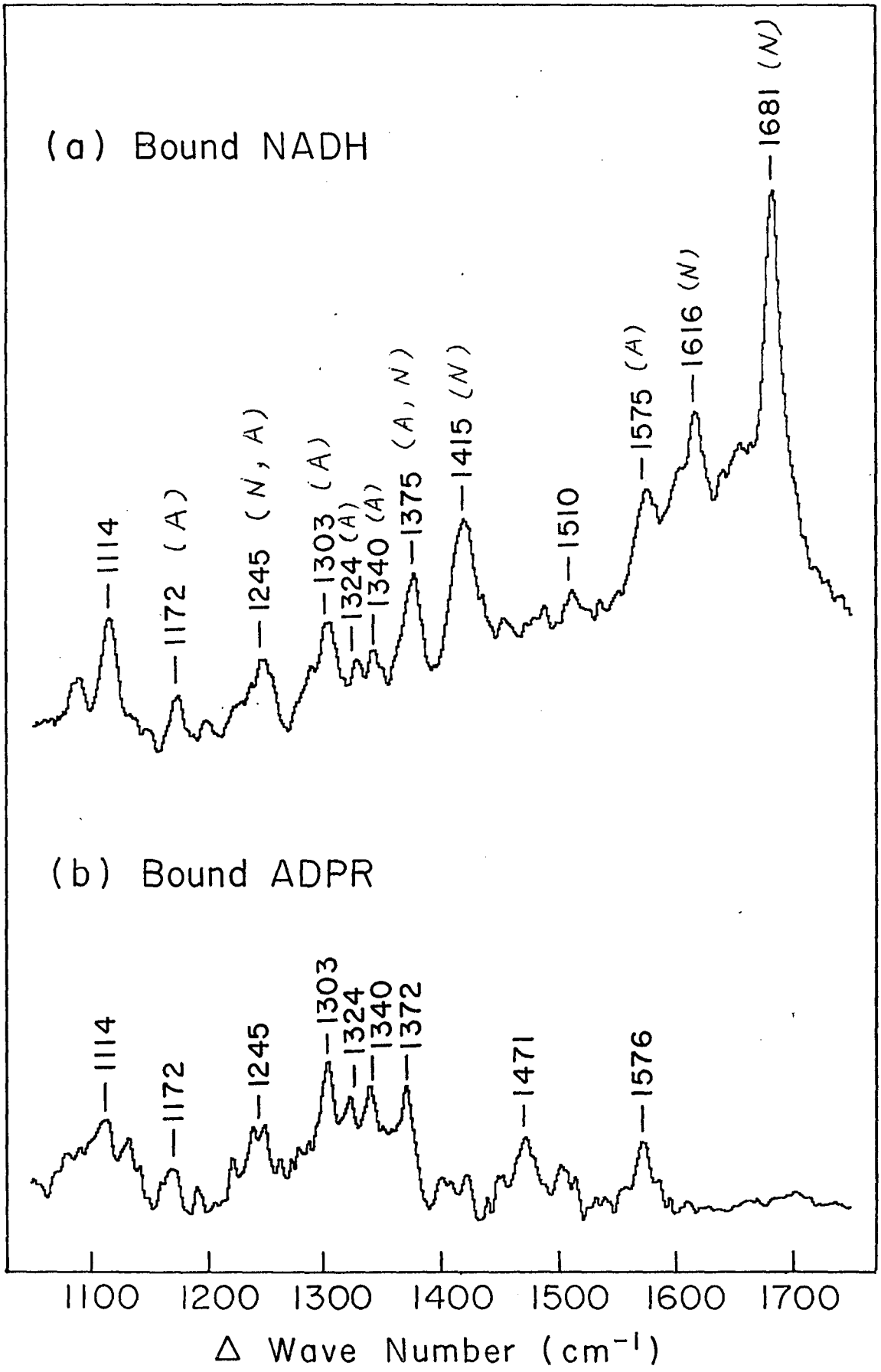
(a) Bound NADH
1114
1172 (A)
1245 (N, A)
1303 (A)
1324 (A)
1340 (A)
1375 (A, N)
1415 (N)
1510
1575 (A)
1616 (N)
1681 (N)
(b) Bound ADPR
1114
1172
1245
1303
1324
1340
1372
1471
1576
1100
1200
1300
1400
1500
1600
1700
Δ Wave Number (cm⁻¹)

4.4

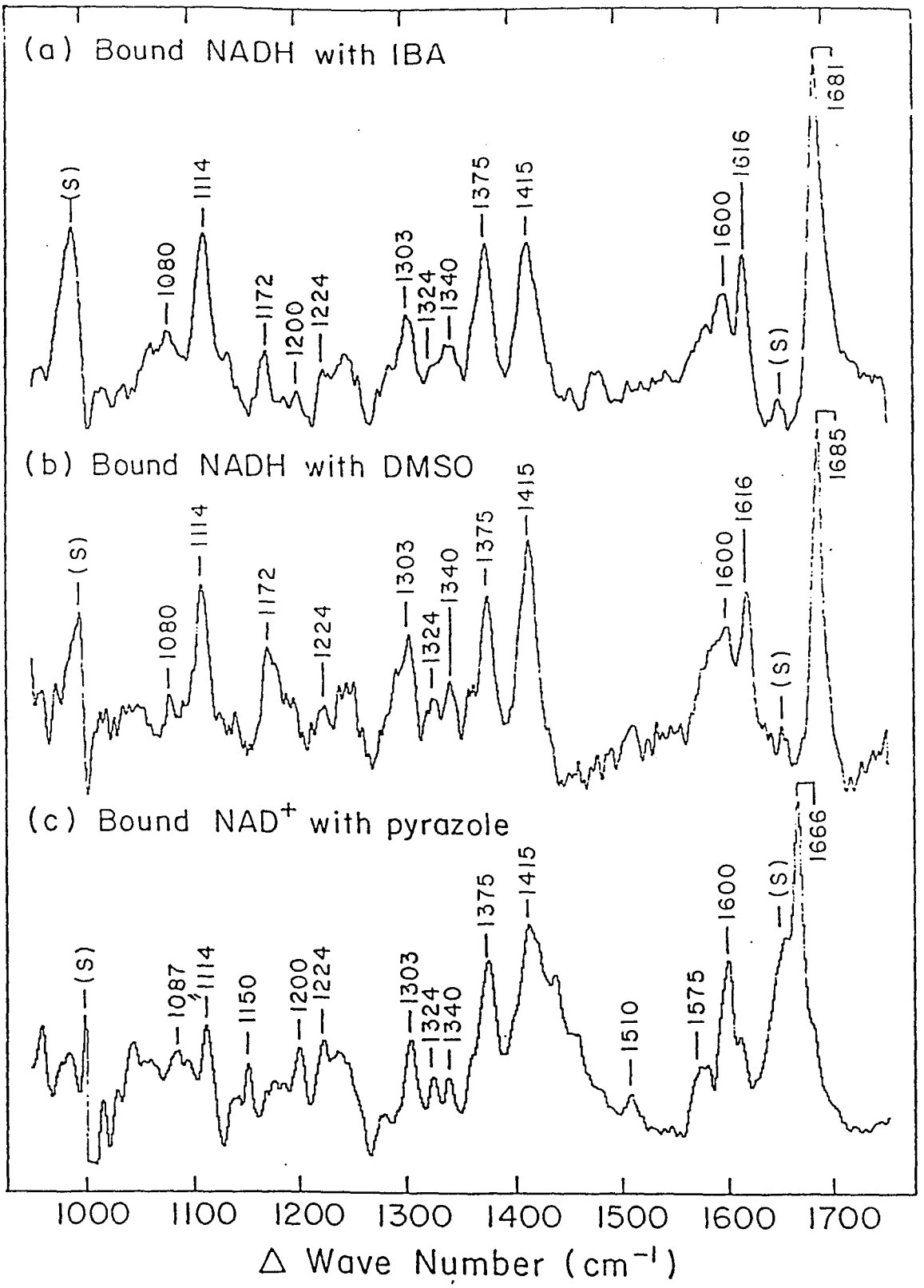
(a) Bound NADH with IBA
(S)
1080
1114
1172
1200
1224
1303
1324
1340
1375
1415
1600
1616
(S)
1681
(b) Bound NADH with DMSO
(S)
1080
1114
1172
1224
1303
1324
1340
1375
1415
1600
1616
(S)
1685
(c) Bound NAD+ with pyrazole
(S)
1087
1114
1150
1200
1224
1303
1324
1340
1375
1415
1510
1575
1600
(S)
1666
1000
1100
1200
1300
1400
1500
1600
1700
Δ Wave Number (cm⁻¹)

4.5

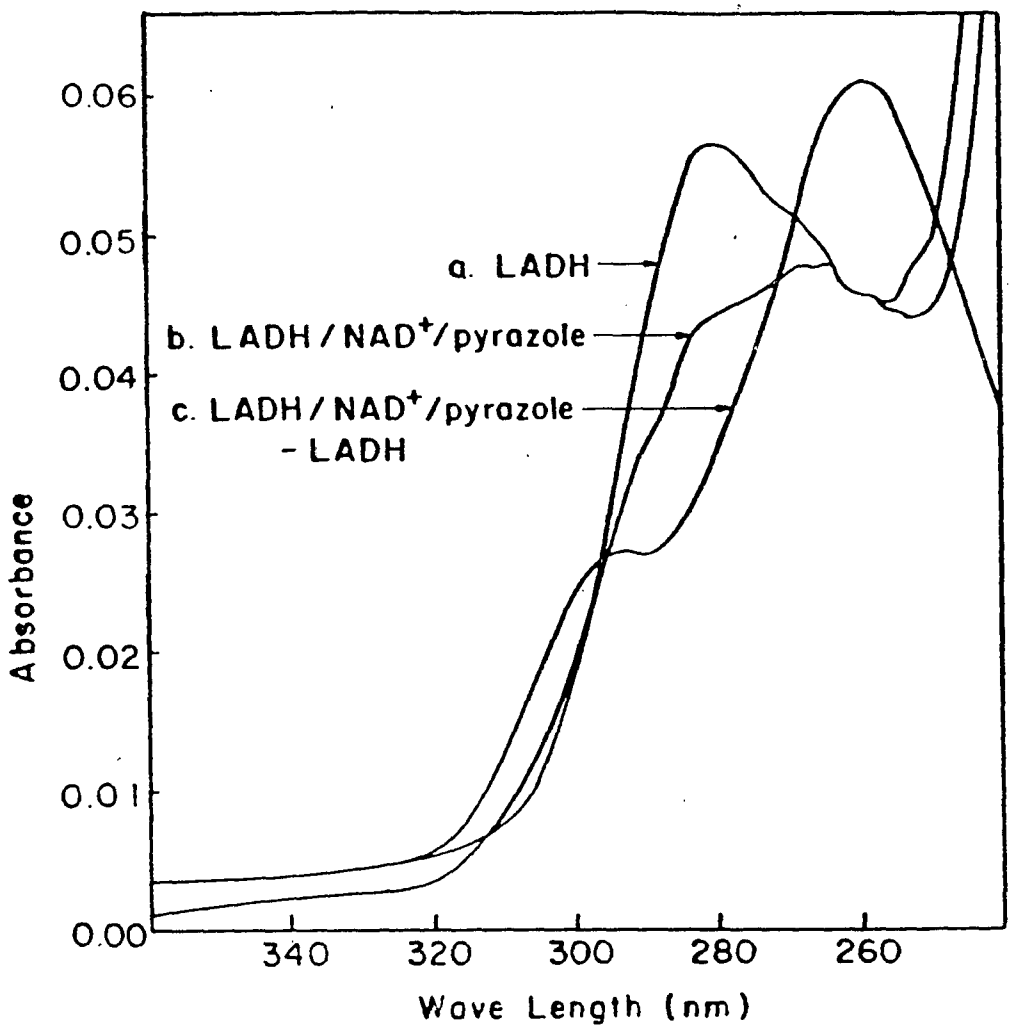
0.06
0.05
0.04
0.03
0.02
0.01
0.00
Absorbance
a. LADH
b. LADH / NAD+/pyrazole
c. LADH / NAD+/pyrazole
- LADH
340
320
300
280
260
Wave Length (nm)

4.6

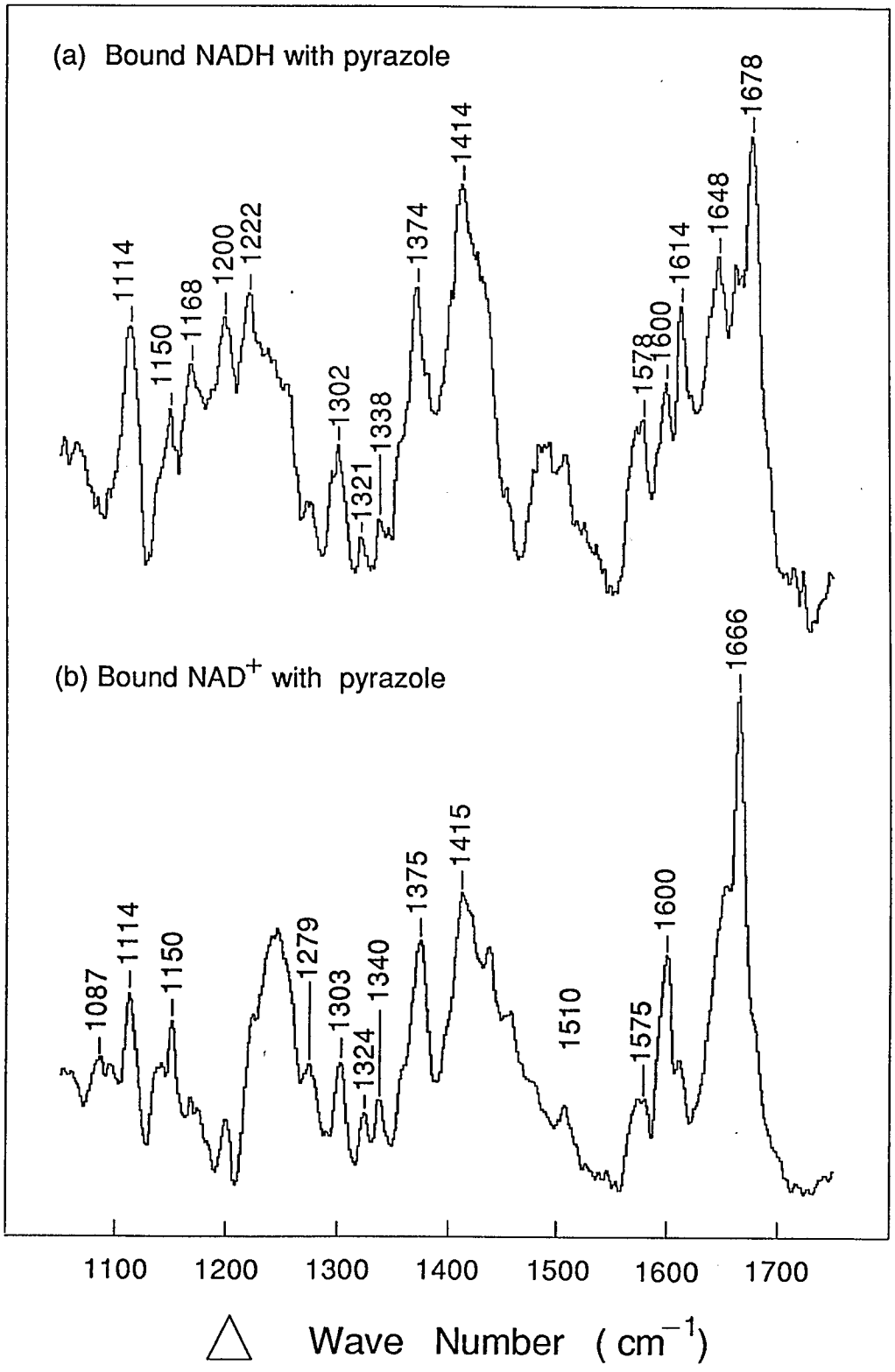
(a) Bound NADH with pyrazole
1114
1150
1168
1200
1222
1302
1321
1338
1374
1414
1578
1600
1614
1648
1678
(b) Bound NAD+ with pyrazole
1087
1114
1150
1279
1303
1324
1340
1375
1415
1510
1575
1600
1666
1100
1200
1300
1400
1500
1600
1700
Wave Number (cm−1)

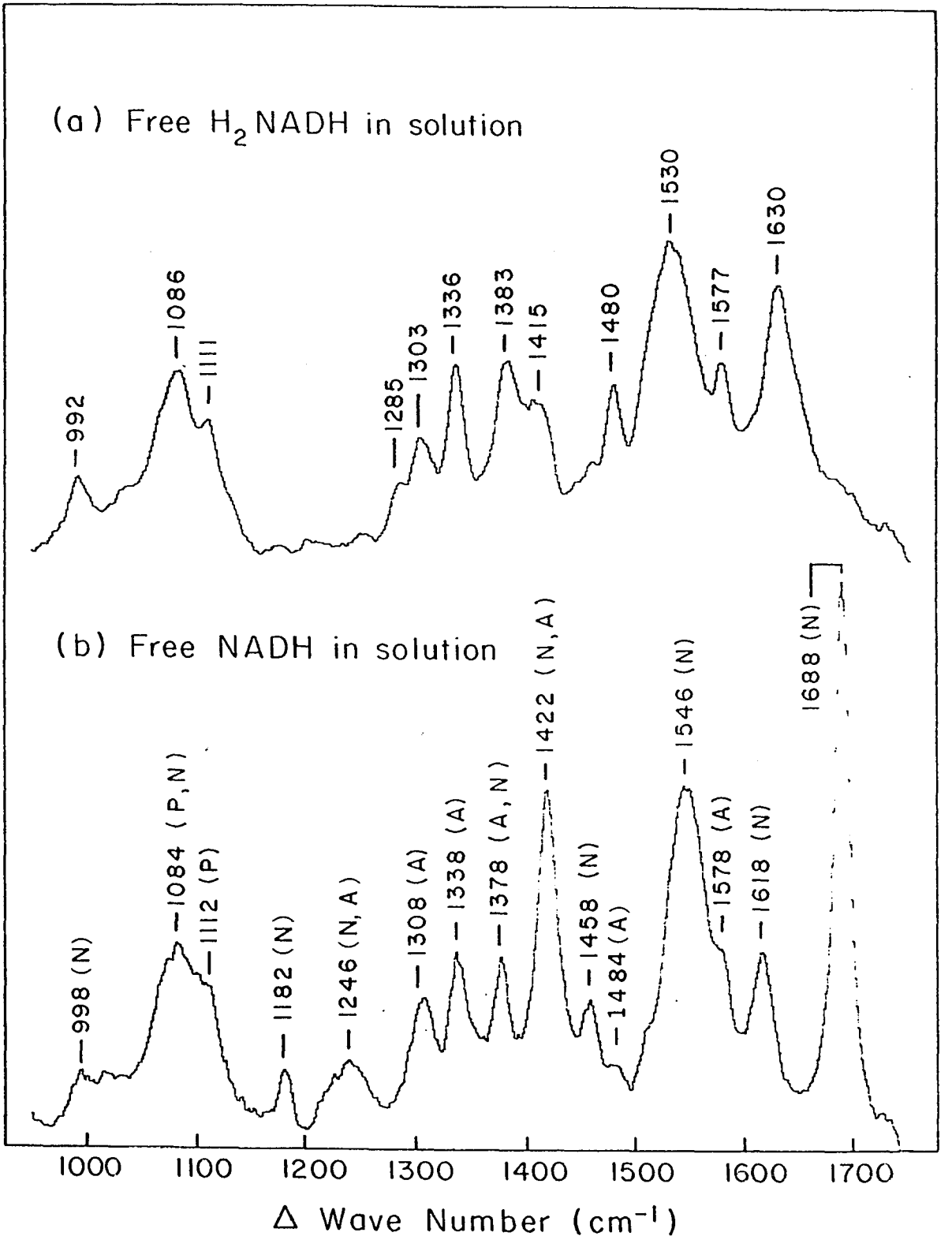
(a) Free H_2NADH in solution
992
1086
1111
1285
1303
1336
1383
1415
1480
1530
1577
1630
(b) Free NADH in solution
998 (N)
1084 (P,N)
1112 (P)
1182 (N)
1246 (N,A)
1308 (A)
1338 (A)
1378 (A,N)
1422 (N,A)
1458 (N)
1484 (A)
1546 (N)
1578 (A)
1618 (N)
1688 (N)
1000
1100
1200
1300
1400
1500
1600
1700
Δ Wave Number (cm^{-1})

4.8

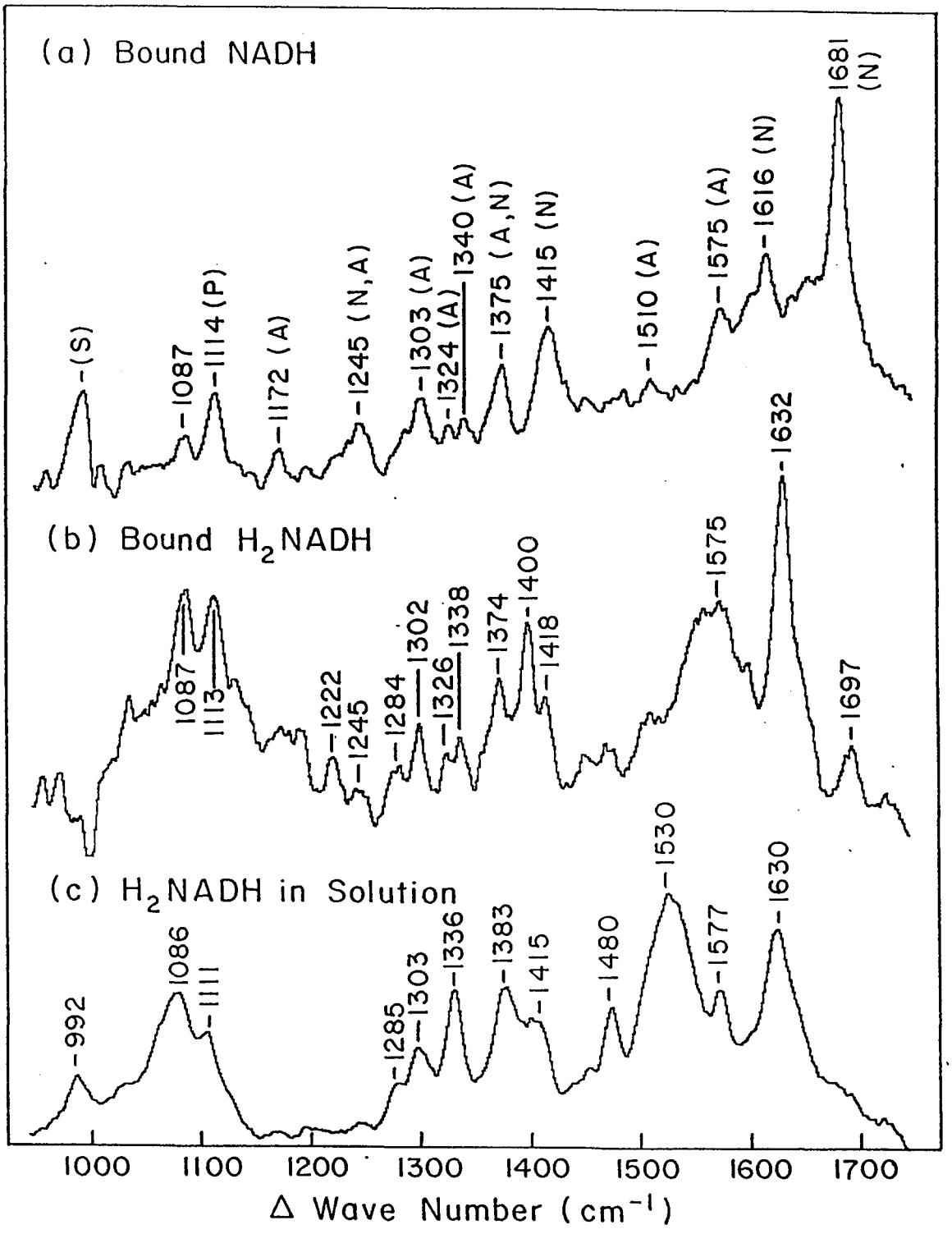
(a) Bound NADH
-(S)
-1087
-1114 (P)
-1172 (A)
-1245 (N,A)
-1303 (A)
-1324 (A)
1340 (A)
-1375 (A,N)
-1415 (N)
-1510 (A)
-1575 (A)
-1616 (N)
1681 (N)
(b) Bound H_2NADH
1087
1113
-1222
-1245
-1284
1302
-1326
1338
-1374
-1400
-1418
-1575
-1632
-1697
(c) H_2NADH in Solution
-992
1086
-1111
-1285
-1303
-1336
-1383
-1415
-1480
-1530
-1577
-1630
1000
1100
1200
1300
1400
1500
1600
1700
Δ Wave Number (cm^{-1})

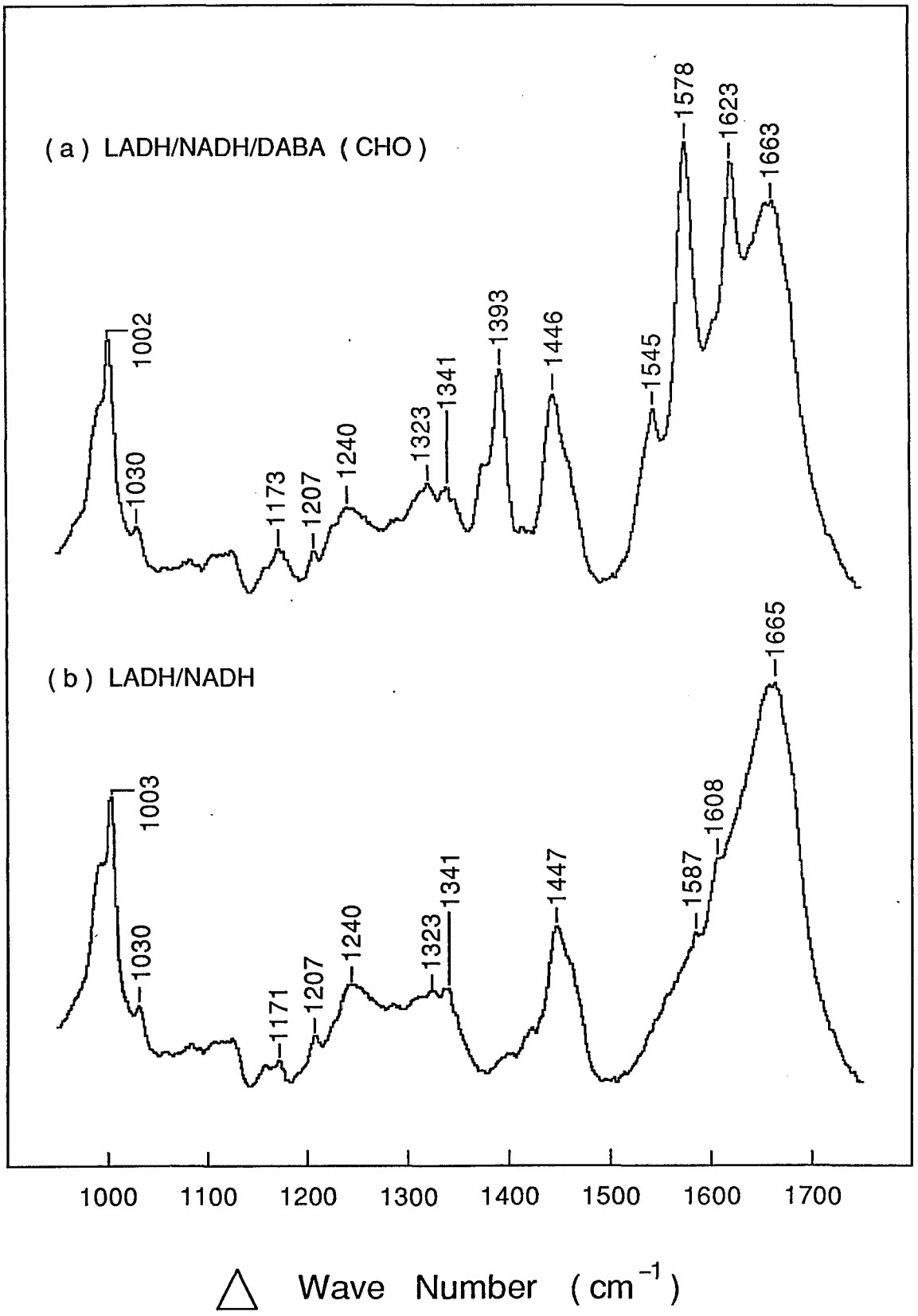
(a) LADH/NADH/DABA (CHO)
1002
1030
1173
1207
1240
1323
1341
1393
1446
1545
1578
1623
1663
(b) LADH/NADH
1003
1030
1171
1207
1240
1323
1341
1447
1587
1608
1665
1000
1100
1200
1300
1400
1500
1600
1700
△ Wave Number (cm⁻¹)

5.1

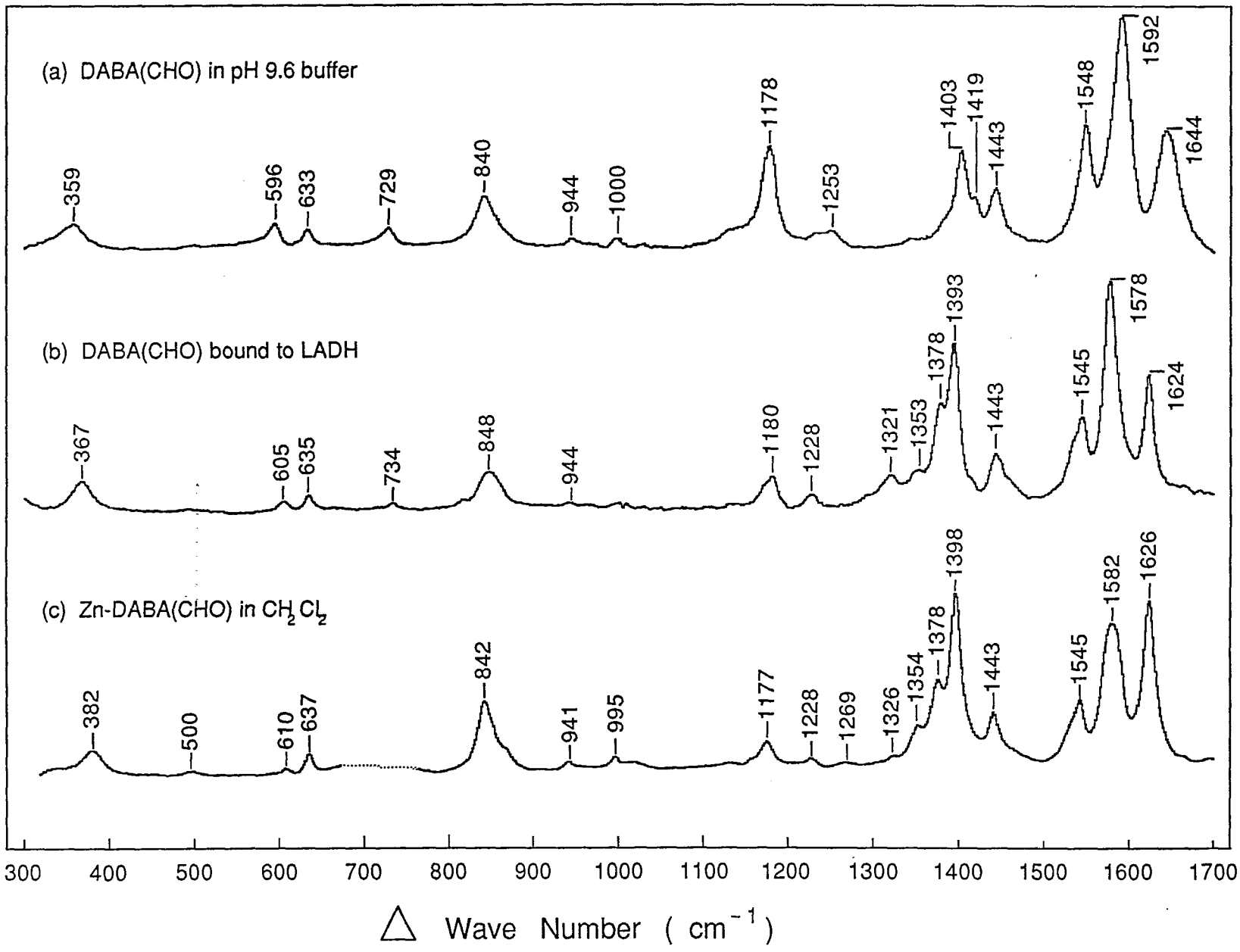
(a) DABA(CHO) in pH 9.6 buffer
359
596
633
729
840
944
1000
1178
1253
1403
1419
1443
1548
1592
1644
(b) DABA(CHO) bound to LADH
367
605
635
734
848
944
1180
1228
1321
1353
1378
1393
1443
1545
1578
1624
(c) Zn-DABA(CHO) in CH2 Cl2
382
500
610
637
842
941
995
1177
1228
1269
1326
1354
1378
1398
1443
1545
1582
1626
300
400
500
600
700
800
900
1000
1100
1200
1300
1400
1500
1600
1700
△ Wave Number (cm-1)

5.2

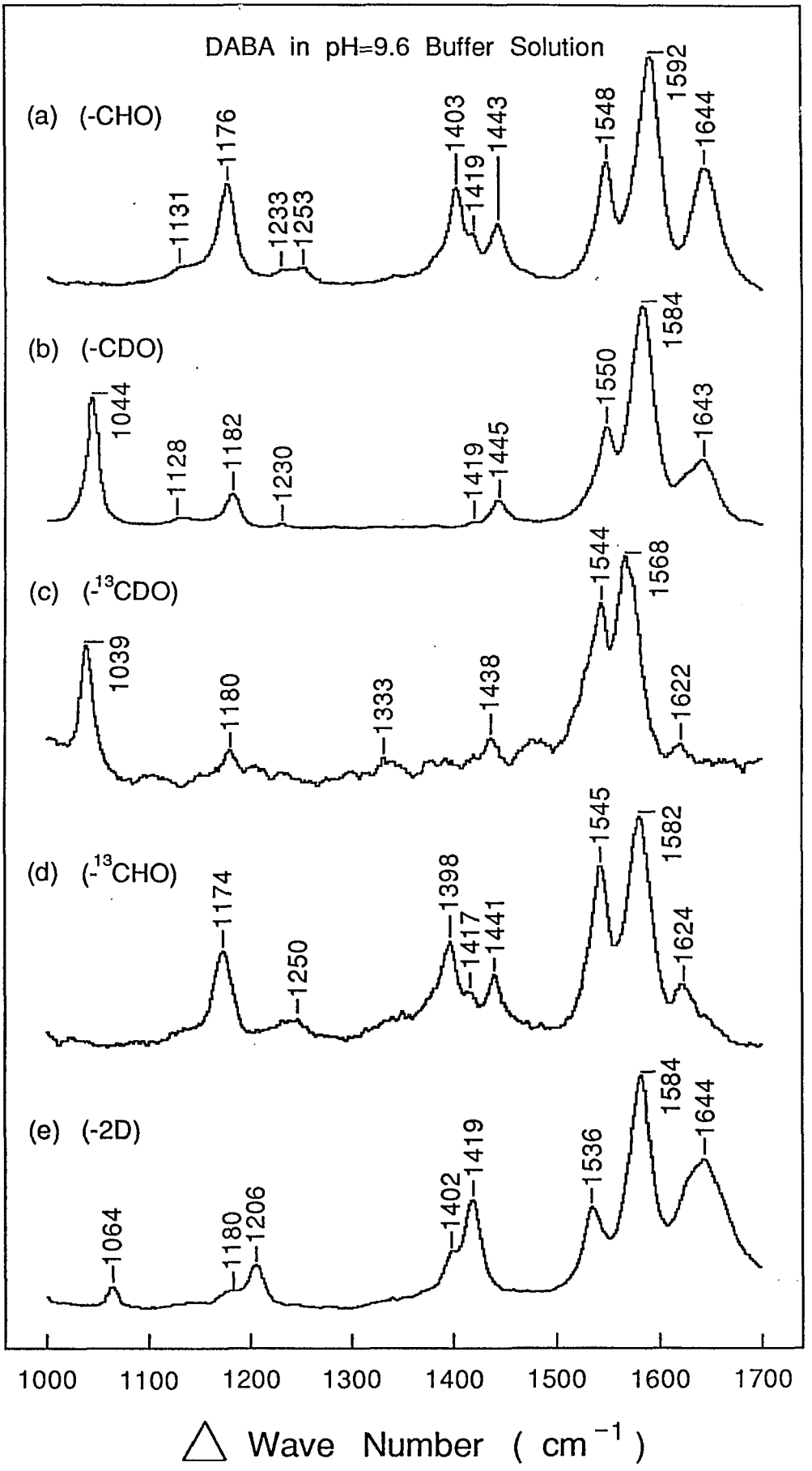
DABA in pH=9.6 Buffer Solution
(a) (-CHO)
1131
1176
1233
1253
1403
1419
1443
1548
1592
1644
(b) (-CDO)
1044
1128
1182
1230
1419
1445
1550
1584
1643
(c) (-13CDO)
1039
1180
1333
1438
1544
1568
1622
(d) (-13CHO)
1174
1250
1398
1417
1441
1545
1582
1624
(e) (-2D)
1064
1180
1206
1402
1419
1536
1584
1644
1000
1100
1200
1300
1400
1500
1600
1700
△ Wave Number (cm-1)

5.3

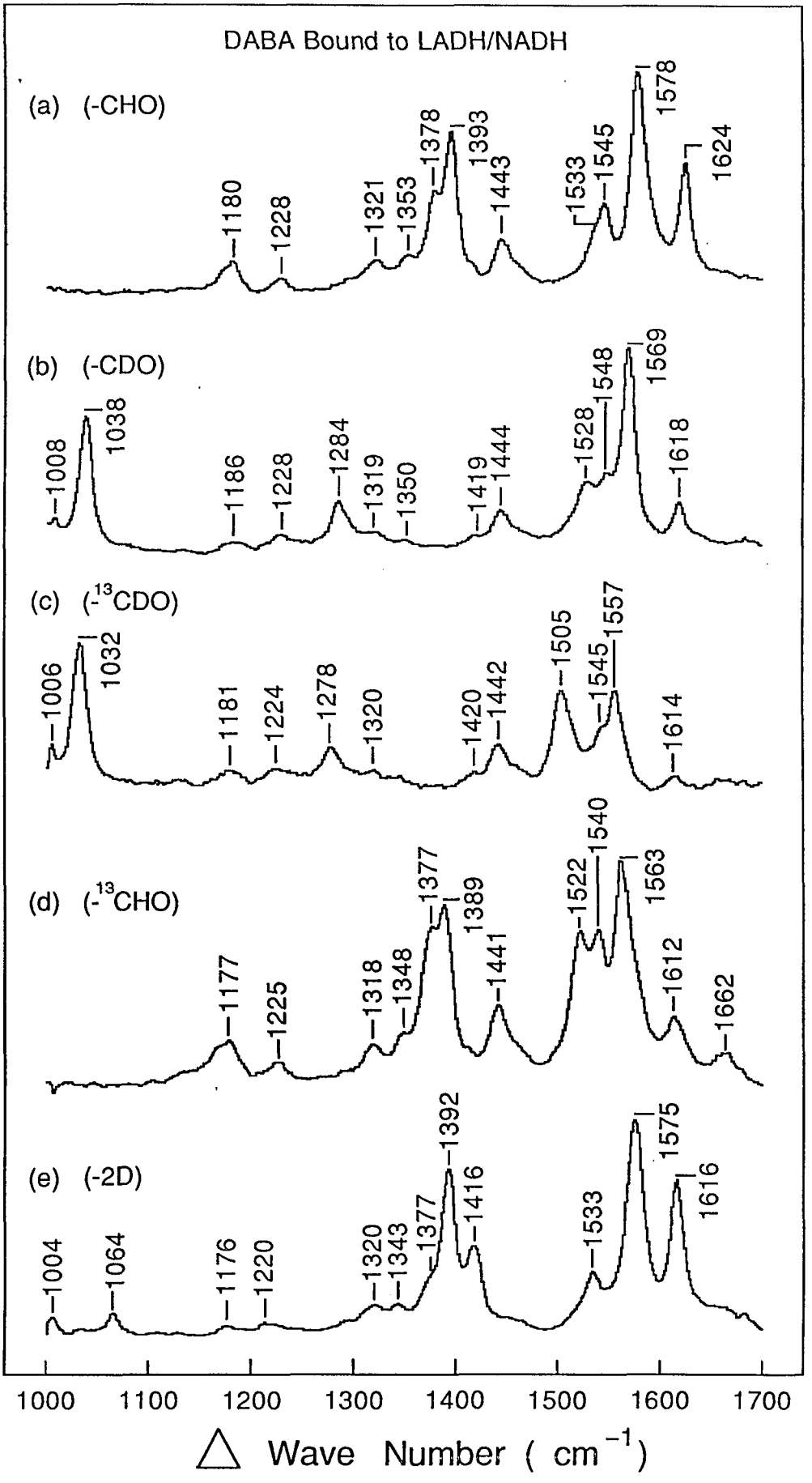
DABA Bound to LADH/NADH
(a) (-CHO)
1180
1228
1321
1353
1378
1393
1443
1533
1545
1578
1624
(b) (-CDO)
1008
1038
1186
1228
1284
1319
1350
1419
1444
1528
1548
1569
1618
(c) (-13CDO)
1006
1032
1181
1224
1278
1320
1420
1442
1505
1545
1557
1614
(d) (-13CHO)
1177
1225
1318
1348
1377
1389
1441
1522
1540
1563
1612
1662
(e) (-2D)
1004
1064
1176
1220
1320
1343
1377
1392
1416
1533
1575
1616
1000
1100
1200
1300
1400
1500
1600
1700
△ Wave Number (cm-1)

5.4

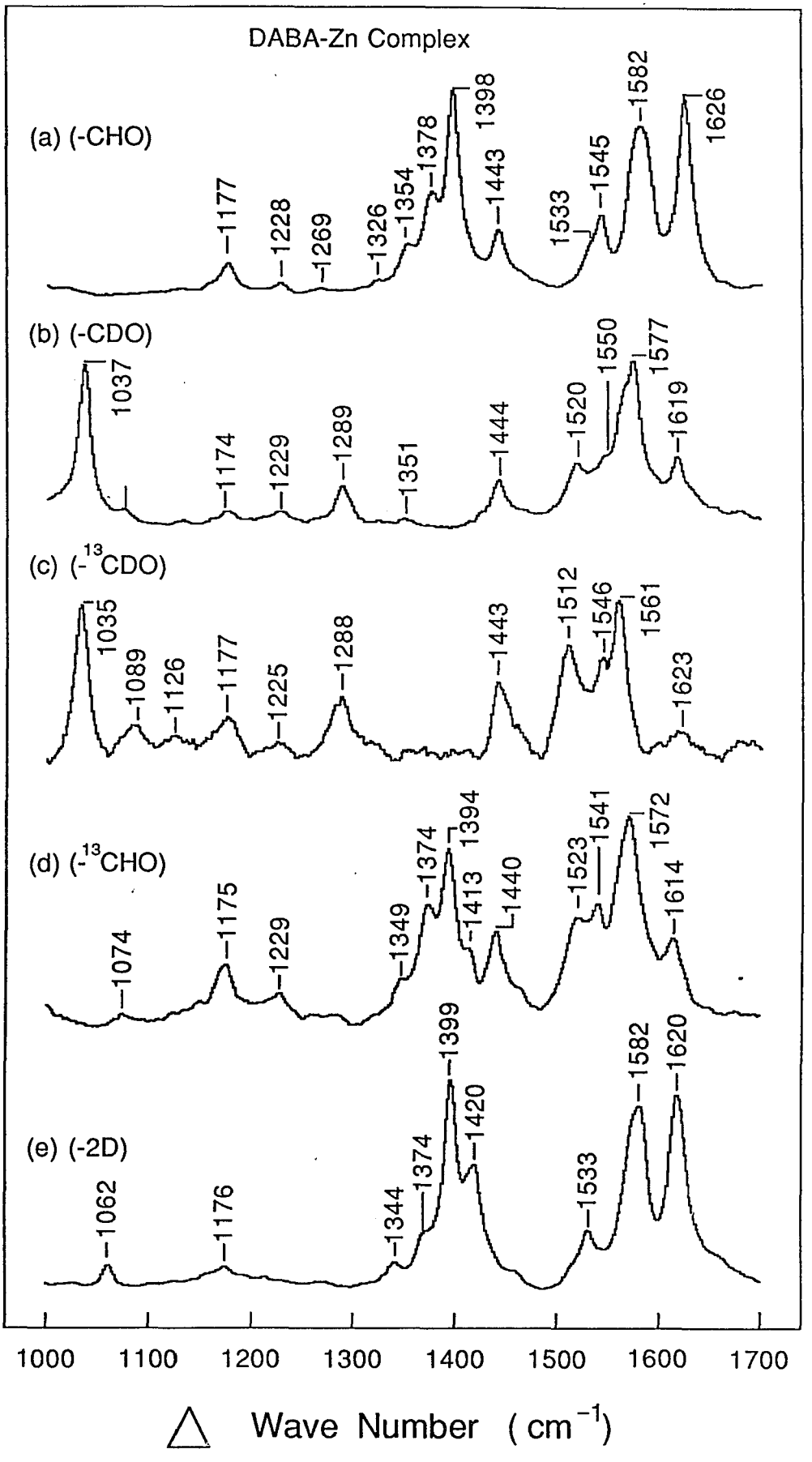
DABA-Zn Complex
(a) (-CHO)
1177
1228
1269
1326
1354
1378
1398
1443
1533
1545
1582
1626
(b) (-CDO)
1037
1174
1229
1289
1351
1444
1520
1550
1577
1619
(c) (-13CDO)
1035
1089
1126
1177
1225
1288
1443
1512
1546
1561
1623
(d) (-13CHO)
1074
1175
1229
1349
1374
1394
1413
1440
1523
1541
1572
1614
(e) (-2D)
1062
1176
1344
1374
1399
1420
1533
1582
1620
1000
1100
1200
1300
1400
1500
1600
1700
Wave Number (cm-1)

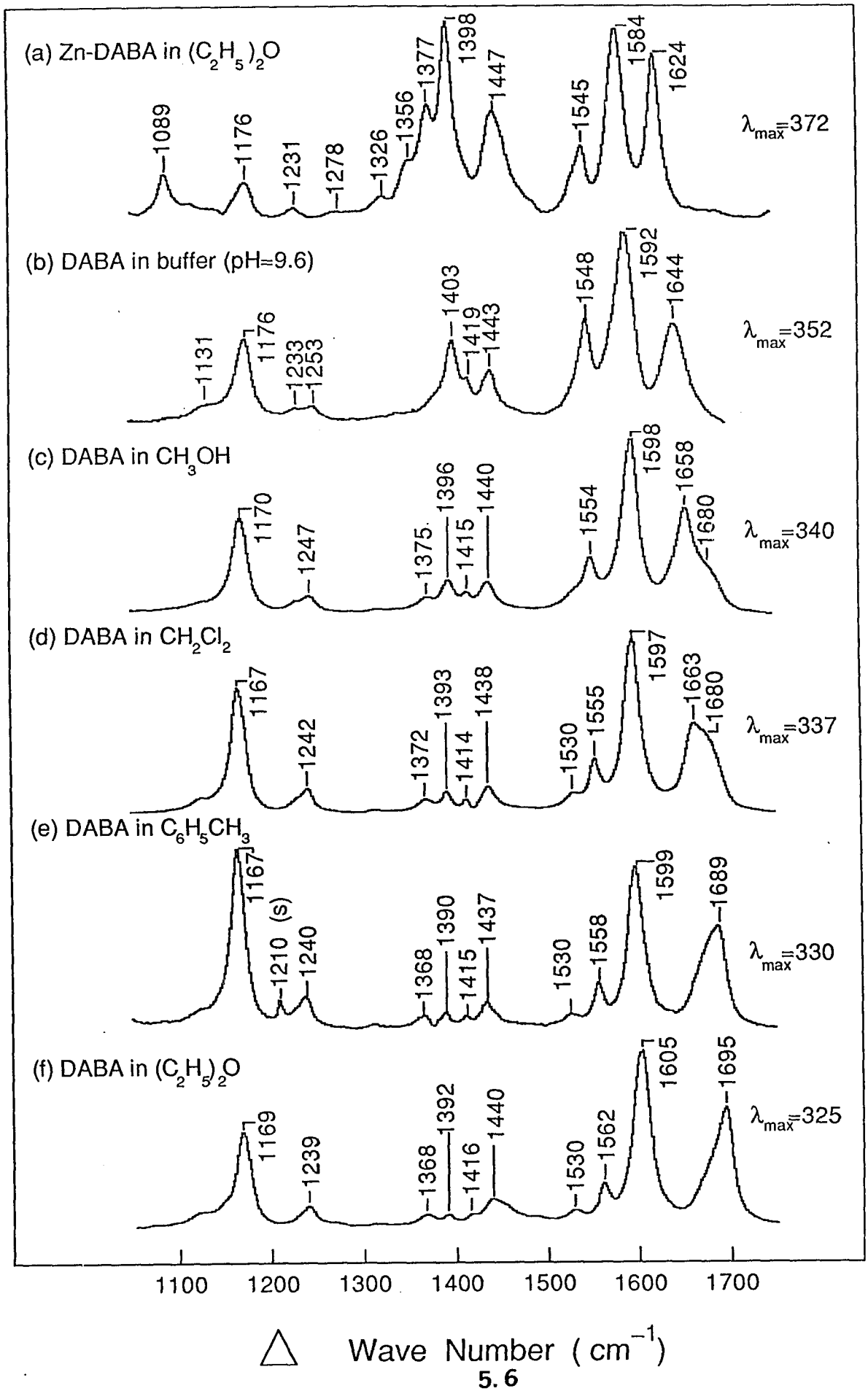
(a) Zn-DABA in $(C_2H_5)_2O$
1089
1176
1231
1278
1326
1356
1377
1398
1447
1545
1584
1624
λ_{max}=372
(b) DABA in buffer (pH=9.6)
1131
1176
1233
1253
1403
1419
1443
1548
1592
1644
λ_{max}=352
(c) DABA in CH_3OH
1170
1247
1375
1396
1415
1440
1554
1598
1658
1680
λ_{max}=340
(d) DABA in CH_2Cl_2
1167
1242
1372
1393
1414
1438
1530
1555
1597
1663
1680
λ_{max}=337
(e) DABA in $C_6H_5CH_3$
1167
1210 (s)
1240
1368
1390
1415
1437
1530
1558
1599
1689
λ_{max}=330
(f) DABA in $(C_2H_5)_2O$
1169
1239
1368
1392
1416
1440
1530
1562
1605
1695
λ_{max}=325
1100
1200
1300
1400
1500
1600
1700
Wave Number (cm^{-1})

5.6

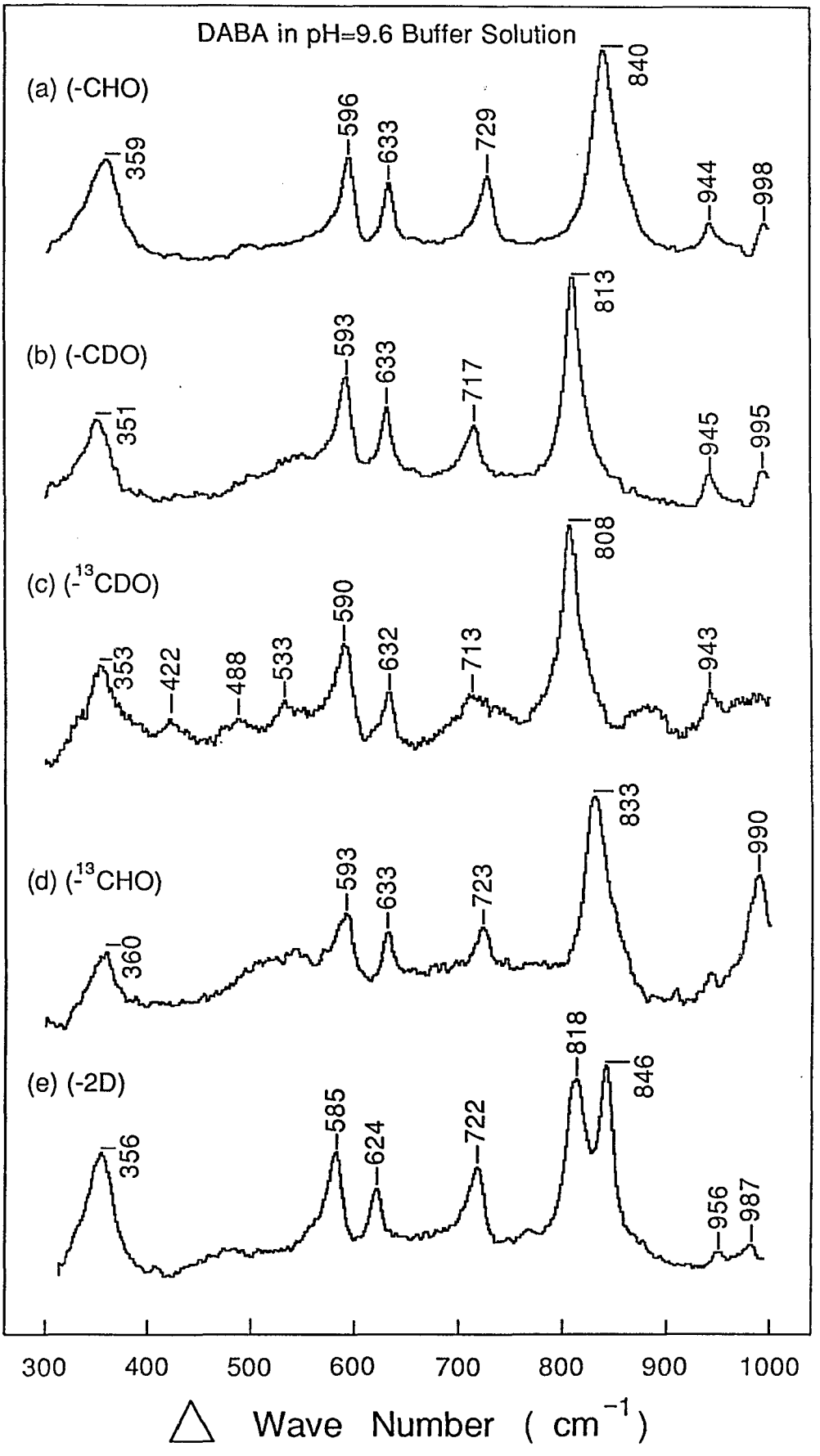
DABA in pH=9.6 Buffer Solution
(a) (-CHO)
359
596
633
729
840
944
998
(b) (-CDO)
351
593
633
717
813
945
995
(c) (-13CDO)
353
422
488
533
590
632
713
808
943
(d) (-13CHO)
360
593
633
723
833
990
(e) (-2D)
356
585
624
722
818
846
956
987
300
400
500
600
700
800
900
1000
Wave Number (cm-1)

5.7

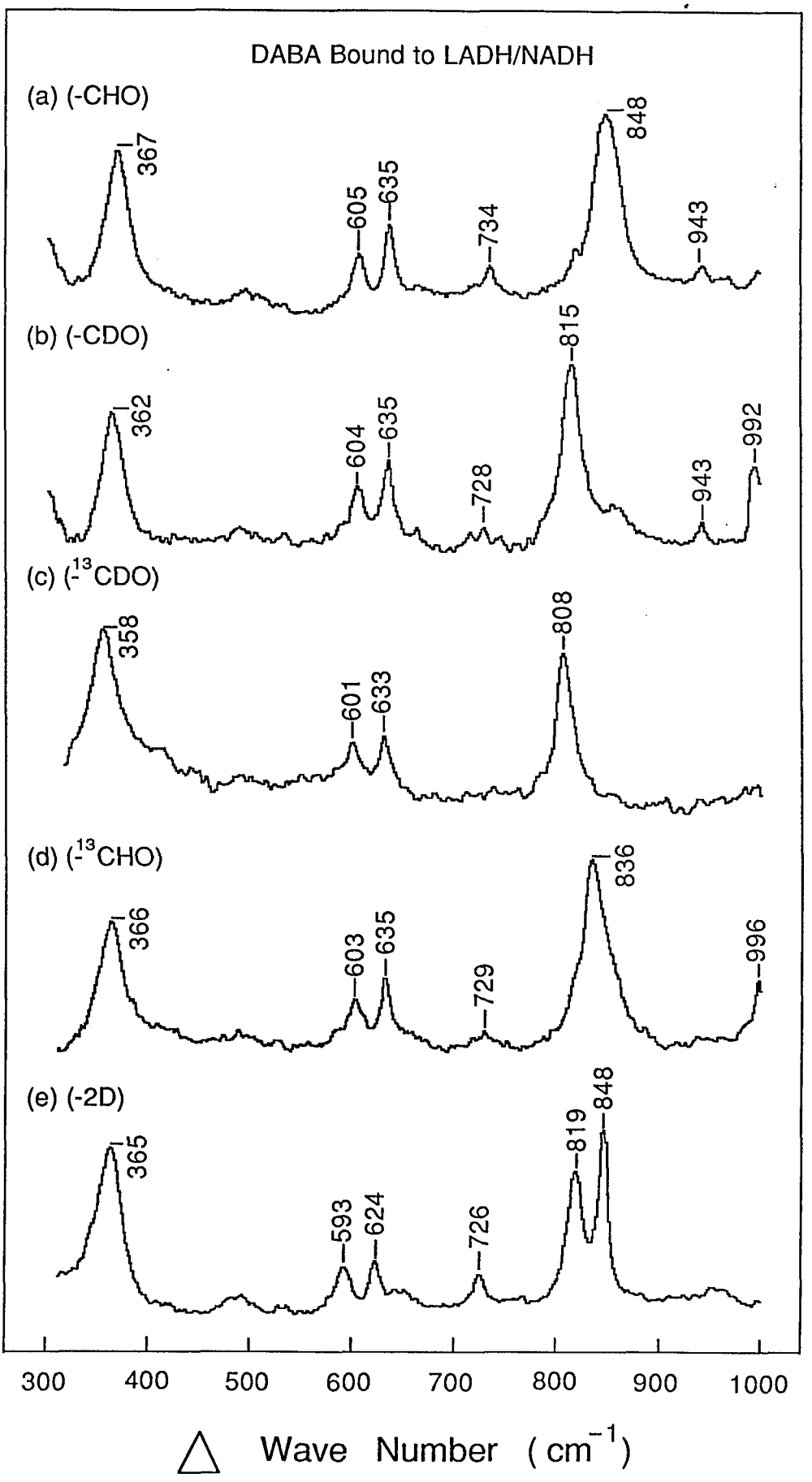
DABA Bound to LADH/NADH
(a) (-CHO)
367
605
635
734
848
943
(b) (-CDO)
362
604
635
728
815
943
992
(c) (-13CDO)
358
601
633
808
(d) (-13CHO)
366
603
635
729
836
996
(e) (-2D)
365
593
624
726
819
848
300
400
500
600
700
800
900
1000
Wave Number (cm-1)

5.8

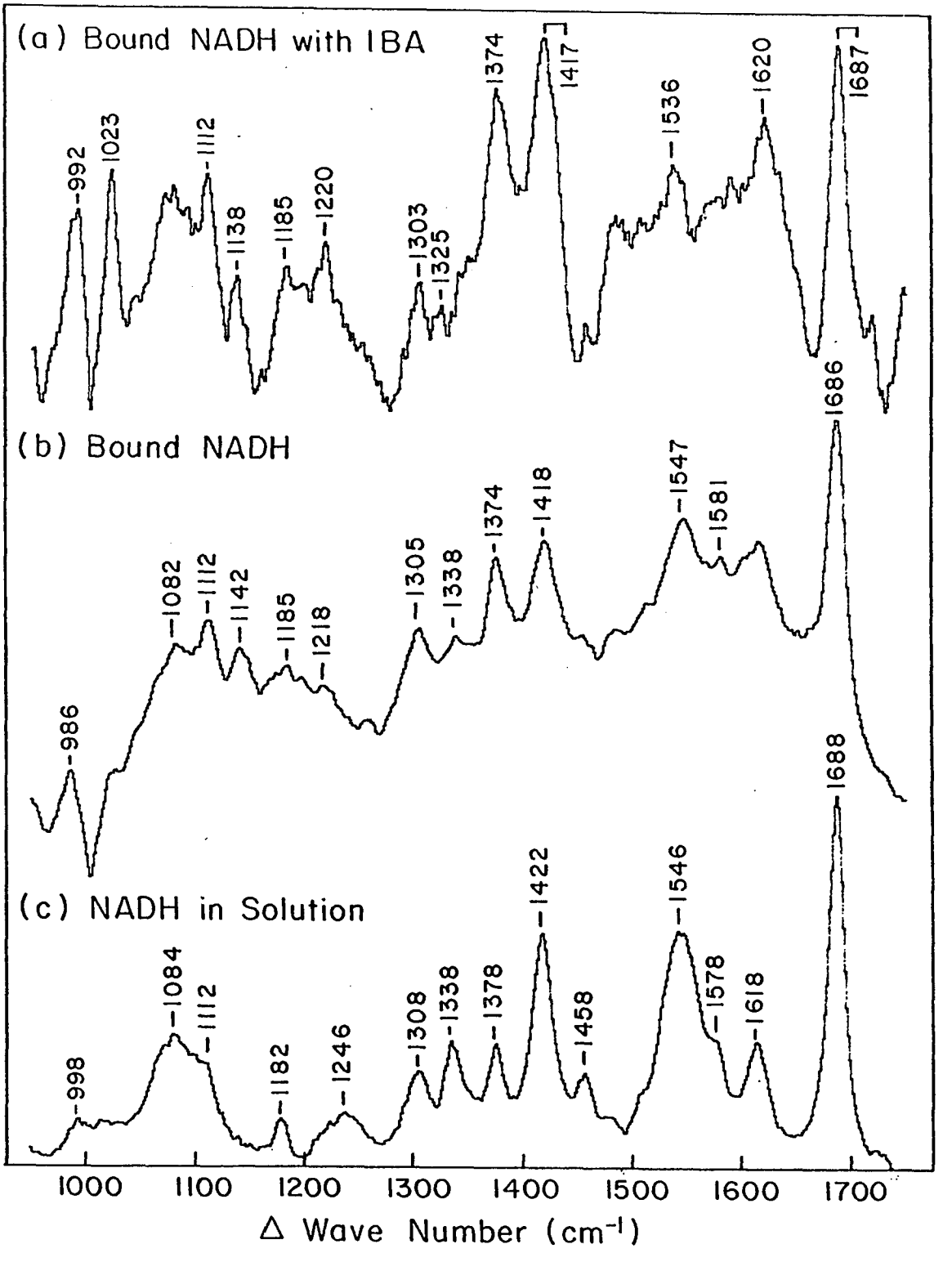
(a) Bound NADH with IBA
992
1023
1112
1138
1185
1220
1303
1325
1374
1417
1536
1620
1687
(b) Bound NADH
986
1082
1112
1142
1185
1218
1305
1338
1374
1418
1547
1581
1686
(c) NADH in Solution
998
1084
1112
1182
1246
1308
1338
1378
1422
1458
1546
1578
1618
1688
1000
1100
1200
1300
1400
1500
1600
1700
Δ Wave Number (cm⁻¹)

6.1

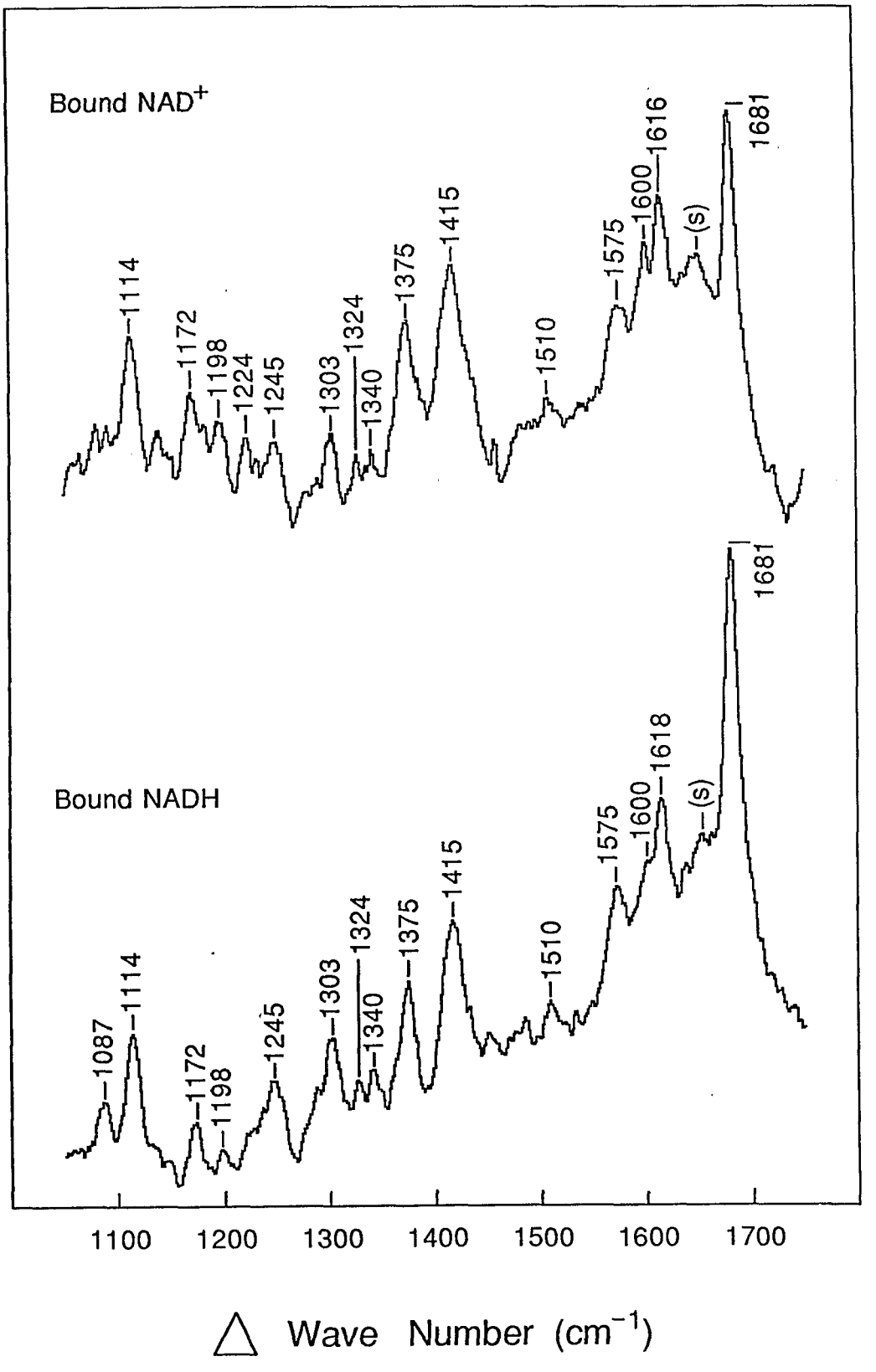
Bound NAD+
1114
1172
1198
1224
1245
1303
1324
1340
1375
1415
1510
1575
1600
1616
(s)
1681
Bound NADH
1087
1114
1172
1198
1245
1303
1324
1340
1375
1415
1510
1575
1600
1618
(s)
1681
1100
1200
1300
1400
1500
1600
1700
△ Wave Number (cm⁻¹)

8.1

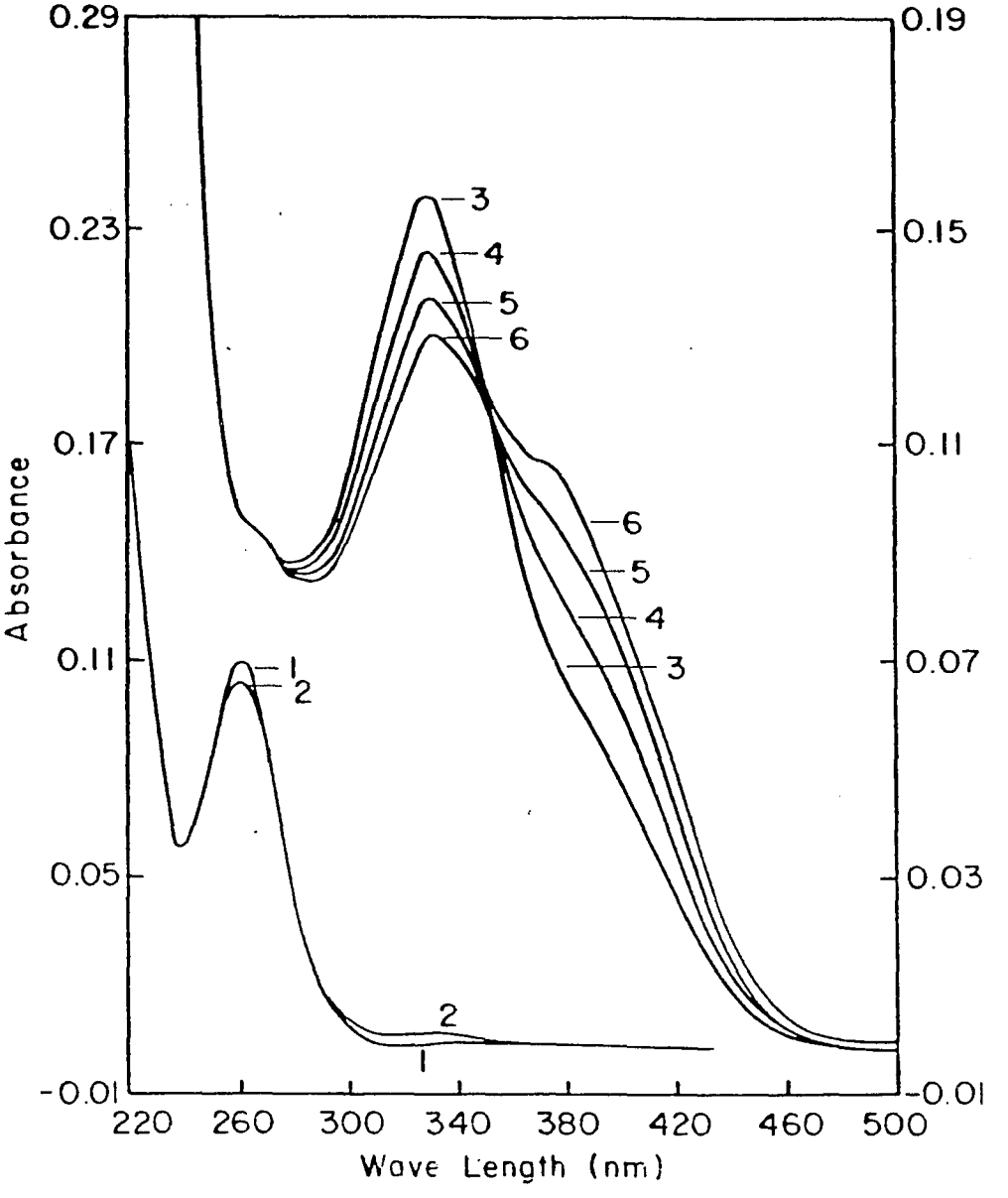
0.29
0.23
0.17
0.11
0.05
-0.01
0.19
0.15
0.11
0.07
0.03
-0.01
Absorbance
220
260
300
340
380
420
460
500
Wave Length (nm)
1
2
3
4
5
6

8.2

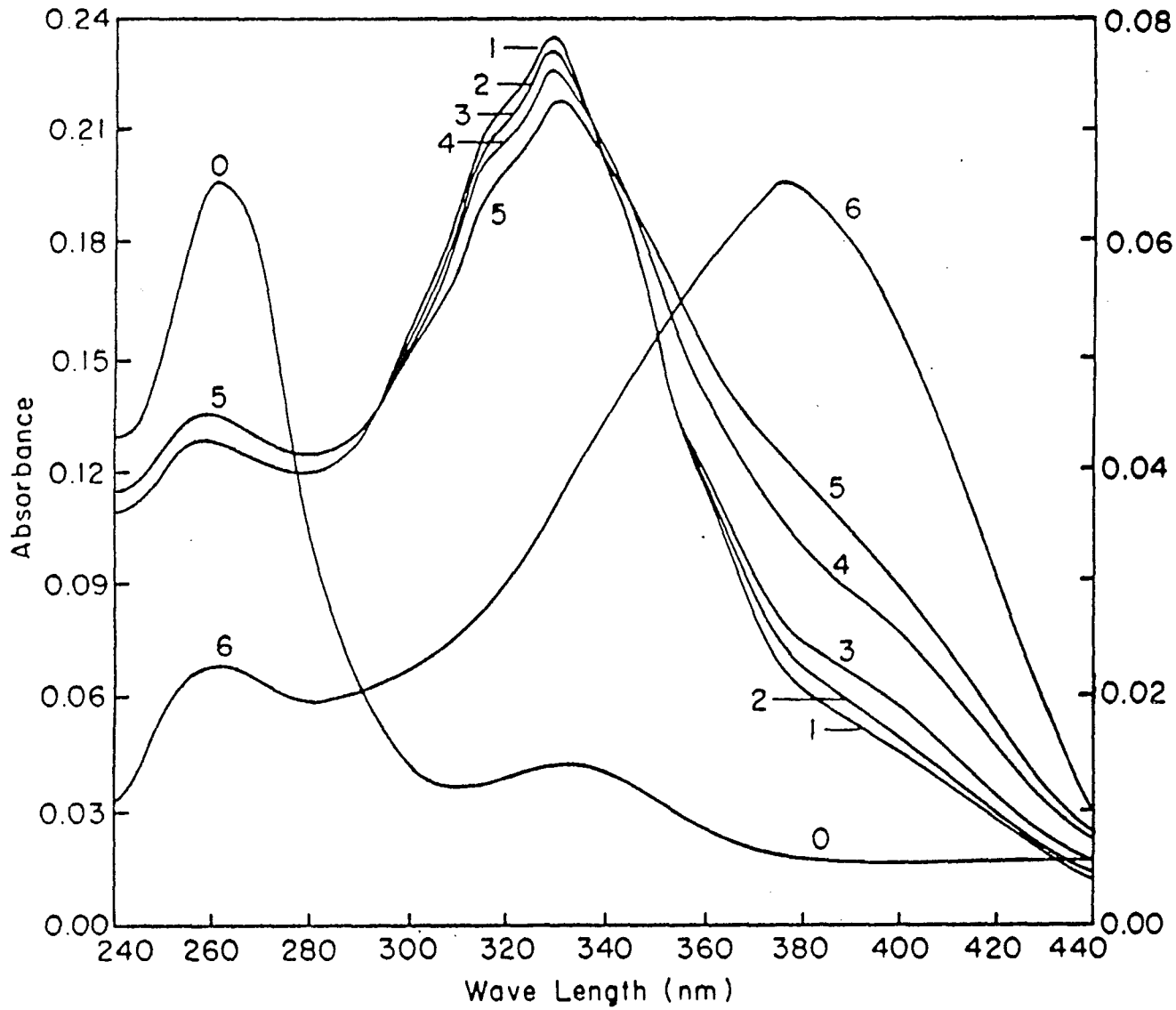
0.24
0.21
0.18
0.15
0.12
0.09
0.06
0.03
0.00
0.08
0.06
0.04
0.02
0.00
Absorbance
240 260 280 300 320 340 360 380 400 420 440
Wave Length (nm)
0
1
2
3
4
5
6

8.3

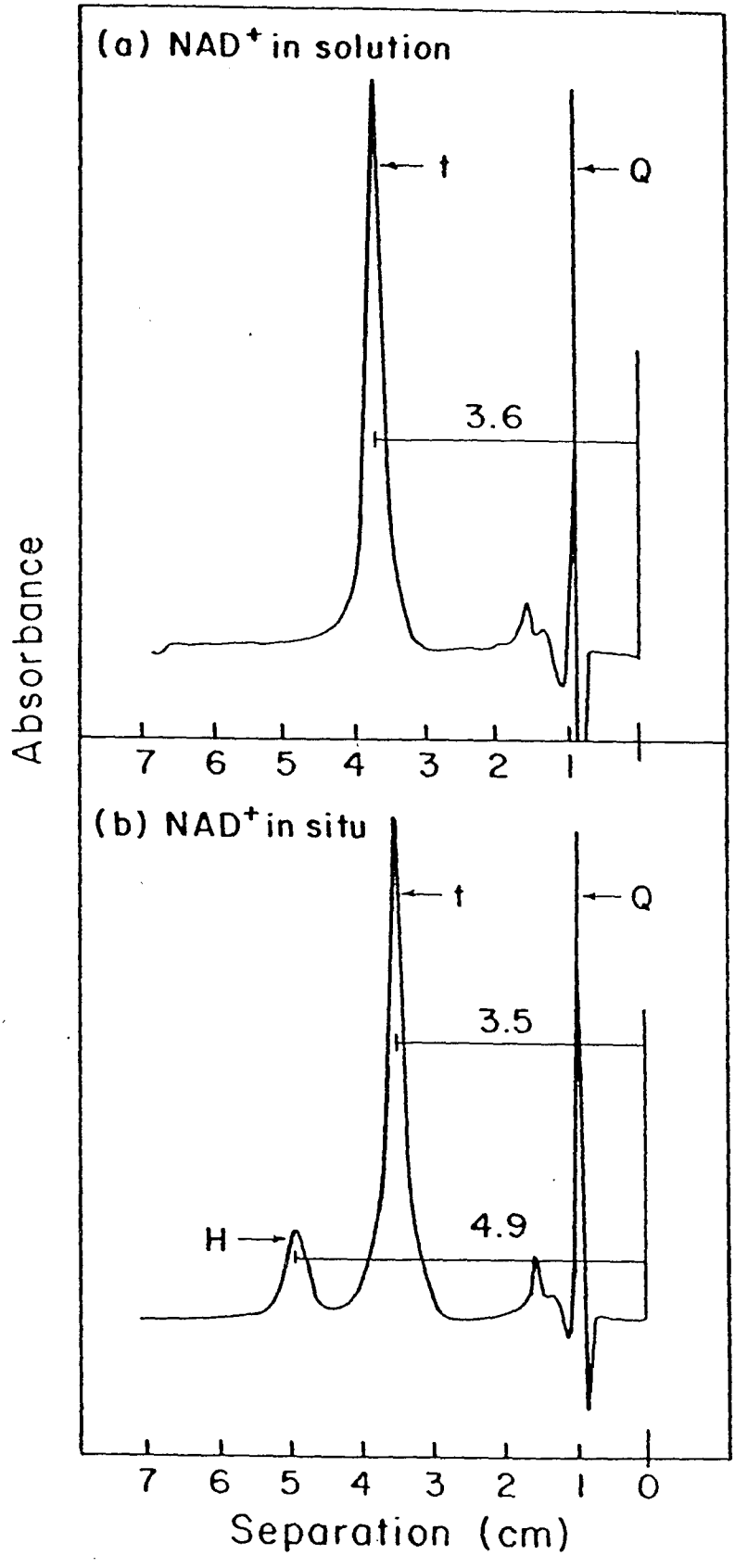
(a) NAD+ in solution
t
Q
3.6
Absorbance
7 6 5 4 3 2 1
(b) NAD+ in situ
t
Q
3.5
H
4.9
7 6 5 4 3 2 1 0
Separation (cm)

8.4

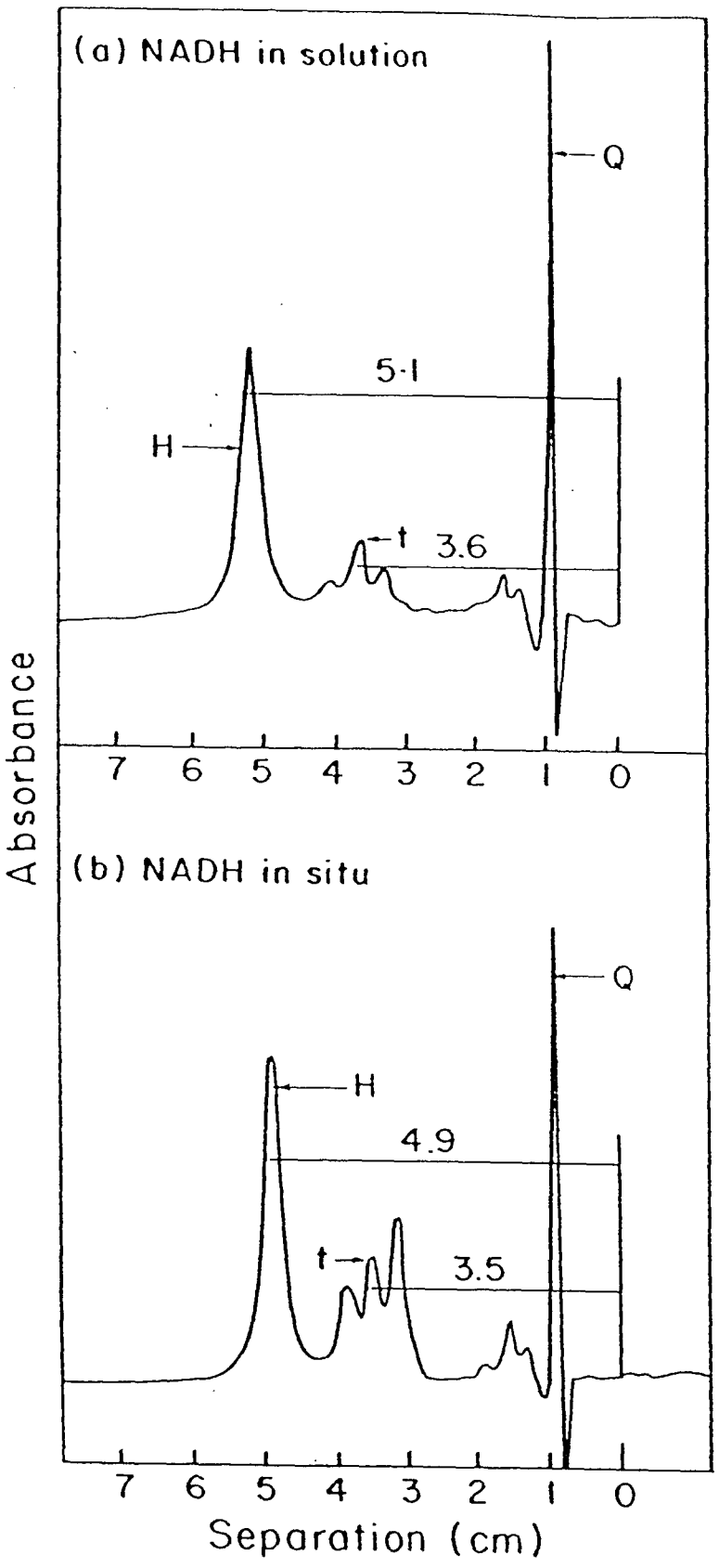
(a) NADH in solution
Q
5·1
H
t
3.6
7 6 5 4 3 2 1 0
Absorbance
(b) NADH in situ
Q
H
4.9
t
3.5
7 6 5 4 3 2 1 0
Separation (cm)

8.5

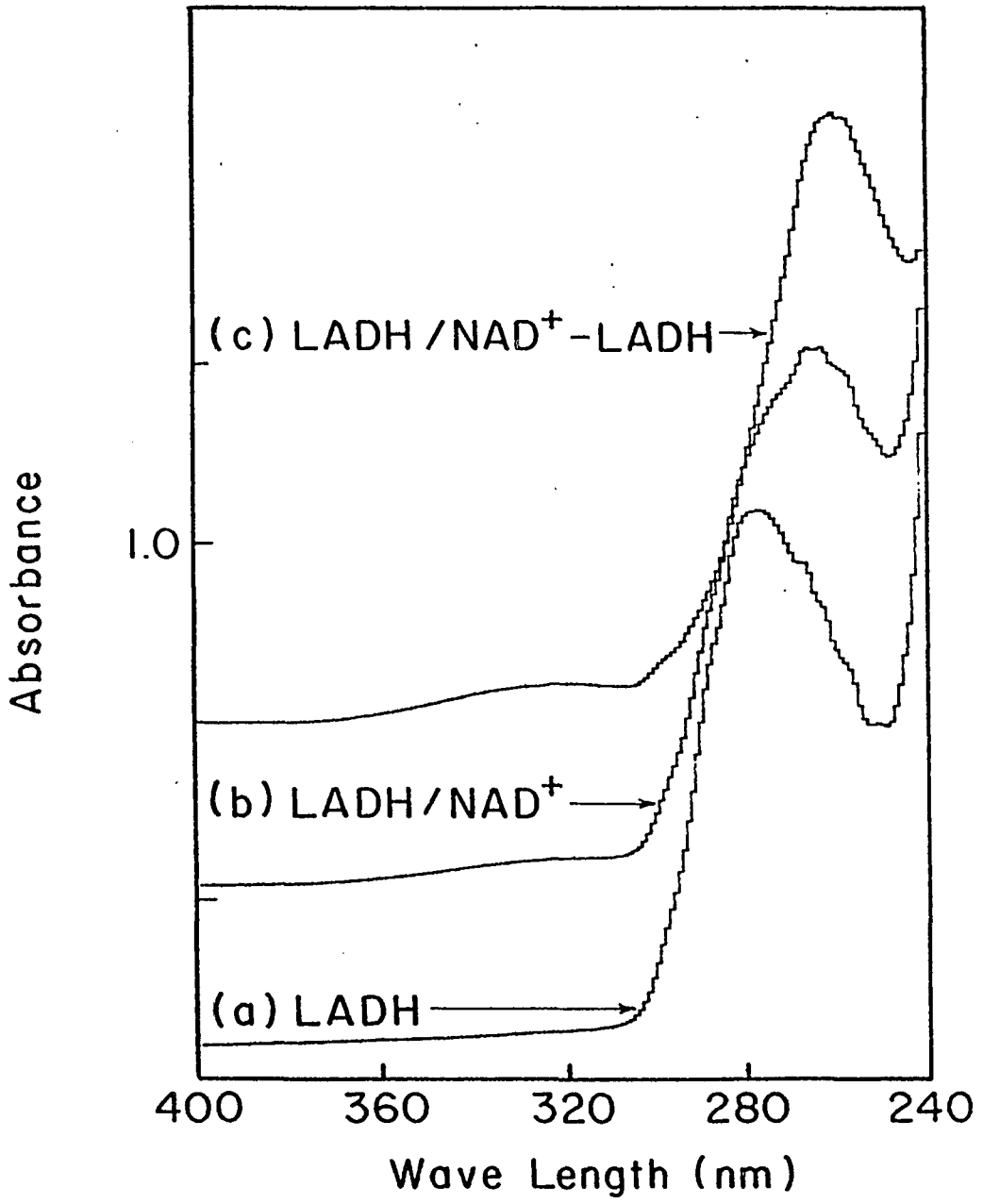
(c) LADH / NAD+ - LADH
(b) LADH / NAD+
(a) LADH
Absorbance
1.0
400
360
320
280
240
Wave Length (nm)

8.6

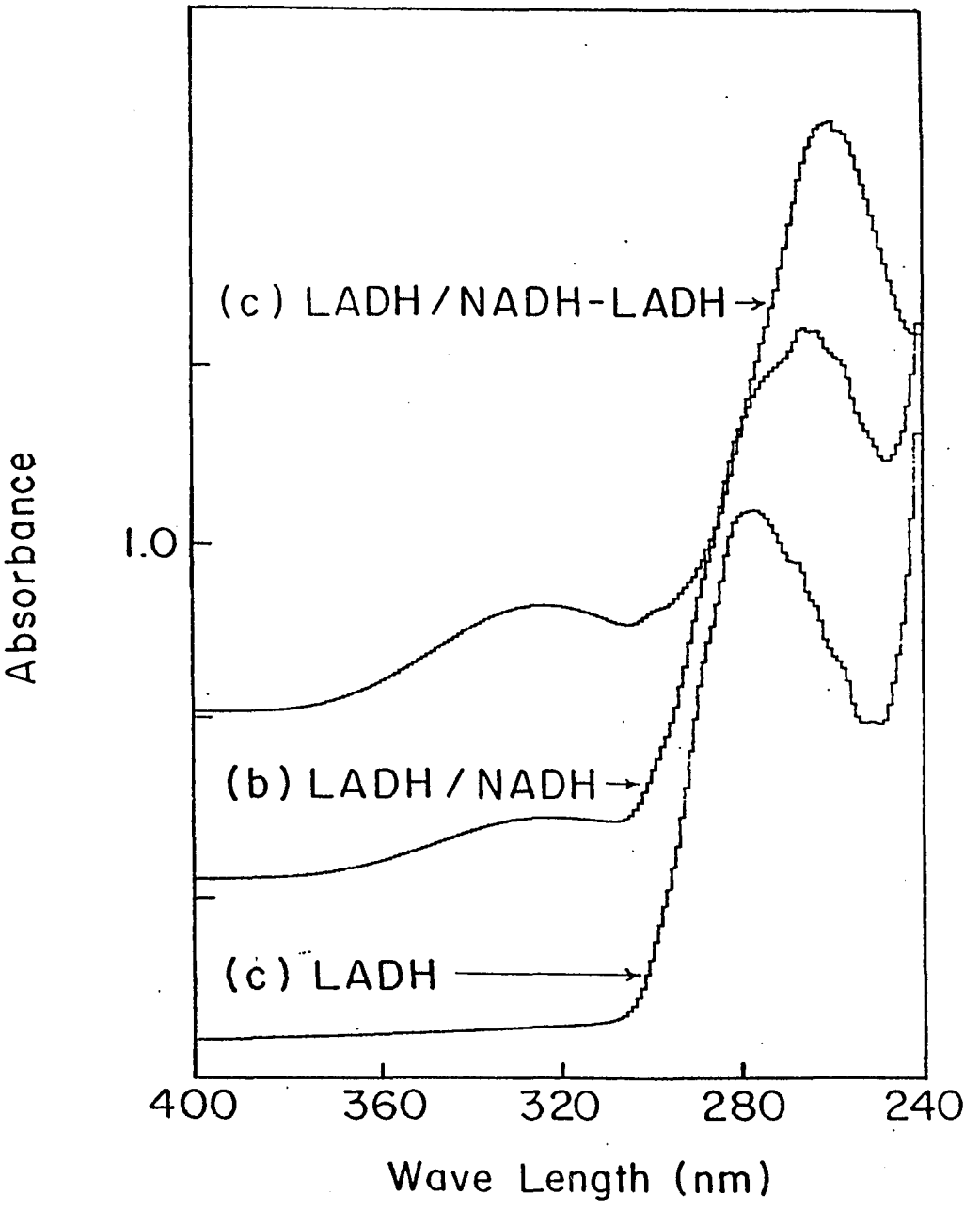
(c) LADH/NADH-LADH
(b) LADH/NADH
(c) LADH
Absorbance
1.0
400
360
320
280
240
Wave Length (nm)

8.7

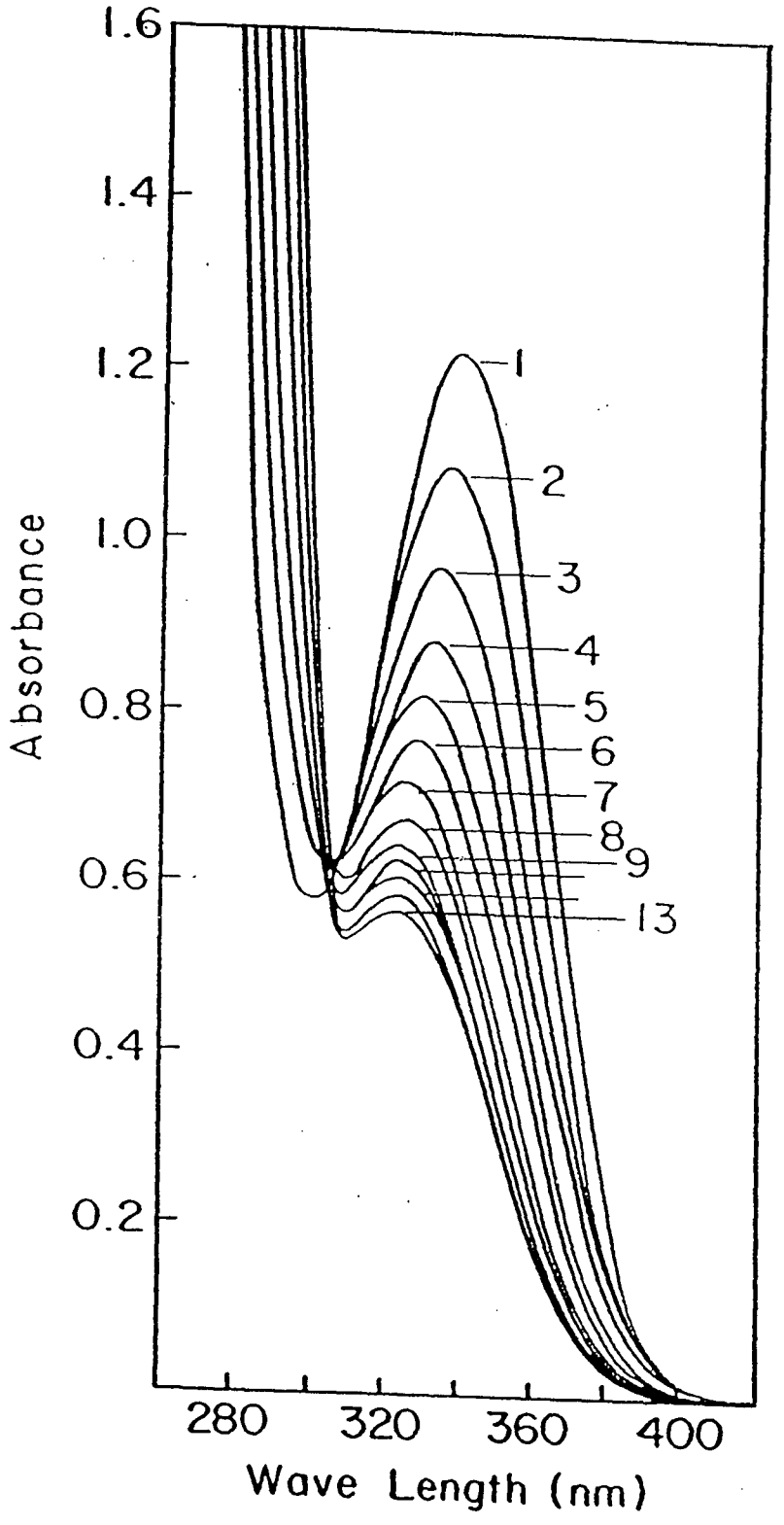
1.6
1.4
1.2
1.0
0.8
0.6
0.4
0.2
Absorbance
1
2
3
4
5
6
7
8
9
13
280
320
360
400
Wave Length (nm)

8.8

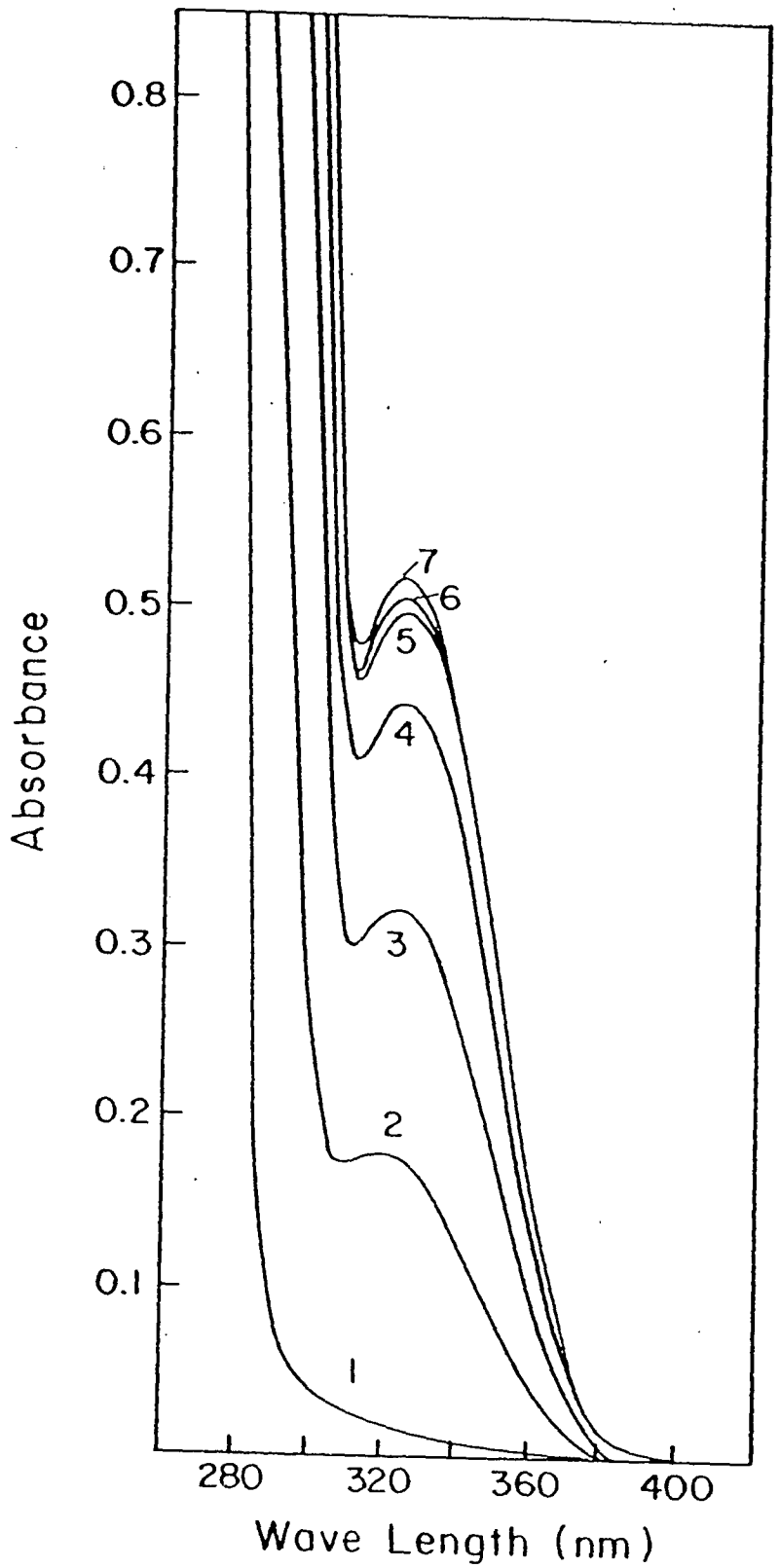
Absorbance
0.8
0.7
0.6
0.5
0.4
0.3
0.2
0.1
1
2
3
4
5
6
7
280
320
360
400
Wave Length (nm)

8.9

REFERENCES

Åkenson, Å. (1964). Biochem. Biophys. Res. Comm. 17, 211-214.

Angelis, C. T., Dunn, M. F., Muchemore, D. C. & Wing, R. M. (1977). Biochemistry 16, 2922-2931.

Andersson, P., Kvassmann, J., Lindstrom, A., Olden, B., & Pettersson, G. (1981). Eur. J. Biochem. 113, 425-433.

Bert L. Vallee & Frederic L. Hoch (1955). National Academy of Sciences, 41 No. 6,327.

Biellmann, J.-F. & Jung, M. J. (1971) Eur. J. Biochem. 19, 130-134.

Biellman, J.-F., Samama, J.-P., Bränden, C.-I., & Eklund, H. (1979). Eur. J. Biochem. 102, 107-110.

Bignetti, E., Rossi, G. L. & Zeppezauer, E. (1979). FEBS Letters, 100, No. 1, 17-22.

Blackwell, L. F. & Hardman, M. J. (1975). Eur. J. Biochem. 55, 611-615.

Bodenheimer, J. S., Berenblut, B. J., Wilkinson, G. R. (1972). Chem. Phys. Lett. 14, 535-536.

Bowman, W. D., & Spiro, T. G. (1980). J. Raman Spectrosc. 9, 369-371.

Bränden, C.-I. (1965). Arch. Biochem. Biophys. 112, 215-217.

Bränden, C.-I., Jörnvall, H., Eklund, H., & Funrugren, B. (1975). Enzymes, 3rd ED. 11, 103-190.

Bränden, C.-I., & Eklund, H. (1978). Ciba Foundation Symposium 60 p. 63.

Carey, P. R., & Storer, A. C. (1984). Ann. Rev. Biophys. Bioeng. 13, 25-49.

Cedergren-Zeppezauer, E., Samama, J.-P., & Eklund, H. (1982). Biochemistry, 21,

4895-4908.

Chi-Yu Lee, Eichener, R. D. & Kaplan, N. O. (1973). Proc. Nat. Acad. Sci. USA. 70, No. 5, pp. 1593-1597.

Cook, P. F. & Cleland, W. W. (1981). Biochemistry, 20, 1805-1816.

Cook, P. F., Oppenheimer, N. J. & Cleland, W. W. (1981). Biochemistry, 20, 1817-1825.

Colowick, S. P., Van Eys, J., & Park, J. H. (1966). Comp. Biochem. 14, 1-98.

Cotton, F. A. & Francis, R. J. Amer. Chem. Soc. 82, 2986.

Czeizler, J. L. & Hollis, D. P. (1973). Biochemistry, 12, No. 9, 1684-1689.

Dahl, K., & Dunn, M. F. (1984). Biochemistry 23, 4094-4100.

Dalzeil,K. (1957).Acta Chem. Scand. 11 No. 2, 397-398.

Dalziel, K. (1975). The Enzymes, 3rd ED. 11, 1-60.

Dickinson, F. M. & Monger, G. P. (1973) Biochem. J. 131, 262-270.

Dickinson, C. J. & Dickinson, F. M. (1975). Biochem. J. 147, 303-311.

Dickinson, F. M. (1970). Biochem. J. 120, 821-830.

Dickinson, F. M. (1974). Eur. J. Biochem., 41, 31-36.

Dickinson, C. J. & Dickinson, F. M. (1977). 161, 73-82.

Dickinson, F. M. & Dickinson, C. J. (1978). 171, 629-637.

Drum, D. E. & Vallee, B. L. (1970). Biochem. Biophys. Res. Comm. 41, 33-39.

Drysdale, B.-E. & Hollis, D. P. (1980). Arch. Biochem. Biophys. 205, 267-279.

Dunn, M. F. (1974). Biochemistry, 13, 1146-1151.

Dunn, M. F., & Hutchison, J. S. (1973). Biochemistry 12, 4882-4892.

Dunn, M. F., Biellmann, J. -F., & Branlant, G. (1975). Biochemistry 14, 3176.

Dworschack, R. T. & Plapp, B. V. (1977). Biochemistry 16, No. 12, 2716-2725.

Eklund, H., Nordstrom, B., Zeppezauer, E., Soderlund, G., Ohlsson, I., Boiwe, T., Sorderberg, B.-O., Tapia, O., & Bränden, C.-I., (1976). J. Mol. Biol., 102, 27-59.

Einarsson, R., Eklund, H., Zeppezauer, E., Boiwe, T., & Bränden, C.-I. (1974). EUR. J. Biochem. 49, 41-47.

Eklund, H., Samama, J. -P., Wallen, L., Bränden, C.-I., Åkenson, Å. & Jones, T. A. (1980). J. Mol. Biol. 146, 561-587.

Eklund, H., Samama, J.-P., & Jones, T. A. (1984). Biochemistry 23, 5982-5996.

Eklund, H., & Bränden, C.-I. (1986). In Pyridine Nucleotides, John Wiley and Sons, New York.

Eklund, H., Samama, J.-P., Wallen, L., Bränden, C.-I., Åkenson, A., & Jones, T. A. (1981). J. Mol. Biol. 146, 561-587.

Fisher, H. F., Adija, D. L., Cross, D. G. (1969). Biochemistry 8, 4424-4430.

Fisher, R. F., Harris, A. C., Mathias, A. P., & Rabin, B. R. (1967). Biochem. Biophys. Acta 139, 169-170.

Forrest, G. (1976). J. Phys. Chem. 80, 1127-1128.

Gronenborn, A. M. & Clore, G. M. (1982) J. Mol. Biol. 157, 155-160.

Hardman, M. J., Blackwell, L. F., Boswell, C. R., & Buckley, P. D. (1974). Eur. J. Biochem., 50, 113-118.

Harris, I. I., & Waters, M. (1976). The Enzymes, 3 rd Ed. !3, 1-49.

Holbrook, J. J., LilJas, A., Steindel, S. J., & Rossmann, M. G. (1975). The Enzymes, 3 rd ED. 11, Part A pp. 191-292.

Hollis, D. P. (1967). Biochemistry 6, 2080-2087.

Hope, H. (1969). Acta, Cryst. B25, 78-87.

Jagodzinski, P. W. & Peticolas, W. L. (1981). J. Am. Chem. Soc. 103, 234-236.

Jagodzinski, P. W., Funk, G. F., & Peticolas, W. L. (1982). Biochemistry 21, 2193-2202.

Jan Van Eys & Kaplan, N. O. (1957) Biochem. Biophys. Acta 23, 574-587.

Jencks, W. P. (1969). In Catalysis in Chemistry and Enzymology, Part I, pp. 1-320, McGraw-Hill, New York.

Jörnvall, H. (1970). Eur. J. Biochem. 16, 25.

Jörnvall, H., Eklund, H., & Bränden, C.-I. (1978). J. Biol. Chem. 253, 8414-8419.

Kaplan, N. O. (1960). The Enzymes 2nd ED. 3, 105-169.

Karle, I. L. (1961). Acta Cryst. 14, 497.

Karlovic, D., Amiguet, P., Bonner, F. J. & Luisi, P. L. (1976) Eur. J. Biochem . 66, 277-284.

Kiefer, W. (1973). Applid Spectroscopy 27, 253-258.

Klinman, J. (1975). J. Biol. Chem. 250, 2569-2573.

Kint, S., & Tomimatsu, Y. (1979). Biopolymers 18, 1073-1079.

Kvassmann, J., Larsson, A., & Pettersson, G. (1981). Eur. J. Biochem. 14, 555-562.

Lafleur, L., Rice, J., & Thomas, Jr., G. J. (1972). Biopolymers 11, 2423-2437.

Leskovac, T. & Pavkov- Pericin, D. (1974). Blochem. J. 145, 581-590.

Lippert, J. L., Tyminski, D., & Desmeules, P. (1976). J. Am. Chem. Soc. 98, 7075-7080.

Lord, R. C., & Thomas, G. J. Jr. (1967). Spectrchim. Acta, Part A 23A, 2551-2591.

Luisi, P. L., & Favilla, R. (1970). Eur. J. Biochem. 17, 91-94.

Maret, W., Andersson, I., Dietrich, H., Schneider-Brenlohr, H., Einarsson, R., & Zeppeauer, M. (1979). Eur. J. BIOchem. 98, 501-512.

Maret, W., Dietric, H.,Ruf, H.-H., & Zeppezauer, M. (1980). J. Inorg. Biochem. 12, 241-252.

Maurice R. E & Katarina B (1986). Biochemistry 25, 6624-6630.

Nishimura, Y., & Tsuboi, M. (1980). Science (Washington, D. C.) 210, 1358-1360.

Nygard, A. P. & Therorell, H. (1955). Acta, Chem. Scand. 9, No 8.

Ohlsson, I., Nordstrom, B., & Bränden, C.-I., (1974). J. Mol. Biol. 89, 339-354.

Patrick, D. M., II, Wilson, J. E., & Leroi, G. E. (1974). Biochemistry 13, 2813-2817.

Perlman, R. L. (1968). Science 160, 317-319.

Plapp, B. V., Eklund, H., & Bränden, C.-I. (1978). J. Mol. Biol. 122, 23-32.

Reynier, M. (1969). Acta Chem. Scand. 23, 1119-1129.

Rizzo, V., Pande, A., & Luisi, P. L. (1987) In Coenzymes and Cofactors to be published.

Rodgers, E. G., & Peticolas, W. L. (1980). J. Raman Spectrosc. 9, 372-375.

Rousseau, D. L. (1981). J. Raman spectroscopy 10, 94-99.

Samama, J.-P., Wrixon, A. D., & Biellmann, J. -F. (1981). Eur. J. Biochem. 118, 479-486.

Schlessinger, J. Steinberg, I. Z., & Levitzki, A. (1975). J. Mol. Biol. 91, 523-528.

Shelnutt, J. A., Rousseau, D. L., Friedman, J. M. & Simon, S. R. (1979). Proc. Natl. Acad. Sci. (USA) 76, 4409-4414.

Shore, J. D., & Gilleland, M. J. (1970). J. biol. Chem. 245, 3422-3425.

Shore, J. D. Gutfreund, H., Brooks, R. L., Santiago, D.,& Santiago, P. (1974). Biochemistry 13, 4185-4190.

Sloan, D. L., Young, J. M., Mildvan, A. S. (1975). Biochemistry 14, 1998.

Subramanian, S., & Ross, P. D. (1978). J. of Biol. Chem. 254, 7827-7830.

Subramanian, S., & Ross, P. D. (1977). Biochem. Biophys. Res. Commum. 78, 461-466.

Subramanian, S., & Ross, P. D. (1978). Biochemistry 17, 2193-2197.

Subramanian, S., Ross, J. B. A., Ross, P. D., & Brand, L. (1981). Biochemistry 20, 4086-4093.

Sund, H. & Therorell, H. (1963). Alohol Dehydrogenases. In The Enzymes, (Boyer, P. D., Lardy, H. and Myrback, K. eds.) 2nd ED. Vol. 7, p. 25, Academic Press, New York.

Sytkowski, A. J. & Vallee, B. L. (1978). Biochemistry 17, 2850-2857.

Taniquchi, S., Therorell, H. & Åkenson, Å. (1967). Arch. Chem. Scand. 21, 1903-1920.

Temler, R. S., & Kagi, J. H. R. (1974) Experientia 30, 687.

Therorell, H., & Chance, B. (1951). Acta Chem. Scand. 5, 1127-1144.

Therorell, H., & Mckinley-Mckee, J. S. (1961). Acta. Chem. Scand. 15, 1811-1833.

Therorell, H. & Yonetani, T. (1963). Biochem. Z. 338, 537-553.

Therorell, H., & Yonetani, T. (1964). Arch. Biochem. Biophys., 106, 252-258.

Therorell, H., Yonetani, T., & Sjoberg, B. (1969). Acta. Chem. Scand. 23, 255-260.

Therorell, H. & Tatemoto, K. (1971). Arch. Biochem. Biophys., 142, 69-82.

Tsuboi, M. Takahashi, S., & Harada, I. (1973) in Physico-Chemical Properties of Nucleic Acid (Duchesne, J., Ed.) Vol. 2, pp 91-145. Academic Press, London & New York.

Yamada, T. & Yamato, M. (1973). J. Biochem. 74, 971-984.

Yonetani, T. (1963). Acta. Chem. Scand. 17, suppl. 1, 971-984.

Yu, N.-T., Jo, B. H., Chang, R. C. C., & Huber, J. D. (1974). Arch. Biochem. Biophys. 160, 614-622.

Yue, K. T., Yang, J. P., Martin, C. L., Sloan, D. L., & Callender, R. H. (1984a).Biochemical and Biophysical research communications 122, No. 1, 225-229.

Yue, K. T., Yang, J. P., Martin, C. L., Lee, S. K., Sloan, D. L., & Callender, R. H. (1984b). Biochemistry 23, 6480-6483.

Yue, K. T. Martin, C. L., Chen D., Nelson, P., Sloan, D. L., & Callender, R. H. (1986). Biochemistry 25, 4941-4947.

Zeppezauer, E., Soderberg, B.-O., Bränden, C. -I., Åkenson, Å., & Therorell, H. (1967). Acta. Chem. Scand. 21, 1099-1101.

Zeppezauer, E., Samama, J.-P., & Eklund, H. (1982). Biochemistry 21, 4895-4908.